5-10-2003

Development of a Nonlinear Model for Subgrid Scale Turbulence and it's Applications

Shanti Bhushan

DEVELOPMENT OF A NONLINEAR MODEL FOR SUBGRID SCALE TURBULENCE AND ITS APPLICATIONS

By

Shanti Bhushan

A Dissertation
Submitted to the Faculty of
Mississippi State University
in Partial Fulfillment of the Requirements
for the Degree of Doctor of Philosophy
in Aerospace Engineering
in the Department of Aerospace Engineering

Mississippi State, Mississippi

May 2003

DEVELOPMENT OF A NONLINEAR MODEL FOR SUBGRID SCALE TURBULENCE AND ITS APPLICATIONS

By

Shanti Bhushan

Approved:

Z. U. A. Warsi Emiritus Professor of Aerospace Engineering (Director of Dissertation)	Boyd Gatlin Interim Head and Associate Professor of Aerospace Engineering (Committee Member)
Mark Janus Associate Professor of Aerospace Engineering (Committee Member)	Seth Oppenheimer Associate Professor of Mathematics and Statistics (Committee Member)
David Bridges Associate Professor of Aerospace Engineering (Committee Member)	A. Wayne Bennett Dean of the College of Engineering

Name: Shanti Bhushan

Date of Degree: May 10, 2003

Institution: Mississippi State University

Major Field: Aerospace Engineering

Major Professor: Dr. Z.U.A. Warsi

Title of Study: DEVELOPMENT OF A NONLINEAR MODEL FOR SUBGRID SCALE TURBULENCE AND ITS APPLICATIONS

Pages in Study: 136

Candidate for Degree of Doctor of Philosophy

The present work addresses the basic question involving the modeling of subgrid-scale turbulence. A new model has been developed which extends the nonlinear Reynolds' stress constitutive equation to subgrid scale turbulence. Effort has been made to model the terms forming the subgrid stresses, i.e, Reynolds', Leonard's and cross terms, separately which play different roles in the physics of subgrid scale turbulence. Modeling of these terms independently helps to capture the physics of the problem accurately such as the filtering process for subgrid scale turbulence, backscatter of energy and dissipation of energy. Some of the answers of the questions such as backscatter of energy comes from the spectral decomposition of the stresses and from homogeneous isotropic turbulence. The model coefficients are expressed as universal constants for a Gaussian filter using the Kolmogrov's hypothesis. The model coefficients have been tested for the *plane homogeneous shear* and *plane homogeneous strain* flows. An *a priori* test has been performed to compare the model results with the mixed-nonlinear model and Smagorinsky model.

In this study Enviornmental Fluid Dynamics Computer code (EFDC) has been used. An *a posteriori* analysis has been performed for the two-dimensional flow over a backward facing step, where the vertically hydrostatic boundary layer equations are solved. The top boundary is assumed to be a free surface and a terrain following coordinate system has been used. Because of the non-negativity of the subgrid scale dissipation term the solution becomes unstable and the

steady state solution is obtained by clipping the dissipation term. The results are compared with the available experimental and numerical results for the velocity profiles, subgrid scale kinetic energy profiles and the reattachment length.

The model is further extended for the diffusion of scalar variables and to include the buoyancy effect. It is implemented to explore the hydrostatic flow over two-dimensional elliptical mountain ridge, where the Boussinesq approximation is used for variable density. An attempt has been made to model the mean square vorticity fluctuation to understand the effect of turbulent flow and the buoyancy effect on vortex generation. The effect of turbulent flow on the phenomenon of upstream blocking and lee-vortex generation has been studied numerically for varying Froude number.

ACKNOWLEDGMENTS

I would like to express my sincere gratitude to my major professor, Dr.Z. U. A Warsi, for his valuable moral support and guidance. I would also like to thank Dr. David Huddleston for providing me the *EFDC code* which was used in my research work. Further, this work would not have been complete without the support of my committee members.

In addition I would like to thank Aerospace Department for funding me throughout the research work. I would like to give special thanks to the personnel in the library for their cooperation in my literature search.

Finally, I offer my heartfelt gratitude to my parents, friends and family members for all their support and encouragement. I would also like to thank everyone who has made my stint at MSU a wonderful learning experience.

TABLE OF CONTENTS

CHAPTER Page

LIST OF TABLES

LIST OF FIGURES

FIGURE Page

NOMENCLATURE

Fluid Dynamic Variables:

$\hat{.}$	Filtered/resolved component of the variable
$\acute{.}$	Subgrid/fluctuating component of the variable
$\grave{.}$	Fourier Component of the variable
$\langle\ .\rangle$	Volume Averaging
C_k	Kolmogorov's constant
Δ	Grid Scale
f	Coriolis Parameter
η	Dissiaption Length Scale
κ	Fluid Thermal Conductivity
ϕ	Mean Square Vorticity Fluctuation
N	Brunt-Vaisala Frequency
p_0	Synoptic Scale Fluid Pressure
p	Perturbation Pressure
ρ_0	Synoptic Scale Fluid Density
ρ	Perturbation Density
T	Fluid Temperature
$\mathbf{x}$	Cartesian Coordinate Vector
$\boldsymbol{\xi}$	Curvilinear Coordinates Vector
t	Time
Pr	Prandtl Number
Re	Reynolds Number

Sc	Schmidt Number
Fr	Froude Number
Ri	Richardson Number
$\mathbf{u}$	Fluid Velocity Vector
$\mathbf{w}$	Grid Velocity Vector
$\mathbf{G}$	Filter Function
$\mathbf{k}$	Wavenumber vector
$\boldsymbol{\omega}$	Vorticity Vector
$\mathbf{I}$	Identity Tensor
$\mathbf{D}$	Rate-of-strain tensor
$\boldsymbol{\tau}$	Stress Tensor
$\boldsymbol{\mathcal{L}}$	Leonard Stress Tensor
$\boldsymbol{\mathcal{C}}$	Cross Stress Tensor
$\boldsymbol{\mathcal{R}}$	Reynolds Stress Tensor
$\boldsymbol{\sigma}$	Deviatoric Stress Tensor
$\mathbf{H}$	Subgrid scalar flux tensor
K_{sgs}	Subgrid Scale Kinetic Energy
K_r	Resolved Scale Kinetic Energy
ϵ	Dissipation
c_b , $c_{b\theta}$	Backscatter Coefficients
δ_{ij}	Kronecker Symbol

Tensor Operators:

div	Divergence
$grad$	Gradient
$curl$	Curl

CHAPTER I

INTRODUCTION

Big whorls have little whorls,
which feed on their velocity,
and little whorls have lesser whorls,
and so on to viscosity (in molecular sense).

The above rhyme as enunciated by Richardson (1922) captures the physics of fluid turbulence which states that the turbulent flow can be exactly resolved if the numerical solution is carried out up to the Kolmogrov's length scale (η) where the dissipation of energy occurs. This forms the basis of Direct Numerical Simulation (DNS). Fully developed turbulent flow consists of a wide range of scales, and as DNS requires the resolution of all scales of motion, which restricts its application to low Reynolds number (Re) flow as Reynolds number is directly proportional to the scales in flow. Hirt [8] approximately estimated that number of mesh points on a three dimensional grid is proportional to $Re^{9/4}$ which yields 10^9 mesh points for $Re = 5 \times 10^4$. The situation gets even worse in real physical problems, such as atmospheric and oceanographic flows, where Re may be as large as 10^8. Because of these limitations the DNS calculations have been carried out to low Reynolds' numbers. The alternative approach classified as Large Eddy Simulations 'LES' is to separate the scales of motion as large and small scales, where large scales contain most of the energy and dominate the transport of mass, momentum, and heat. On the other hand the small scale includes the dissipative range responsible for the energy dissipation. The space average of the variable can be obtained by integrating over a volume, l^3, using a filter function $G(\xi)$ with filter width Δ such that the flow variable is decomposed into the averaged or large scale component and the small scale or subgrid scale component. Similarly time average can also be used. It must be observed that $l \to 0$ implies DNS, whereas $l \to \infty$ yields ensemble average and results in Reynolds Averaged Navier-Stokes (RANS). In a RANS solution all the scales below the largest energy containing eddies (L)are averaged out satisfying the Reynolds

assumption. In this process the dynamical information of the smaller scales are lost. Although these filters are used implicitly to formulate the transport equations of the averaged variables but they have to be solved on numerically discrete grids. Hence the averaging is over a finite volume rather than over infinite volume. Thus the scale separating the large and small scale must be related to the grid scale (Δ). In turbulent flow there is no clear cut distinction of length scales except that some have most of the energy, some merely transport energy, and some dissipate energy thus have a broad spectral representation. Hence the filtering operation averages out scales less than $O(\Delta)$ and eddies of scale larger than Δ are resolved. So in general the Reynolds' assumption is not satisfied. This forms the underlying assumption for Large Eddy Simulation (LES). For LES, resolved and subgrid scales are more appropriate than large and small scale respectively and will be used here henceforth. From the above discussion it is apparent that LES and RANS are equivalent except for the filtering scale. In RANS the small scale effects the evolution of the large scale through the Reynolds stress but more interactions appear for LES. In LES the interaction of the resolved and subgrid scale of the flow field is also present and needs to be parameterized accurately through subgrid stresses. The simplifying assumption used in LES is that the resolved scale motions are flow dependent and represent the evolution of large eddies whereas subgrid scale are universal in character and thus can be modeled as subgrid stresses. The fundamental question that needs to be addressed is how to model subgrid stresses as a functional of resolved fields.

LES is a technique intermediate between the DNS and RANS. This fact can be seen easily from the fact that DNS requires filter width $\Delta \sim O(\eta)$ and RANS requires $\Delta \sim O(L)$ whereas in LES the scale Δ lies somewhere in between this range. The self-consistency requires that the results of LES approach RANS when grid size is increased and approaches the results of DNS as the grid size is decreased. The fundamental question of the self-consistency of LES modeling is the independence of the results on filter width. The Kolmogrov's hypothesis of scale invariance answers the above question, according to which there exists an equilibrium range where the subgrid scale components are isotropic and independent of the detailed structure of the resolved scale. This phenomenon of scale invariance has received much attention over the past decade and forms the useful ingredient in turbulence modeling.

The purpose of this dissertation is to use the technique of LES to solve the problem of turbulence. The LES involves the modeling of the subgrid stresses which have been considered

by various authors, e.g. Smagorinsky [9],Deardorff [10], Lilly [11], [12], Leonard [13], Mason [14], Leslie and Quarini [15], Kosovic [16], Speziale [17], Pope [18], Meneveau and Katz [19], Ghosal *et al.* [20], Chasnov [21] Horiuti [22], Cabot and Moin [22] and others. The subgrid scale turbulence models are based on scale-invariance which has proven beneficial. The LES turbulence modeling so far inspires the following variation of the Richardson's rhyme as quoted by Meneveau and Katz [19]

LES whorls have subgrid whorls,
which feed on their velocity,
but small whorls copy larger whorls,
so we don't need viscosity (in molecular sense).

In this research a new nonlinear model has been proposed which extends the algebraic stress model for the Reynolds' stresses developed by Warsi [23]. Rate equation of the subgrid scale kinetic energy is formed and the terms are collected as the production, diffusion and dissipation term. The nonlinear constitutive equation is formed for the subgrid stresses and new nonlinear model is obtained as a second order approximation. Smagorinsky model is obtained for the first order approximation. The model coefficients are thus computed based on the dissipation criteria for homogeneous isotropic turbulence. An attempt has been made to identify the terms of the model with the Leonard's, cross and Reynolds stress term. The model coefficients thus obtained are tested for the homogeneous plane shear and plane strain cases, which gives a good approximation of stresses.

The new nonlinear model which includes the backscatter of energy renders the resolved scale motion stochastic. This phenomenon has been reported by Chasnov [21] and Mason and Thompson [24] who modeled the stresses to have stochastic variation. This phenomenon was also observed for the *dynamic models* for which the deterministic solution was obtained by averaging along homogeneous direction. Meneveau *et al.* [25] moved a step further to obtain the *Lagrangian dynamic model* which helps to get rid of *ad-hoc* principles, but requires solution of another rate equation and modeling of terms. The simplistic approach to obtain deterministic solution is to clip the negative production as suggested by Ghosal *et al.* [20], which has been used in this research.

The new nonlinear model has been implemented in the code which solves the hydrostatic Navier-Stokes equation, where the grid size normal to the plane is fine enough to yield Reynolds stresses but in the plane the subgrid stresses have to be computed. The Reynolds stresses are computed based on Mellor and Yamada model [26] which is a modified form of the one-equation model. The numerical solution is not carried out up to the wall hence wall function is used based on the *surface roughness height.*

In this study we have used the " *Three-Dimensional Environmental Fluid Dynamics Code*" written by John M. Hamrick [27]. The code uses the RANS model in the vertical direction and LES model in the plane. The code is cabable of solving stratified mesoscale flow. The theoretical and numerical methods used in the code are discussed in the subsequent chapters. The code is modified by introducing the new nonlinear model for the subgrid stresses and scalar fluxes with buoyancy effect.

The flow over a backward facing step is solved as a test case. This type of flow forms a very good test problem and has been used by different authors for varying boundary conditions and Reynolds number. An attempt has been made to collect from the available literature, the possible recirculation zones that can be formed for various top boundary condition and flow regimes. The results have been tabulated to give an idea of the recirculation zones that can be formed for the specific case. The reattachment length of the primary recirculation zone also varies depending on various flow parameters such as expansion ratio (E), top boundary condition, surface skin friction and the flow regime. Results of the reattachment lengths have been tabulated from both experimental and numerical simulations for all three types of boundary condition for turbulent flow case. The results seem to vary over a wide range. The reattachment length of $5.2h_s$ obtained in our case although an underprediction but seems reasonable. The stresses from the different models namely Smagorinsky, nonlinear and new-nonlinear model have been compared based on the velocity data obtained from the numerical simulation using Smagorinsky model. The results show that new-nonlinear model shows correlation with Smagorinsky model but has the nature of a mixed nonlinear model. An *a posteriori* analysis has been done and the results compared with the experimental data and good comparisons have been obtained.

The second problem that has been considered is stratified flow over two-dimensional elliptic mountain. The lee wave generation and upstream blocking effect have been studied as a function of the density gradient parameter. Much work has been done to simulate the stratified flow

over an elliptic mountain, but most of the authors end up simulating the baroclinically produced vortices. The effect of turbulence is lost in the baroclinic nature of the vortex. Here we have kept the stratification constant so that the baroclinic effects are absent. Thich also helps us to get rid of the Kelvin-Helmholtz instability which is generated at the interface of the two layers and complex the flow. To understand explicitly the vortex generation phenomenon due to turbulence the Mean Square Vorticity Fluctuation (MSVF) equation has been modeled, which explains the appearance of the lee vortices. The numerical simulation has been performed for neutral, stable and unstable atmosphere. The lee vortices are observed in the neutral atmosphere case as the Reynolds number is increased. For the stable atmosphere case no lee vortices are observed as the buoyant production is negative of the shear production. The stratification when increased further gives upstream blocking effect which occurs in accordance to the Shepphard's theory according to which the flow isn't able to overcome the potential of the mountain. In the simulation of the unstable atmosphere case, for which both buoyancy and shear lead to the production mechanism, the lee vortices are observed. The other phenomenon which has been bought to light through the vorticity production mechanism is that the production of turbulent kinetic energy and MSVF depend upon the same parameter Richardson number, hence the vorticity generation is characterized by the concentration of the turbulent kinetic energy.

CHAPTER II

FORMULATION OF LES MODEL

We consider the incompressible flow governed by the Navier-Stokes equations which referred to rectangular cartesian coordinates are

$$\frac{\partial u_i}{\partial t} + \frac{\partial u_i u_j}{\partial x_j} = -\frac{1}{\rho}\frac{\partial p}{\partial x_i} + \nu \nabla^2 u_i \quad , i = 1,\ 2,\ 3$$

Integrating the above equation with a filter function $G(\boldsymbol{\xi}) = G_1(\xi_1)\, G_2(\xi_2)\, G_3(\xi_3)$ such that the resolved scale motion is defined as

$$\hat{u}_i(\mathbf{x}) = \int_{-\infty}^{\infty} G(\boldsymbol{\xi})\, u_i(\mathbf{x} - \boldsymbol{\xi})\, d\boldsymbol{\xi}$$

Further assuming that the filter function and differentiation commute the momentum equation for the resolved scale motion is obtained as

$$\frac{\partial \hat{u}_i}{\partial t} + \frac{\partial \hat{u}_i \hat{u}_j}{\partial x_j} = -\frac{1}{\rho}\frac{\partial \hat{p}}{\partial x_i} + \nu \nabla^2 \hat{u}_i - \frac{\partial}{\partial x_j}\left(\widehat{u_i u_j} - \hat{u}_i \hat{u}_j\right) \tag{2.1}$$

The above equation reduces to the Reynolds averaged equation if the Reynolds' approximation, $\widehat{u_i'} = 0$, is applicable. The subgrid stresses can thus be expressed as

$$\tau_{ij} = \widehat{u_i u_j} - \hat{u}_i \hat{u}_j \tag{2.2}$$

In the above definition of stress correlation the total velocity components appear which can be further decomposed into resolved and subgrid components ($u = \hat{u} + \acute{u}$) to get three stress

components, as proposed by Leonard [13]

$$\begin{aligned} \tau_{ij} &= L_{ij} + C_{ij} + R_{ij} \\ L_{ij} &= \widehat{\hat{u}_i \hat{u}_j} - \hat{u}_i \hat{u}_j \\ C_{ij} &= \widehat{\hat{u}_i \acute{u}_j} + \widehat{\acute{u}_i \hat{u}_j} \\ R_{ij} &= \widehat{\acute{u}_i \acute{u}_j} \end{aligned} \tag{2.3}$$

In the above definition the Leonard (L_{ij}), cross (C_{ij}) and Reynolds (R_{ij}) represent the components of the subgrid stresses which have different characteristics and can be modeled independently. Reynolds stresses are of the same form as in RANS model. Cross stresses represent the interaction between resolved and subgrid stresses and Leonards term is the totality of resolved stresses, which Leonard interpreted as the nonlinear interaction of resolved scale motion. These can be better understood in the wave number space. One of the main effort here is to identify the physical behavior of each term. Most important drawback of this decomposition is that these individual stresses are not Galilean invariant. Thus they can not be modeled separately unless expressed in Galilean invariant form. Germano [28], [29], [30] proposed the Galilean invariant form of these stresses as

$$\begin{aligned} \tau_{ij} &= \mathcal{L}_{ij} + \mathcal{C}_{ij} + \mathcal{R}_{ij} \\ \mathcal{L}_{ij} &= \widehat{\hat{u}_i \hat{u}_j} - \hat{\hat{u}}_i \hat{\hat{u}}_j \\ \mathcal{C}_{ij} &= \widehat{\hat{u}_i \acute{u}_j} - \hat{\hat{u}}_i \hat{\acute{u}}_j + \widehat{\acute{u}_i \hat{u}_j} - \hat{\acute{u}}_i \hat{\hat{u}}_j \\ \mathcal{R}_{ij} &= \widehat{\acute{u}_i \acute{u}_j} - \hat{\acute{u}}_i \hat{\acute{u}}_j \end{aligned} \tag{2.4}$$

The above definition will be considered further to model the subgrid stresses. The modeling of subgrid stresses requires detailed understanding of interaction between resolved and subgrid scale of motion. These interactions between resolved and subgrid stress are dependent on the type of filter used in LES. The most important of such interactions are the energy transfer, which appears as a complex phenomenon as splitting of variables into resolved and subgrid scale such that resolved scale contain most of the kinetic energy and subgrid scale contain all the viscous dissipation is not feasible especially close to the wall where the scales of motion are small. The

effect of subgrid stresses can also be expressed through the resolved kinetic energy equation K_r

$$\frac{\partial K_r}{\partial t} + \hat{u}_j \frac{\partial K_r}{\partial x_j} = -\frac{\partial}{\partial x_j}\left[\hat{u}_i\left(\hat{P}\delta_{ij} + \tau_{ij}\right) - \nu\frac{\partial K_r}{\partial x_j}\right] - 2\nu\hat{D}_{ij}\hat{D}_{ij} + \tau_{ij}\hat{D}_{ij} \tag{2.5}$$

The second term on the right hand side represents the dissipation of resolved energy directly by molecular viscosity which is negligible for high Reynolds numbers or for large Δ/η. The largest effect of subgrid scale appears in terms of SGS dissipation by third term on right, which also appears in the subgrid scale kinetic energy as production term. When the grid filter Δ is in inertial subrange and under equilibrium condition this term is exactly equal to the dissipation, ϵ. Hence the evolution of the resolved scale kinetic energy depends directly on the modeling of the subgrid stresses. In the wave number space the Eq. (2.5) is (cf. to Eq. (4.10))

$$\frac{\partial \grave{K}_r}{\partial t} = -2\nu k^2 \grave{K}_r + T_f + T_r$$

where the positive value of T_r represent the energy transfer from the subgrid scale motion to the resolved scale motion which represents the backscatter of energy. This term has been discussed further in Appendix A.2.

2.1 Smagorinsky Model

One of the most pioneering work in LES was done by Smagorinsky [9], who modeled the anisotropic stress component (where $K_{sgs} = \frac{1}{2}\tau_{ii}$, is the subgrid scale kinetic energy)

$$\sigma_{ij} = \tau_{ij} - \frac{2}{3}K_{sgs}$$

by a eddy viscosity type model, which can be traced back to the Boussinesq hypothesis for the Reynolds stresses. A linear relationship between SGS stress tensor and rate of strain is assumed:

$$\sigma_{ij} = -2\nu_T\hat{D}_{ij}$$

In the inertial subrange the usual dimensional argument demands $\nu_T = c^{4/3}\epsilon^{1/3}\Delta^{4/3}$. Finally assuming the equilibrium condition it can be shown that $\nu_T = (C_s\Delta)^2\left(2\hat{D}_{ij}\hat{D}_{ij}\right)^{1/2}$, hence

follows the Smagorinsky model.

$$\sigma_{ij} = -2\left(C_s\Delta\right)^2\left(2\hat{D}_{ij}\hat{D}_{ij}\right)^{1/2}\hat{D}_{ij} \tag{2.6}$$

The above definition of turbulent viscosity is the generalization of the Prandlt's mixing length hypothesis with length scale $l = C_s\Delta$. This makes perfect sense for isotropic grid because the grid scale is same in all directions. For anisotropic grid the grid scale needs to be defined in terms of grid size. Deardorff [10] used Smagorinsky's model in channel flow problem and defined $\Delta = \left(\Delta_1\Delta_2\Delta_3\right)^{1/3}$. Some other authors have used $\Delta^2 = \Delta_1^2 + \Delta_2^2 + \Delta_3^2$, such as Germano [31], Ferziger [22],Bardina [32]. Orzag [22] showed that in the vicinity of the wall, for Chebyshev grid spacing in the wall normal direction (Δ_y) and constant grid spacing in the plane (Δ_x and Δ_z) yields $\tau_{xy} \sim y^{2/3}$ and *constant* as compared to $\sim y^3$, for the above two definition respectively. Hence Deordroff's definition is an obvious choice and is used commonly. However Scotti *et al.* [33] generalized the Smagorinsky's model for anisotropic grid using energy equilibrium condition and expressed length scale as $l = C\ f\left(a_1, a_2\right)\Delta_{eq}$ where $\Delta_{eq} = \left(\Delta_1\Delta_2\Delta_3\right)^{1/3}$, grid aspect ratios are $a_1 = \frac{\Delta_1}{\Delta_3}$, $a_2 = \frac{\Delta_2}{\Delta_3}$ for $\Delta_1 < \Delta_2 < \Delta_3$ and

$$f\left(a_1, a_2\right) = cosh\sqrt{\frac{4}{27}\left(\left[lna_1\right]^2 - lna_1 lna_2 + \left[lna_2\right]^2\right)}$$

Further Lieth [34] modified the grid scale term for nonhomogeneous turbulence by adding a triple correlation term. The length scale have also been modified in the near wall region by Mason [35], Mason and Callen [14] as

$$\frac{1}{l^n} = \frac{1}{l_0^n} + \frac{1}{\left(\kappa z - \kappa z_0\right)^n}$$

where $l_0 = C_s\Delta$,z_0 is the surface roughness height and $n \sim O\left(1\right)$ is a constant . However Moin and Kim [36] introduced a wall function $f\left(y\right)$ in the definition of length scale such that it increases monotonically with y. The major drawback of Smagorinsky's model is the choice of the Smagorinsky constant C_s. Lilly [11] deduced its value to be 0.17 for spectral cut-off filter in the inertial subrange, but turned out to be too large causing much of the turbulence energy to reside in subgrid scale. Choice of $C_s = 0.1$ seemed optimum but didn't allow turbulent flow to become excessively large. Canuto and Cheng [37] have concluded that overestimation of the Smagorinsky

coefficient is due to the equilibrium assumption. He further expressed dynamical nature of the constant as a function of P/ϵ, where P is the production and ϵ the dissipation of energy. In spite of the drawbacks of the model it has been widely used for atmospheric flow case, as in Deardorff [38] [39], Mason and Callen [35]. Mason [35], Brown *et al.* [40] further extended the model to include the buoyancy effect. Mason and Thompson [24] introduced the stochastic backscatter model by introducing backscatter of energy to Smagorinsky model. Brown and Mason [40] discussed this model in details and concluded that it shows departure from the logarithmic profile. Mason and Brown [41] concluded that "*..... subgrid model determines the filter operation (and better be called subfilter model). The numerical resolution should be sufficient to allow good resolution of filter. The constant of Smagorinsky's model C_s measures the ratio of filter scale and numerical resolution*". This emphasizes on the fact that filtering and modeling are dependent. There are other variants of the eddy viscosity model that has been proposed and used over the years. The time scale can be obtained from the subgrid scale kinetic energy, K_{sgs} which is equivalent to the one equation model [42]. Karaichan [43] and others [44] [21] solved the equations of motion in the wave number space and used the eddy viscosity type model. Leonard [13] suggested that the Leonard's stress term can be estimated directly as it represents the interaction between large scales and the cross plus Reynolds stress terms may be modeled together by eddy viscosity type model. Many other researches have used the advantages of the partition of stresses and modeled them independently [32] [42],[36]. Some of the major drawbacks of the Smagorinsky's model can be listed as

i. The constant is not universal and cannot be predicted uniquely.

ii. Does not predict asymptotic behavior near a wall.

iii. Eddy viscosity does not vanish in laminar region.

iv. Does not allow backscatter of energy.

v. Model is too dissipative and it poorly correlates with DNS data in homogeneous flow.

vi. Assumes that principal axes of SGS stress tensor is aligned with those of resolved strain rate tensor, which is not supported by DNS data shown by Bardina [45]

These drawbacks of the eddy-viscosity type model overshadows the simplicity and wide use of the model and demands improved modeling of subgrid stresses.

2.2 Scale Similarity Model

Bardina [45] introduced the scale similarity model where he introduced the concept of smallest resolved motion and approximated the subgrid scale terms in terms of smallest resolved motion. The decomposition of the velocity is extended as

$$u = \tilde{\hat{u}} + \left(\hat{u} - \tilde{\hat{u}}\right) + \acute{u} \tag{2.7}$$

where the ' ~ ' represents the test filter. The second term in the decomposition is the smallest resolved scale motion motion. In the Fourier space it represents the component of the velocity which lies within the length scales $\hat{\Delta}$ and $\tilde{\hat{\Delta}}$. If grid and test scales are the same then $\tilde{\hat{\Delta}} = 2\hat{\Delta}$, and thus according to the scale similarity model the subgrid scale motion can be represented from the resolved motion between the length scales $\hat{\Delta}$ and $2\hat{\Delta}$ [46]. This fact was further looked into by Germano *et al.* [31] who used different test filters width and supports the above assumption. Bardina introduced the modeling of cross and Reynolds' term as

$$\begin{aligned} \widehat{\acute{u}_i\acute{u}_j} &\approx \hat{\acute{u}}_i\hat{\acute{u}}_j = \left(\hat{u}_i - \hat{\hat{u}}_i\right)\left(\hat{u}_j - \hat{\hat{u}}_j\right) \\ \widehat{\acute{u}_i\hat{u}_j} &\approx \hat{\acute{u}}_i\hat{\hat{u}}_j = \left(\hat{u}_i - \hat{\hat{u}}_i\right)\hat{\hat{u}}_j \end{aligned} \tag{2.8}$$

On using Eq. (2.8) in Eq. (2.3) we get

$$\sigma_{ij} = C_{ss}\left(\widehat{\hat{u}_i\hat{u}_j} - \hat{\hat{u}}_i\hat{\hat{u}}_j\right) \tag{2.9}$$

It must be noted that at the time Bardina's model was proposed the Galilean invariant form of the stresses were not available but the above model recovers the Galilean invariancy. If the filtered equation are filtered again using test filter, $\tilde{\Delta}$, then the resulting equation takes the form

$$\frac{\partial\tilde{\hat{u}}_i}{\partial t} + \frac{\partial\tilde{\hat{u}}_i\tilde{\hat{u}}_j}{\partial x_j} = -\frac{1}{\rho}\frac{\partial\tilde{\hat{p}}}{\partial x_i} + \nu\nabla^2\tilde{\hat{u}}_i - \frac{\partial}{\partial x_j}\left(\widetilde{\widehat{u_iu_j}} - \tilde{\hat{u}}_i\tilde{\hat{u}}_j\right) \tag{2.10}$$

where the stress at the filter level $\tilde{\hat{\Delta}}$ is

$$T_{ij} = \widetilde{\widetilde{u_i u_j}} - \tilde{\hat{u}}_i \tilde{\hat{u}}_j$$

From inspection we observe that the stresses obtained at these two levels (T_{ij} and τ_{ij}) can be subtracted to obtain the Leonard's stress

$$\mathcal{L}_{ij} = T_{ij} - \tilde{\tau}_{ij} \tag{2.11}$$

Since the Leonard's stress represents the stresses due to the resolved scale motion it can be computed numerically. The numerical computation of the Leonard's stress requires explicit filtering which may work by using a top hat filter but is not so appealing in comparision to smooth filters like Gaussian and sharp-spectral filter. These filtering can be applied as suggested by Pruett and Socchacke [47] or by interpolating intermediate values by Lagrange interpolation. Explicit filtering can be avoided by modeling the Leonard's stress term by using Taylor's series expansion [13] [48]. A realistic feature of the scale similarity model is that it can produce backscatter, but it is not sufficiently dissipative. It can be combined further with the Smagorinsky's model to obtain the mixed model. Although it overcomes the problems that stress tensor is not aligned to rate of strain tensor, it produces backscatter. However the determination of the model coefficient still remains a problem.

2.3 Dynamic Model

Dynamic model helps to determine the model coefficient dynamically which works on the assumption that the Leonard's stress can be computed directly from the resolved fields. The coefficient can be obtained by multiplying both sides of Eq. (2.11) by resolved rate of strain and introducing Smagorinsky's model for both grid and test scale level stresses and proceeding, we obtain

$$C_s = \frac{1}{2} \frac{\langle \mathcal{L}_{mn} \hat{D}_{mn} \rangle}{\tilde{\hat{\Delta}}^2 \langle |\tilde{\hat{D}}| \tilde{\hat{D}}_{mn} \hat{D}_{mn} \rangle - \hat{\Delta}^2 \langle \widetilde{|\hat{D}|} \hat{D}_{mn} \hat{D}_{mn} \rangle}$$

The above constant is obtained by assuming that C_s is constant for both the filter levels, which might not be true. Secondly, the constant is brought out of the filtering. To obtain the stable value of constant the whole term is averaged ($\langle . \rangle$) along the direction of isotropy. Lilly [12] further modified the method such that the constant obtained minimizes the square of the error, E^2 where

$$E = (\mathcal{L}_{ij} - 1/3\mathcal{L}_{kk} + 2C_s N_{ij})$$

where N_{ij} represent the modeled $T_{ij} - \tilde{\tau}_{ij}$ component. Satisfying $\frac{\partial E^2}{\partial C_s} = 0$ we get

$$C_s = -\frac{1}{2}\frac{\mathcal{L}_{mn}N_{mn}}{N_{mn}N_{mn}}.$$

The above formulation does not require averaging as in earlier formulation because the numerator does not go to zero unless all the five components of the tensor N_{ij} go to zero. If all the components go to zero independently then numerator also goes to zero. But numerical simulation by Moin reported that coefficient was occasionally large enough to blow up the solution. The limitation of the above model was taken care by Ghosal [20] by solving a constrainted variational problem coupled with spatial averaging. Further Meneveau [25] developed a Lagrangian dynamic model in which transport equations need to be solved along pathline to obtain the coefficient, instead of spatial averaging. This equation is similar to the two-equation model and depends on the past data with exponentially dependent memory. The biggest disadvantage of such model is that of memory requirement and computational cost. The assumption that the *model constant* is same for both test and grid scale which fails outside the inertial subrange does not remain a constant anymore. Meneveau and Lund [49] proposed a scale dependent coefficient based on Pao's spectrum. Another option explored by them was solving for two coefficient in bi-dynamic model.

2.4 Mixed model

The Smagorinsky's and scale similarity model can be combined together to form the mixed model. The mixed model combines the advantages of both the models and eliminated the few of the major disadvantages, viz., as the stress tensor is not proportional to the rate of strain tensor,

produces sufficient dissipation and can produce backscatter too.

$$\sigma_{ij} = C_s \left(\widetilde{\hat{u}_i \hat{u}_j} - \tilde{\hat{u}}_i \tilde{\hat{u}}_j \right) - 2C\hat{\Delta}^2 |\hat{D}| \hat{D}_{ij} \tag{2.12}$$

On the other hand the problem requires the determination of two unknown constants. The dynamic coefficient determination can be extended to the mixed model. Zang *et al.* [30] computed the second coefficient dynamically and used $C_s = 1$, which is suggested by Speziale [17] for Galilean invariance criteria. Both the coefficients can be computed using the dynamic method as suggested by Sarghani *et al.* [50] by minimizing the error, which can be defined as in the earlier case, with respect to both the variables,

$$\frac{\partial E^2}{\partial C_s} = 0 \quad \text{and} \quad \frac{\partial E^2}{\partial C} = 0.$$

This model has been named as *bi-dynamic model.* Implementing dynamic model in mixed model further increases the cost and involves additional computation expense due to secondary filtering. Moreover explicit filtering needs to be used which always complicates the situation.

2.5 Mixed Non-Linear Model

From the Taylor's expansion it can be shown that

$$\widetilde{\hat{u}_i \hat{u}_j} - \tilde{\hat{u}}_i \tilde{\hat{u}}_j \cong C_{nl} \Delta^2 \frac{\partial \hat{u}_i}{\partial x_k} \frac{\partial \hat{u}_j}{\partial x_k} \tag{2.13}$$

This expansion when introduced in the mixed model is equivalent to the model

$$\sigma_{ij} = -2\nu_T \hat{D}_{ij} + c_1 \Delta^2 \hat{D}_{ik} \hat{D}_{kj} + c_2 \Delta^2 \left(\hat{\omega}_{ik} \hat{D}_{kj} + \hat{\omega}_{jk} \hat{D}_{ki} \right) + c_3 \hat{\omega}_{ik} \hat{\omega}_{kj} \tag{2.14}$$

Meneveau and Katz [19] have suggested $c_1 = c_2 = c_3$. The above formulation is the general representation of the Reynolds stress obtained from the phenomenological theory, compare with Eq. (2.15). Speziale's $k - \epsilon$ model is based on the phenomenological theory which has been used by some authors to model the subgrid stresses [22] [51]. Kosovic [16] formulated the stresses from the above theory but neglected the fourth term in Eq. (2.14) and assumed that backscatter can be approximated from the second term. In this section we will look further into the assumptions

involved in Kosovic's model. We will formulate the non-linear model as suggested by Meneveau and Katz and compute the coefficients later.

The phenomenological models subjected to extended Galilean invariance gives the general representation of Reynolds stress tensor as discussed by Speziale [7]. The same model can be extended for the subgrid scale turbulence as proposed by Kosovic [16].

$$\tau_{ij} = \frac{2}{3}K\delta_{ij} - 2\frac{l_0^2}{\tau_0}\hat{D}_{ij} + \alpha_1 l_0^2(\hat{D}_{ik}\hat{D}_{kj} - \frac{1}{3}\hat{D}_{mn}\hat{D}_{nm}\delta_{ij}) + \alpha_3 l_0^2(\hat{D}_{ik}\hat{\omega}_{kj} + \hat{D}_{jk}\hat{\omega}_{ik}) + \alpha_2 l_0^2(\hat{\omega}_{ik}\hat{\omega}_{kj} - \frac{1}{3}\hat{\omega}_{mn}\hat{\omega}_{nm}\delta_{ij}) + \alpha_4 l_0^2(\frac{\partial \hat{D}_{ij}}{\partial t} + \hat{\mathbf{u}} \cdot \nabla \hat{D}_{ij}) \quad (2.15)$$

where $\hat{D}_{ij} = \frac{1}{2}(\frac{\partial \hat{u}_i}{\partial x_j} + \frac{\partial \hat{u}_j}{\partial x_i})$; $\hat{\omega}_{ij} = \frac{1}{2}(\frac{\partial \hat{u}_i}{\partial x_j} - \frac{\partial \hat{u}_j}{\partial x_i})$ and $\alpha_1 ....\alpha_4$ are dimensionless constants. The length scale l_0 and the time scale τ_0 are modeled as invariants of $\hat{D}_{ij}$. When $\alpha_i = 0$ then we obtain the eddy viscosity model by Smagorinsky [9]. If $\alpha_4 = 0$ then deviatoric part of the stress is of the general form $\tau_{ij} = A_{ijkl}\frac{\partial \hat{u}_k}{\partial_l}$, where A_{ijkl} depends algebraically on the mean velocity gradient, which is the Stokesian stress tensor [23]. This term can be neglected assuming Taylors hypothesis, according to which advection of the rate-of-strain by the mean velocity field is balanced by its time rate of change. Kosovic [16] and Pope [52] further dropped the fourth term on right hand side as it gives erroneous prediction for isotropic turbulence for solid-body rotation [53]. Here we will keep this term as suggested by Meneveau and Katz [19]. This additional term helps us to simplify the algebraic expression in the same form as the mixed model. The model coefficients can be estimated comparing the terms with the Galilean-invariant decomposition of subgrid stresses as discussed earlier. The cross term and Reynolds' stress terms can be together modeled by the first term (which is the eddy viscosity term) as used by Leonard [13]. The significance of these terms can be best understood in wave number space, which shows that cross+Reynolds terms must account for the backscatter of energy in the wave number space, which appears as a stochastic fluctuation in physical space. Here we will try to understand the physics behind backscatter and model it the best way it can be done. The rest of the terms resolve the Leonard stress which causes only forward scatter of energy. The dissipation due to Leonard's term can be computed for isotropic flow as discussed in following section. Here the grid filter, $G(r)$, is assumed to be a Gaussian filter but results corresponding to other filters have also been discussed. Kosovic [16] considered spectral cutoff filter in his non-linear model. As the contribution of Leonard stress to the dissipation is zero for spectral cutoff filter the earlier model

works for spectral filter, but spectral cut off filter should not be used as it does not satisfy the realizibility condition. Gaussian filter is reasonably compact both in physical and wave number space, hence the computation here will be carried for Gaussian filter. Gaussian filter function and its transfer function is given in subsequent chapters. In the inertial subrange for Gaussian filter (also for top hat filter) the dissipation by the Leonard's stresses can be approximated using the isotropic turbulence, discussed in appendix A.7, as:

$$-\langle \mathcal{L}_{ij}\hat{D}_{ij}\rangle = \epsilon_{RS} = -\frac{35}{24}\Delta^2\langle\left(\frac{\partial \hat{u}_1}{\partial x_1}\right)^3\rangle \tag{2.16}$$

where $\langle\left(\frac{\partial \hat{u}_1}{\partial x_1}\right)^3\rangle$ can be related to the total dissipation for isotropic turbulence in the inertial subrange. This value is twice the value estimated by Leonard using the L_{ij} term. In the inertial subrange Kolmogrov's hypothesis can be extended for a filter function, as discussed in Appendix (A.5), to obtain

$$\hat{E}(k) = C_k\epsilon^{2/3}k^{-5/3}|\grave{G}(k)|^2 \tag{2.17}$$

The filtered energy spectrum is related to velocity gradient for isotropic case as given below:

$$\int_0^\infty k^2\hat{E}(k)dk = \frac{15}{2}\langle\left(\frac{\partial \hat{u}_1}{\partial x_1}\right)^2\rangle \tag{2.18}$$

Evaluating the integral on left

$$\int_0^\infty k^2\hat{E}(k)dk = C_k\epsilon^{2/3}\int_0^\infty k^{1/3}e^{-\Delta^2k^2/12}dk$$

we obtain,

$$\langle\left(\frac{\partial \hat{u}_1}{\partial x_1}\right)^3\rangle = -\frac{12}{\Delta^2}\left[\Gamma\left(\frac{5}{3}\right)\frac{C_k}{10}\right]^{3/2}\overline{S}\epsilon \quad \text{and} \quad \overline{S} = -\frac{\langle(\frac{\partial \hat{u}_1}{\partial x_1})^3\rangle}{\langle(\frac{\partial \hat{u}_1}{\partial x_1})^2\rangle^{3/2}} \tag{2.19}$$

where $\overline{S}$ is the skewness factor, ϵ is the total dissipation, C_k is the Kolmogrov's constant and $\Gamma(.)$ is the gamma function. Separating the forward and backward component of inertial transfer

of energy the forward and backward dissipation coefficient can be related as:

$$(C_f - C_b) = 1 \tag{2.20}$$

where C_f is the coefficient of the forward scatter of energy and C_b is coefficient of backward scatter of energy. The backward scatter of energy occurs due to interaction of modes with wavenumber greater than cutoff wavenumber hence is caused by cross and Reynolds' stresses , as discussed in details in Appendix A.2. Furthermore Leonard stresses contributes to the forward scatter as approximated in Appendix A.7. Kosovic postulated that the second term in Eq. (2.14) accounted for backscatter, which actually approximates the Leonard's stress as discussed later, Eq. (2.30). His model does not account for Leonard's stress, which is of course true for spectral cut off filter for which Leonard's stress is zero. However the same is not true for the smooth filters like the Gaussian filter so Leonard's stress term has to be accounted. The modeling of the dissipation is obtained as

$$\epsilon = -\langle \sigma_{ij}\hat{D}_{ij}\rangle = \langle (C_s\Delta)^2\, 2\left(2\hat{D}_{mn}\hat{D}_{mn}\right)^{1/2}\hat{D}_{ij}\hat{D}_{ij} + C_1\hat{D}_{ik}\hat{D}_{kj}\hat{D}_{ij} - C_2\hat{\omega}_{ik}\hat{\omega}_{kj}\hat{D}_{ij} + C_3\left(\hat{D}_{ik}\hat{\omega}_{kj}\hat{D}_{ij} + \hat{D}_{jk}\hat{\omega}_{ik}\hat{D}_{ij}\right)\rangle \tag{2.21}$$

The dissipation ϵ by taking the Leonard's model are given by last three terms of Eq. (2.21). The fourth term on the right is zero and can be shown upon expansion. The second and third terms produce dissipation equal to the Leonard's stresses so that,

$$-\langle \mathcal{L}_{ij}\hat{D}_{ij}\rangle = C_1(C_s\Delta)^2\langle \hat{D}_{ik}\hat{D}_{kj}\hat{D}_{ij}\rangle - C_2(C_s\Delta)^2\langle \hat{\omega}_{ik}\hat{\omega}_{kj}\hat{D}_{ij}\rangle \tag{2.22}$$

Further for locally isotropic velocity field the sixth order isotropic tensor field can be approximate as given by Champagne and Robertson [54], discussed in Appendix A.7, gives the dissipation due to terms appearing in above equation as:

$$\langle \hat{D}_{ik}\hat{D}_{kj}\hat{D}_{ij}\rangle = \frac{105}{8}\langle\left(\frac{\partial\hat{u}_1}{\partial x_1}\right)^3\rangle \quad \text{and} \quad \langle \hat{\omega}_{ik}\hat{\omega}_{kj}\hat{D}_{ij}\rangle = -\frac{35}{8}\langle\left(\frac{\partial\hat{u}_1}{\partial x_1}\right)^3\rangle \tag{2.23}$$

Hence subsituting the approximated values the dissipation due to the modeled Leonard's stress is obtained, which must be equal to the dissipation by the improved Leonard's term as obtained

above. Comparing the two terms we get the equation

$$\frac{105}{8}C_s^2C_1 + \frac{35}{8}C_s^2C_2 = \frac{35}{24} \tag{2.24}$$

which is satisfied for a linear relationship in between C_1 and C_2 .The simplifying assumption of $C_1 = C_2$ gives us the value of constants as:

$$C_s^2C_1 = C_s^2C_2 = \frac{1}{12} \tag{2.25}$$

For Gaussian filter the dissipation due to the total subgrid stresses given by the right hand side of the equation can be approximated in terms of the total dissipation term as shown above. We get the relation

$$\epsilon = (C_s\Delta)^2\langle(\frac{\partial\hat{u}_1}{\partial x_1})^2\rangle^{3/2}[(15)^{3/2} - \frac{105}{8}C_1\overline{S} - \frac{35}{8}C_2\overline{S})] \tag{2.26}$$

Here the last two terms on right hand side correspond to Leonard's stress and gives forward scatter only, for which the coefficients have already been computed. The first term gives the rest of forward as well as backward scatter. To account for the backscatter we improve the coefficient of the Smagorinsky's term as $C_s^2(1-D)$ as adopted by Mason and Thomson [24]. It should be noted that positivity of the coefficients are maintained so that forward and backward scatter is accurately accounted. Thus the dissipation equation above is written as:

$$C_f - C_b = 12\left[\Gamma\left(\frac{5}{3}\right)\frac{3C_k}{2}\right]^{3/2}C_s^2(1-D) + \frac{35}{2}\left[\Gamma\left(\frac{5}{3}\right)\frac{C_k}{10}\right]^{3/2}\overline{S} \tag{2.27}$$

Comparing the terms corresponding to forward and backward scatter and using $C_k = 1.62$, $C_b = 0.176$ for smooth filter Schumann [55] and $\overline{S} = 0.5$ as used by Kosovic we obtain the coefficients as:

$$C_s = 0.1326 \quad \text{and} \quad D = 0.2565 \tag{2.28}$$

If we consider $C_2 = C_1 = C_3$ then for the plane shear stress the anisotropic diagonal stresses are

$$\sigma_{11} = \frac{8}{3}\mathcal{C} \quad , \sigma_{22} = -\frac{4}{3}\mathcal{C} \quad \text{and} \quad \sigma_{33} = -\frac{4}{3}\mathcal{C} \tag{2.29}$$

This deviates from the experimental values where $\sigma_{22} \neq \sigma_{33}$. But because of the above assumption the terms on expansion results in Leonards stress term.

$$\begin{aligned} \left(\hat{D}_{ik}\hat{D}_{kj} - \frac{1}{3}\hat{D}_{mn}\hat{D}_{nm}\right) \quad & + \left(\hat{\omega}_{ik}\hat{D}_{kj} - \hat{D}_{ik}\hat{\omega}_{kj}\right) - \left(\hat{\omega}_{ik}\hat{\omega}_{kj} - \frac{1}{3}\hat{\omega}_{mn}\hat{\omega}_{nm}\right) \\ \Rightarrow \quad & \frac{\partial \hat{u}_i}{\partial x_k}\frac{\partial \hat{u}_j}{\partial x_k} - \frac{1}{3}\frac{\partial \hat{u}_m}{\partial x_n}\frac{\partial \hat{u}_m}{\partial x_n} \end{aligned} \tag{2.30}$$

Here the right hand side can be obtained by Taylor series exapnsion of the Leonard's stress, Appendix A.4. So the nonlinear model yields the mixed model, which models the Leonard's stress explicitly whereas the Reynolds' and cross term are modeled together by a eddy-viscosity type model. Thus this model can be called the *mixed nonlinear model.* As Leslie and Quarini [15], Chasnov [21] suggest that since the physics of the forward and backward scatter of energy are different they must be modeled separately. The above model violates this hypothesis as the eddy-viscosity type term contains the information about the forward and backward scatter of energy and represents the net averaged energy transfer. Since the model coefficients are obtained based in the the net dissipation hence the model is totally dissipative and yields a deterministic solution. The nonlinear model can be written in coordinate invariant form as

$$\boldsymbol{\tau} = \frac{2}{3}K_{sgs}\mathbf{I} - 2\nu_T\hat{\mathbf{D}} + C\Delta^2\left[grad\ \hat{\mathbf{u}} \cdot (grad\ \hat{\mathbf{u}})^T - \frac{1}{3}grad\ \hat{\mathbf{u}} : grad\ \hat{\mathbf{u}}\ \mathbf{I}\right] \tag{2.31}$$

The above model can be extended to model the scalar flux term, $H_{\theta i}$, appearing in the scalar (θ) transport equation such as temperature, salinity, vapor pressure etc. Since the third term on the right is the Taylor's series expansion of the Leonard's stress term, its counterpart can be obtained similarly as shown in Appendix A.1. The turbulent viscosities for the stress and scalar flux can be related by the Prandlt-Schmidt number (Pr, Sc) for scalars as used by Mason [56], Brown [40] and others. Extending the nonlinear model for the scalar flux we get the coordinate

invariant form as

$$\mathbf{H} = -2\frac{\nu_T}{Pr} grad\ \hat{\theta} + C\Delta^2 grad\ \hat{\theta} \cdot (grad\ \hat{\mathbf{u}})^T \tag{2.32}$$

As shown by Leonard [13] the Leonard's stress term only produces dissipation, which can be estimated from the isotropic turbulence. Leonard applied Taylors series expansion of the stress term which has been used later by other authors, Brun and Friedrich [48], Aldama [22]. Leonard's expansion required representation of the stress term by second order derivative so as to satisfy the dissipation criteria. We use the modified Leonard's stress term and find that first order term exactly satisfies the dissipation. The backward scatter has been studied in detail in the fourier space by Leslie and Quarini [15], Lesieur [57], Chasnov [21], Stefano and Vasilyev [58], Aupoix [44] and others using the EDQNM theory. It has been shown that the backscatter of energy may occur due to the cross and Reynolds stresses. But only the backscatter due to the Reynolds' stresses can be estimated using the non-local expansion. More insight into this fact can be obtained from the triadic interactions. The cross term represents the interaction of the scales across the grid filter. They form the near local energy transfer term in the wave number space and cause both forward and backward scatter of energy. From the numerical simulation in wave number space it is evident that the net energy transfer or net dissipation in physical space is zero for cross term. Better understanding of this term is still required and this term is absent in the model, Eq. (2.31). The Reynolds' stress term accounts for the rest of the dissipation as well as the backward scatter. In developing the new nonlinear model, as described in the next chapter we have tried to model the backscatter phenomenon of energy separated from the forward scatter and have obtained the coefficients of the model based on the above physics.

CHAPTER III

NEW NONLINEAR MODEL

Here we present the development of a new nonlinear model for subgrid scale turbulence from the transport equation of subgrid stresses and subgrid scale energy. The transport equation of subgrid scale stresses ($\widehat{\mathbf{uu}} - \hat{\mathbf{u}}\hat{\mathbf{u}}$) can be obtained from the Navier-Strokes equation as :

$$\begin{aligned}
\frac{\hat{D}}{Dt}\tau_{ik} &= -\left[\frac{\partial \widehat{u_i u_j u_k}}{\partial x_j} - \frac{\partial \hat{u}_i \tau_{kj}}{\partial x_j} - \frac{\partial \hat{u}_j \widehat{u_i u_k}}{\partial x_j} - \frac{\partial \widehat{u_k}\tau_{ij}}{\partial x_j}\right] \\
&\quad -\frac{1}{\rho}\left[\frac{\partial \widehat{pu}_i \delta_{kj}}{\partial x_j} - \frac{\partial \hat{p}\hat{u}_i\delta_{kj}}{\partial x_j} + \frac{\partial \widehat{pu_k}\delta_{ij}}{\partial x_j} - \frac{\partial \hat{p}\widehat{u_k}\delta_{ij}}{\partial x_j}\right] + \frac{1}{\rho}\left[\widehat{p\frac{\partial u_k}{\partial x_i}} - \hat{p}\frac{\partial \widehat{u_k}}{\partial x_i} + \widehat{p\frac{\partial u_i}{\partial x_k}} - \hat{p}\frac{\partial \hat{u}_i}{\partial x_k}\right] \\
&\quad +\nu\nabla^2\tau_{ik} - 2\nu\left[\frac{\partial \widehat{u_i}}{\partial x_l}\frac{\partial \widehat{u_k}}{\partial x_l} - \frac{\partial \hat{u}_i}{\partial x_l}\frac{\partial \widehat{u_k}}{\partial x_l}\right] - \left[\tau_{ij}\frac{\partial \widehat{u_k}}{\partial x_j} + \tau_{kj}\frac{\partial \hat{u}_i}{\partial x_j}\right] \qquad (3.1)
\end{aligned}$$

Here the terms can be interpreted physically as diffusion, dissipation, production as in the case of Reynolds stress. The correlation term in the subgrid sense can be defined analogous to the Reynolds's stresses as given by Germano [28] and Warsi [23].

$$\begin{aligned}
P_{ij} &= -\left[\tau_{ik}\frac{\partial \hat{u}_j}{\partial x_k} + \tau_{kj}\frac{\partial \hat{u}_i}{\partial x_k}\right] \\
Q_{ij} &= \frac{1}{\rho}\left[\widehat{p\frac{\partial u_i}{\partial x_j}} - \hat{p}\frac{\partial \hat{u}_i}{\partial x_j} + \widehat{p\frac{\partial u_j}{\partial x_i}} - \hat{p}\frac{\partial \hat{u}_j}{\partial x_i}\right] \\
F_{ij} &= -\frac{\partial}{\partial x_k}\left[\left(\widehat{u_i u_j u_k} - \hat{u}_i\tau_{jk} - \hat{u}_j\tau_{ik} - \widehat{u_k}\tau_{ij} - \hat{u}_i\hat{u}_j\widehat{u_k}\right) + \frac{1}{\rho}\left(\widehat{pu}_i\delta_{kj} - \hat{p}\hat{u}_i\delta_{kj} + \widehat{pu_j}\delta_{ik} - \hat{p}\hat{u}_j\delta_{ik}\right)\right] \\
\epsilon_{ij} &= 2\nu\left[\frac{\partial \widehat{u_i}}{\partial x_k}\frac{\partial \widehat{u_j}}{\partial x_k} - \frac{\partial \hat{u}_i}{\partial x_k}\frac{\partial \hat{u}_j}{\partial x_k}\right] \qquad (3.2)
\end{aligned}$$

where the substantive derivative is,

$$\frac{\hat{D}}{Dt} = \frac{\partial}{\partial t} + \hat{u}_k\frac{\partial}{\partial x_k}$$

Before we proceed forward we note that the substantive derivative and the filter function do not commute and are related as:

$$\widehat{\frac{D\phi}{Dt}} = \frac{\hat{D}}{Dt}\hat{\phi} + \widehat{(grad\ \phi)} \cdot \mathbf{u} - \left(grad\ \hat{\phi}\right) \cdot \hat{\mathbf{u}} \tag{3.3}$$

Hence, the rate equation for subgrid stresses becomes:

$$\frac{\hat{D}}{Dt}\tau_{ij} = P_{ij} + Q_{ij} + F_{ij} - \epsilon_{ij} + \nu\nabla^2\tau_{ij} \tag{3.4}$$

From the above equation the energy rate equation can be expressed as:

$$\frac{\partial K_{sgs}}{\partial t} + \hat{u}_k\frac{\partial K_{sgs}}{\partial x_k} = P + D - \epsilon + \nu\nabla^2 K_{sgs} \tag{3.5}$$

where $P = \frac{1}{2}P_{ii}$; $D = \frac{1}{2}F_{ii}$; $\epsilon = \frac{1}{2}\epsilon_{ii}$ and $Q_{ii} = 0$ from continuity equation. These terms carry the same significance as for the turbulent kinetic energy equation [23], hence can be modeled in the same fashion. Using the modeling of pressure-velocity correlation by return term and dissipation by isotropic term Rodi and later Warsi [23] obtained the nonlinear constitutive relation as:

$$\tau_{ij} = \frac{2}{3}K_{sgs}\delta_{ij} - \frac{2AK_{sgs}^2}{\epsilon}\hat{D}_{ij} + 3A^2\frac{K_{sgs}^3}{\epsilon^2}\left[\hat{D}_{ik}\frac{\partial\hat{u}_j}{\partial x_k} + \hat{D}_{jk}\frac{\partial\hat{u}_i}{\partial x_k} - \frac{2}{3}\delta_{ij}\hat{D}_{mn}\frac{\partial\hat{u}_m}{\partial x_n}\right] \tag{3.6}$$

which is the same form as the algebraic Reynolds stress model developed by Speziale if substantive part of the Oldroyd derivative is neglected. The model obtained by Speziale has been used by different authors to obtain the non-linear model. The above model requires solution of two additional differential equations which are the equations of motion of subgrid scale kinetic energy and dissipation. Further simplification can be obtained if dissipation (ϵ) is expressed in terms of the subgrid scale kinetic energy (K_{sgs}) and subgrid length scale (Δ). Using the one-equation model approach we use the following form for dissipation,

$$\epsilon = C_\epsilon\frac{K_{sgs}^{3/2}}{\Delta} \tag{3.7}$$

The value of the constant C_ϵ has been computed in the inertial subrange for Gaussian filter as discussed in Appendix A.6. Wong [51] used the above assumption in the model developed by Speziale and suggested dynamic calculation of the coefficients. These type of model was used by

Schmidt and Schumann, Moeng [59]. Here we will proceed from the constitutive model concept presented above and extend it considering more terms to model the pressure-velocity correlation. The model coefficients are computed based on the dissipation produced by each term. The stress terms will be considered in the form of Leonard's, cross and Reynolds stress terms. Backscatter will also be considered and calculation will be carried out for the Gaussian filter as opposed to spectral filter as used by most of the authors. The coefficients thus obtained will be expressed as universal constants. From the algebraic stress closure we get (cf., Rodi, Warsi [23])

$$T_{ij}\left(P-\epsilon\right)=P_{ij}+Q_{ij}-\epsilon_{ij}$$

where $T_{ij}=\tau_{ij}/K_{sgs}$. In the above equation we introduce the modeling of the dissipation term in isotropic form

$$\epsilon_{ij}=\frac{2}{3}\epsilon\delta_{ij}$$

and the pressure velocity correlation term is modeled as suggested by Launder, where we keep the return and rapid terms and the wall term is assumed to be small.

$$Q_{ij}=3c_1\frac{\epsilon}{K_{sgs}}\left(\frac{2}{3}K_{sgs}\delta_{ij}-\tau_{ij}\right)+\alpha\left(\frac{2}{3}P\delta_{ij}-P_{ij}\right)+\left(\frac{2}{3}P\delta_{ij}-\Delta_{ij}\right)-\gamma K_{sgs}\hat{D}_{ij} \qquad (3.8)$$

where the coefficients α,β andγ are expressed in terms of the constants c_1 and c_2, Eq. (6.303) in Warsi [23]. It must be noted that we have considered more terms of the correlation as compared to the Reynolds stress modeling. These models will be used to develop the nonlinear constitutive equation for subgrid stresses similar to the equation developed for Reynolds stress as done by Warsi [23].

3.1 Nonlinear constitutive equation

Introducing the quantity

$$M_{ij}=\frac{K_{sgs}}{\epsilon}\frac{\partial\hat{u}_i}{\partial x_j}$$

the production term can then be expressed as

$$\begin{aligned} P_{ij} &= -\epsilon \left(T_{ik} M_{jk} + T_{jk} M_{ik} \right) \\ P &= -\epsilon T_{kl} M_{kl} \end{aligned} \tag{3.9}$$

Substituting the expressions in the algebraic stress equation we get the nonlinear algebraic equation for the determination of stress. Following Warsi [23] a deductive iterative scheme is used to obtain the zero, first and second order approximation as

$$\begin{aligned} a_0 T_{ij}^{(n+1)} = T_{ij}^n T_{kl}^n M_{kl} + \frac{2}{3}\delta_{ij}\left[a_0 + \left(\gamma_0 - 1 - \beta \right) T_{kl}^n M_{kl} \right] - \\ \gamma \left[M_{ij} + M_{ji} \right] - \gamma_0 \left[T_{ik}^n M_{jk} + T_{jk}^n M_{ik} \right] + \beta \left[T_{ik}^n M_{kj} + T_{jk}^n M_{ki} \right] \end{aligned} \tag{3.10}$$

For the zero order approximation we assume isotropic form of the stress tensor, $T_{ij}^0 = \frac{2}{3}\delta_{ij}$ which gives $\tau_{ij}^0 = \frac{2}{3} K_{sgs} \delta_{ij}$. On substituting this approximation we obtain the first order approximation as

$$\tau_{ij}^1 = \frac{2}{3} K_{sgs} \delta_{ij} - \frac{\left(\gamma + 2/3\gamma_0 + 2/3\beta \right)}{a_0} \frac{K_{sgs}^2}{\epsilon} \hat{D}_{ij} \tag{3.11}$$

It is interesting to note that Eq. (3.11) is the Smagorinsky's model, where the eddy coefficient has been defined from, $K_{sgs} - \epsilon$ model. The model can be made independent of ϵ by substituting it as a function of K_{sgs} and Δ. The second order approximation can be also be obtained similarly.

$$\begin{aligned} \tau_{ij} = \frac{2}{3} K_{sgs} \delta_{ij} - 2 \frac{A}{C_\epsilon} K_{sgs}^{1/2} \Delta \hat{D}_{ij} \\ + 2 \frac{A \gamma_0}{C_\epsilon^2 a_0} \Delta^2 \left[2 \frac{\partial \hat{u}_i}{\partial x_k} \frac{\partial \hat{u}_j}{\partial x_k} - \frac{2}{3}\delta_{ij} \frac{\partial \hat{u}_m}{\partial x_n} \frac{\partial \hat{u}_m}{\partial x_n} + \frac{\partial \hat{u}_i}{\partial x_k} \frac{\partial \hat{u}_k}{\partial x_j} + \frac{\partial \hat{u}_j}{\partial x_k} \frac{\partial \hat{u}_k}{\partial x_i} - \frac{2}{3}\delta_{ij} \frac{\partial \hat{u}_m}{\partial x_n} \frac{\partial \hat{u}_n}{\partial x_m} \right] \\ - 2 \frac{A \beta}{C_\epsilon^2 a_0} \Delta^2 \left[2 \frac{\partial \hat{u}_k}{\partial x_i} \frac{\partial \hat{u}_k}{\partial x_j} - \frac{2}{3}\delta_{ij} \frac{\partial \hat{u}_m}{\partial x_n} \frac{\partial \hat{u}_m}{\partial x_n} + \frac{\partial \hat{u}_i}{\partial x_k} \frac{\partial \hat{u}_k}{\partial x_j} + \frac{\partial \hat{u}_j}{\partial x_k} \frac{\partial \hat{u}_k}{\partial x_i} - \frac{2}{3}\delta_{ij} \frac{\partial \hat{u}_m}{\partial x_n} \frac{\partial \hat{u}_n}{\partial x_m} \right] \end{aligned} \tag{3.12}$$

The above algebraic stress model can be further simplified if $\gamma_0 = \beta$, as per the values specified by Launder $\gamma_0 = 0.4$ and $\beta = 0.141$, but the values can be made equal if $c_2 = 0.0796$. However

assuming both the quantities being equal we get the simplified expression of the stress,

$$\begin{aligned}\tau_{ij} &= \frac{2}{3}K_{sgs}\delta_{ij} - 2\frac{A}{C_\epsilon}K_{sgs}^{1/2}\Delta\hat{D}_{ij} + 2\frac{A\gamma_0}{C_\epsilon^2 a_0}\Delta^2\left[2\frac{\partial\hat{u}_i}{\partial x_k}\frac{\partial\hat{u}_j}{\partial x_k} - \frac{2}{3}\delta_{ij}\frac{\partial\hat{u}_m}{\partial x_n}\frac{\partial\hat{u}_m}{\partial x_n}\right] \\ &\quad -2\frac{A\beta}{C_\epsilon^2 a_0}\Delta^2\left[2\frac{\partial\hat{u}_k}{\partial x_i}\frac{\partial\hat{u}_k}{\partial x_j} - \frac{2}{3}\delta_{ij}\frac{\partial\hat{u}_m}{\partial x_n}\frac{\partial\hat{u}_m}{\partial x_n}\right] \qquad (3.13)\end{aligned}$$

The model coefficients obtained from the constitutive theory have to be adjusted for the subgrid scale turbulence so that the dissipation criteria are satisfied. We modify the model as:

$$\begin{aligned}\sigma_{ij} &= -\alpha_0 K_{sgs}^{1/2}\Delta\hat{D}_{ij} + \alpha_1\Delta^2\left[\frac{\partial\hat{u}_i}{\partial x_k}\frac{\partial\hat{u}_j}{\partial x_k} - \frac{1}{3}\delta_{ij}\frac{\partial\hat{u}_m}{\partial x_n}\frac{\partial\hat{u}_m}{\partial x_n}\right] \\ &\quad -\alpha_2\Delta^2\left[\frac{\partial\hat{u}_k}{\partial x_i}\frac{\partial\hat{u}_k}{\partial x_j} - \frac{1}{3}\delta_{ij}\frac{\partial\hat{u}_m}{\partial x_n}\frac{\partial\hat{u}_m}{\partial x_n}\right] \qquad (3.14)\end{aligned}$$

where the first term of the left represents the *forward scatter* of energy due to the cross+Reynolds' term. The second term can be identified as the improved Leonard's terms obtained from the Taylor's series expansion. The third term represents the *backscatter* of energy and give a negative dissipation. More about the *backscatter* of energy is studied in the wave number space but here we use only the estimated value of *backscatter* coefficient. The new nonlinear model can be written in the coordinate-invariant form as follows:

$$\begin{aligned}\boldsymbol{\tau} &= \frac{2}{3}K_{sgs}\mathbf{I} - \alpha_0 K_{sgs}^{1/2}\Delta\hat{\mathbf{D}} + \alpha_1\Delta^2\left[grad\ \hat{\mathbf{u}}\cdot(grad\ \hat{\mathbf{u}})^T - \frac{1}{3}grad\ \hat{\mathbf{u}} : grad\ \hat{\mathbf{u}}\mathbf{I}\right] \\ &\quad -\alpha_2\Delta^2\left[(grad\ \hat{\mathbf{u}})^T\cdot grad\ \hat{\mathbf{u}} - \frac{1}{3}grad\ \hat{\mathbf{u}} : grad\ \hat{\mathbf{u}}\mathbf{I}\right] \qquad (3.15)\end{aligned}$$

The unknown coefficients above will be obtained assuming that the flow in the subgrid scale is isotropic and hence Kolmogorov law is applicable, and satisfies the dissipation criteria. The coefficients thus obtained are:

$$\begin{aligned}\alpha_0 &= 0.12037 \\ \alpha_1 &= \frac{1}{12} \\ \alpha_2 &= 0.03916 \qquad (3.16)\end{aligned}$$

3.2 Homogeneous Plane Shear Flow

In the plain shear flow only one component of the velocity gradient $\frac{\partial u_1}{\partial x_3} = \mathcal{C}$ exists. We will use the above component of the velocity gradient and estimate the stress component ratios. The stress ratio thus obtained is compared with the experimental values [53]. The components of the anisotropic normal stresses obtained from the above model for the plane shear stress are:

$$\begin{aligned} \sigma_{11} &= 0.2058\mathcal{C} \\ \sigma_{22} &= -0.04416\mathcal{C} \\ \sigma_{33} &= -0.1617\mathcal{C} \end{aligned} \tag{3.17}$$

These are comparable with the experimental values as given in Gatski and Speziale, $0.2 : -0.06 : -0.14$. The shear stress value can also be computed for the plane shear case assuming $P = \epsilon = -\sigma_{13}\frac{\partial \hat{u}_1}{\partial x_3}$ and using the experimental value $\frac{K_{sgs}}{\epsilon}\frac{\partial \hat{u}_1}{\partial x_3} = 6.0$. Further the relation between K_{sgs} and ϵ can be used to obtain its value in terms of earlier constant as $\sigma_{13} = -0.17852\mathcal{C}$. This is a good approximation as compared to -0.15 from experiment. The shear stress value can be improved by including the an additional term $\phi_{ij}\left(\frac{\partial \hat{u}_i}{\partial x_j}\right)$ such that it is symmetric, has a trace equal to zero, does not produce dissipation (for isotropic turbulence) and has no normal components. A function of such form is:

$$\phi_{ij}\left(\frac{\partial \hat{u}_i}{\partial x_j}\right) = \left[\frac{\partial \hat{u}_i}{\partial x_k}\frac{\partial \hat{u}_k}{\partial x_j} - \frac{\partial \hat{u}_j}{\partial x_k}\frac{\partial \hat{u}_k}{\partial x_i}\right]$$

It must be noted that the above function is obtained from the terms which were neglected from the constitutive model. The model is thus improved to:

$$\sigma_{ij,new} = \sigma_{ij,previous} + \alpha_3\phi_{ij}\left(\frac{\partial \hat{u}_i}{\partial x_j}\right)$$

The model coefficient thus obtained to satisfy the shear stress is

$$\alpha_3 = 0.0095 \tag{3.18}$$

It must be noted that the above term does not satisfy the symmetry condition, hence cannot be used for the stresses. Moreover the coefficient of the term is small compared to the other terms. This term will be neglected here.

3.3 Homogeneous Plane Strain Flow

The plane strain flow is defined for which only normal strain components are $\frac{\partial u_1}{\partial x_1} = \mathcal{C}$ and $\frac{\partial u_2}{\partial x_2} = -\mathcal{C}$ and hence the rotation is absent. The mean velocity distribution for this type of flow is

$$u_1 = \mathcal{C}x_1 \quad , \quad u_2 = -\mathcal{C}x_2 \quad \text{and} \quad u_3 = constant$$

This type of flow has been considered by Townsend [60], Tucker and Reynolds [61], Genece and Matheiu [62] [63], Canuto and Cheng [37]. The results from the experimental data will be compared with the results of the present model. From the equation of mean motion and the turbulent intensities the behavior of the normal stress components can be expressed as the linear combination of rapid distortion and ordinary decay.

$$\begin{aligned} \overline{u_3^2} &= \overline{u_1^2}|_0 + \frac{d\overline{u_1^2}}{dt}(t - t_0) \\ \overline{u_1^2} + \overline{u_2^2} &= \overline{u_1^2}|_0 + \overline{u_2^2}|_0 + \frac{d}{dt}\left(\overline{u_1^2} + \overline{u_2^2}\right)(t - t_0) \\ \overline{u_1^2} - \overline{u_2^2} &= \frac{4}{5}\mathcal{C}u_3\left[\overline{u_1^2}|_0 + \overline{u_2^2}|_0\right](t - t_0) \end{aligned} \tag{3.19}$$

From the above equations along with the assumption that there is no sudden change in rate of strain, Townsend [60] introduced structure parameters

$$K_1 = \frac{\overline{u_1^2} - \overline{u_2^2}}{\overline{u_1^2} + \overline{u_2^2}} = \frac{4}{5}\mathcal{C}(t - t_0) \quad \text{and} \quad K_2 = \frac{3\overline{u_3^2}}{K_{sgs}} - 1$$

The parameter K_1 indicates the lack of inequality of the turbulent intensity components and the two structure parameters helps us to determine the relative values of three nonzero intensities. The asymptotic value of the parameter K_1 has been obtained experimentally by Townsend as 0.42, whereas Mathieu and Scott gives its value in the range 0.5-0.6. Tucker and Reynolds estimates its value around 0.55, whereas the value of parameter $K_2 = 0$ is given by all authors.

From the new nonlinear model for the given strains only the three normal stress components exists and others are zero as expected. The non zero components of stresses thus obtained are

$$\begin{aligned}
\tau_{11} &= \frac{1}{3}K_{sgs} - \alpha_0 K_{sgs}^{1/2}\Delta\mathcal{C} + \frac{1}{3}(\alpha_1 - \alpha_2)\Delta^2\mathcal{C}^2 \\
\tau_{22} &= \frac{1}{3}K_{sgs} + \alpha_0 K_{sgs}^{1/2}\Delta\mathcal{C} + \frac{1}{3}(\alpha_1 - \alpha_2)\Delta^2\mathcal{C}^2 \\
\tau_{33} &= \frac{1}{3}K_{sgs}
\end{aligned} \tag{3.20}$$

The sum of the stress components, $\tau_{11} + \tau_{22}$, show independence from K_{sgs} which is also established by results given by Matheiu and Scott [63]. The of parameter $K_2 = 0$ for the new nonlinear model which agrees with the experimental values. But of more importance is the nondimensional quantity

$$K_1 = \frac{\tau_{22} - \tau_{11}}{\tau_{22} + \tau_{11}}$$

whose value has been determined experimentally by various authors ranging from 0.42-0.6. For the present model K_1 takes the form,

$$K_1 = \frac{2\alpha_0\left(\frac{\Delta\mathcal{C}}{K_{sgs}^{1/2}}\right)}{\frac{1}{3}\left[(\alpha_1 - \alpha_2)\left(\frac{\Delta\mathcal{C}}{K_{sgs}^{1/2}}\right)^2 + 2\right]}$$

The factor $\left(\frac{\Delta\mathcal{C}}{K_{sgs}^{1/2}}\right)$ can be determined from the equilibrium condition and using the relation between dissipation and subgrid scale kinetic energy, we get

$$\left(\frac{\Delta\mathcal{C}}{K_{sgs}^{1/2}}\right) = \sqrt{\frac{c_\epsilon}{2\alpha_0}} = 1.645$$

Thus we obtain $K = 0.56$ which is comparable with the value obtained by Tucker and Reynolds.

3.4 Buoyancy Effect

If the buoyancy effect is included, the momentum equation can be obtained as [64]

$$\frac{\partial u_i}{\partial t} + u_j \frac{\partial u_i}{\partial x_j} = -\delta_{i3} g \left[1 - \beta T'\right] - \frac{1}{\rho_0} \frac{\partial p}{\partial x_i} + \nu \nabla^2 u_1$$

The effect of the temperature fluctuation term appears in the rate equation of the subgrid stresses and the subgrid scale turbulent kinetic energy equation. However keeping the same model for the subgrid stresses as discussed before the coefficients are modified to include the buoyancy effect. The rate equation of subgrid scale kinetic energy is

$$\frac{\partial K_{sgs}}{\partial t} + \hat{u}_k \frac{\partial K_{sgs}}{\partial x_k} = P + P_b + D - \epsilon + \nu \nabla^2 K_{sgs} \tag{3.21}$$

where $P_b = \beta g \left[\widehat{wT'} - \hat{w}\widehat{T'}\right]$ is the production due to buoyancy term. If the averaging in the vertical direction is Reynolds average then the subgrid scalar flux producing buoyancy production term reduces to Reynolds flux, i.e. $\left[\widehat{wT'} - \hat{w}\widehat{T'}\right] = \widehat{w'T'}$. For the shallow flow case where $L_z \ll L_x \sim L_y$, the above statement is valid and hence the buoyant production can be related to the total shear production by Richardson number, $R_f = -\frac{P_b}{P}$. The state of local equilibrium for the buoyant flow thus implies

$$P_b + P = \epsilon \Rightarrow \quad P = \left(1 - R_f\right)^{-1} \epsilon$$

using the above structure equilbrium condition in the model coefficient evaluation carried earlier, where $P = \epsilon$ was used, we obtain the new coefficients as

$$\begin{aligned} \alpha_{b0} &= \left(1 - R_f\right) \alpha_0 \\ \alpha_{b1} &= \left(1 - R_f\right) \alpha_1 \\ \alpha_{b2} &= \left(1 - R_f\right) \alpha_2 \end{aligned} \tag{3.22}$$

Mason and Brown [41] used a function of Richardson number depending on the stability of the flow to determine the model coefficient, however here we use the same form for all the stability

regimes. If the averaging is not carried out as discussed above the buoyancy producing scalar flux term can be modeled as Reynolds+cross term as discussed in Appendix A.1.

3.5 Scalar Transport

The turbulent transport equation of an averaged scalar quantity, $\hat{\theta}$, is obtained as

$$\frac{\partial \hat{\theta}}{\partial t} + \hat{u}_j \frac{\partial \hat{\theta}}{\partial x_j} = \nu_\theta \nabla^2 \hat{\theta} - \frac{\partial}{\partial x_j}\left(\widehat{u_j\theta} - \hat{u}_j\hat{\theta}\right) \tag{3.23}$$

where the last term on the right is the subgrid scalar flux term, similar to the subgrid stress term in the momentum equation, which is defined as $H_{j\theta} = \left(\widehat{u_j\theta} - \hat{u}_j\hat{\theta}\right)$. This can also be expressed in Galilean invariant Leonard, cross and Reynolds component terms. The closure of the scalar transport can be obtained by extending the new nonlinear model. The modeling of the subgrid scalar flux has been obtained by Lilly [12], Cabot and Moin [22] by extending dynamic model and by Pantano and Sarkar [65].

$$H_{i\theta} = -\beta_0 K_{sgs}^{1/2} \Delta \frac{\partial \hat{\theta}}{\partial x_i} + \beta_1 \Delta^2 \frac{\partial \hat{\theta}}{\partial x_k}\frac{\partial \hat{u}_i}{\partial x_k} - \beta_2 \Delta^2 \frac{\partial \hat{\theta}}{\partial x_k}\frac{\partial \hat{u}_k}{\partial x_i} \tag{3.24}$$

The second term represents the Leonard's term and can be obtained from the Taylors series expansion. For the Gaussian filter as used earlier the coefficient $\beta_1 = \alpha_1 = \frac{1}{12}$. The third term gives the backscatter of energy, which can be related to the total scatter by a backscatter coefficient, $c_{b\theta}$, whose value has been obtained by Schumann [55], Mason and Thompson [24]. The dissipation by the Leonard's term can be obtained from the scalar correlation term as discussed in Hinze [66]. Defining the mixed derivative skewness [67],

$$S_{k\theta} = -\frac{\langle \frac{\partial \theta}{\partial x_k}\frac{\partial \theta}{\partial x_k}\frac{\partial u_1}{\partial x_1}\rangle}{\langle\left(\frac{\partial \theta}{\partial x_k}\right)^2\rangle\langle\left(\frac{\partial u_1}{\partial x_1}\right)^2\rangle^{1/2}}$$

the dissipation due to the terms can be approximated using the scalar correlation function discussed in appendix. The denominator of the skewness factor can be related to the momentum

dissipation and scalar dissipation using the relation given below

$$\langle \left(\frac{\partial \hat{\theta}}{\partial x_k} \right)^2 \rangle = \int_0^\infty k^2 \hat{E}_\theta dk \tag{3.25}$$

The scalar spectrum can be defined in the inertial subrange similar to the energy spectrum as

$$E_\theta = \beta \epsilon_\theta \epsilon^{-1/3} k^{-5/3} \quad \text{and} \quad \hat{E}_\theta = E_\theta |\grave{G}(k)|^2 \tag{3.26}$$

Schumann [55], Mason and Thompson [24] related the backscatter of energy due to momentum and scalar quantity and obtained the backscatter coefficient ratio $c_{b\theta}/c_b = 0.44$ for smooth filter, and 0.32 for sharp cut-off filter respectively. Schumann related this ratio to the subgrid scale Prandtl number, Pr_{sgs}. From the estimate of the dissipation term we get the ratio of the dissipation coefficients as

$$\begin{aligned} \frac{c_{b\theta}}{c_b} &= Pr_{sgs} = 0.44 - 0.46 = \frac{30}{35} \frac{\beta}{C_k} \frac{\beta_2}{\alpha_2} \frac{S_{k\theta}}{S_k} \\ \frac{c_{L\theta}}{c_L} &= \frac{30}{35} \frac{\beta}{C_k} \frac{S_{k\theta}}{S_k} \\ \frac{c_f}{c_{f\theta}} &= \frac{1}{2} \frac{C_k}{\beta} \frac{\alpha_0}{\beta_0} = \frac{1 + c_b - c_L}{1 + Pr_{sgs}(c_b - c_L)} \end{aligned} \tag{3.27}$$

On a heuristic basis assuming $\frac{c_{L\theta}}{c_L} = Pr_{sgs}$ and using the values of the coefficients $c_b = 0.176$, $c_L = 0.43$, $Pr_{sgs} = 0.45$, $\beta = 0.67$ and $C_k = 1.62$ we get the model coefficients.

$$\beta_1 = \alpha_1 \;\; ; \;\; \beta_2 = \alpha_2 \;\; ; \;\; \beta_0 = \frac{1}{0.7} \alpha_0 \tag{3.28}$$

The coefficient of the eddy-viscosity type term is equivalent to the model used by Brown [40], Mason and Thompson [24], who related the eddy viscosities $\nu_T = \nu_{T\theta}\, Pr$, where Prandtl number, Pr, is assumed to be 0.7, which nearly matches in the interior flow field. The modeled form of the scalar flux can be written in coordinate-invariant form as

$$\mathbf{H} = -\frac{\alpha_0}{Pr} K_{sgs}^{1/2} \Delta grad\, \hat{\theta} + \alpha_1 \Delta^2 grad\, \hat{\theta} \cdot (grad\, \hat{\mathbf{u}})^T - \alpha_2 \Delta^2 grad\, \hat{\theta} \cdot grad\, \hat{\mathbf{u}} \tag{3.29}$$

For any other scalar except temperature Prandtl number should be substituted by Schmidt number.

CHAPTER IV

FILTERING OPERATION IN LES

Because of the random behavior of the turbulence field an averaging process has to be devised to obtain deterministic quantities. Reynolds or ensemble averaging can be used to average the variable for turbulent flow. But the resolution of the scale at which the turbulent phenomenon occurs, involves a large number of scales, is far beyond the computational capabilities. Thus the averaging can only resolve certain portion of the fluctuating variable. The large scale component which can be resolved are usually called the 'filtered/resolved variables' and the remaining part is called 'residual/subgrid-scale variables'. The effect of the subgrid scale variables depends upon the fineness of the grid. For the case of atmospheric and oceanic flows the grid size is quite large hence the subgrid scales turbulence cannot be neglected. One of the most conceptual step in Large-Eddy Simulation (LES) is the filtering operation. Filtering operation is defined to decompose a quantity into resolved and residual component as

$$\phi(x,t) = \overline{\phi(x,t)} + \acute{\phi}(x,t) \tag{4.1}$$

where one of the basic axioms of the Reynolds averaging is

$$\overline{\acute{\phi}(x,t)} = 0 \tag{4.2}$$

The above assumption is true if the averaged field ($\overline{\phi(x,t)}$) is constant over an averaging volume, as discussed by Leonard [13], whereas in the wavenumber space it implies that the spectral decomposition of the fluctuating component is zero. This assumption is not valid in general and thus subgrid stresses replace the well known Reynolds stresses. Thus the filtering operation plays an important role in the definition of the stresses. The filtered variables are obtained by

convolution of filter function and the variable.

$$\hat{\phi}(\mathbf{x},t)=\int_{-\infty}^{\infty}G(\mathbf{x},\mathbf{r})\,\phi(\mathbf{x}-\mathbf{r},t)\,d\mathbf{r} \tag{4.3}$$

where $G(\mathbf{x},\mathbf{r})$ is the filter function. Again any flow variable can be decomposed into 'resolved' and 'subgrid" components as

$$\phi(x,t)=\widehat{\phi}(x,t)+\acute{\phi}(x,t) \tag{4.4}$$

and where the subgrid component does not satisfy the Reynolds assumption

$$\widehat{\acute{\phi}}(x,t)\neq 0 \tag{4.5}$$

4.1 Filter Functions

The decomposition of a variable into resolved and subgrid scale components depends upon the filtering process and hence the physics contained in the subgrid stresses depends on the filter function used. The filter function $G(\mathbf{x},\mathbf{r})$ used earlier has components along the coordinate directions such that

$$G(\mathbf{x},\mathbf{r})=G_1\left(x^1,\xi^1\right)G_2\left(x^2,\xi^2\right)G_3\left(x^3,\xi^3\right)\quad\text{and}\quad\int_{-\infty}^{\infty}G(\mathbf{x},\mathbf{r})\,d\mathbf{r}=1$$

Taking the derivative of the resolved scale variable we get

$$\frac{\partial\hat{u}_i}{\partial x_j}=\widehat{\frac{\partial u_i}{\partial x_j}}+\int_{-\infty}^{\infty}u_i(\mathbf{x}-\mathbf{r},t)\,\frac{\partial G(\mathbf{x},\mathbf{r})}{\partial x_j}d\mathbf{r}$$

From the above expression we can conclude that the filter operation and the differentiation commute if the filter function G is not a function of the space coordinate $\mathbf{x}$. Some authors have used different definitions of the filtering of variable, for example

$$\hat{\phi}(x)=\int_{-\infty}^{\infty}G(\mathbf{x}-\mathbf{r})\,\phi(\mathbf{r})\,d\mathbf{r} \tag{4.6}$$

which satisfies the commutative property when the filter function vanishes at the boundary of its support. This is true for the box and Gaussian filter, but for spectral filter the boundary must be at infinity. At least from the definition the commutative property is satisfied. However here we have assumed filter function independent of '$\mathbf{x}$', hence commutative propoerty is satisfied from its definition. The one dimensional filter functions which are of interest are tabulated in Table 4.1. The properties of the filter function are further revealed by their spectral representation. By taking Fourier transform of the variable and the filter function their relation in wave number space is obtained as

$$\grave{\hat{u}}_i(\mathbf{k}) = \grave{G}(\mathbf{k})\,\grave{u}_i(\mathbf{k})$$

where $\grave{u}_i$ is the Fourier representation of u_i and $\grave{G}(\mathbf{k})$ is the transfer function of the filter such that $\grave{G}(\mathbf{k}) = \prod_{i=1}^{3} G_i(k_i)$. The spectral representation can be used to relate the averaged fluctuating variable to that of the filtered variable from the definition as:

$$\grave{\widehat{u_i'}} = \grave{G}(\mathbf{k})\,\grave{u}_i(\mathbf{k}) - \grave{G}(\mathbf{k})^2\,\grave{u}_i(\mathbf{k}) \tag{4.7}$$

Hence, the Reynolds assumption is not satisfied in general, i.e. $\widehat{u} \neq 0$, unless the spectral representation of the averaged fluctuating variable is zero, which is satisfied exactly for sharp cut-off spectral filter. Of all the filters given in the Table 4.1 box, Gaussian and spectral cut-off filter are used commonly. The box filter which has a been widely used in LES because of its simplicity (in the physical space) and ability to treat a wide range of boundary conditions. Liu *et al.* [46] showed that box filter gives much better result in the scale similarity model and further Pope [18] show that they have good spectral realization. But their biggest disadvantage is the non-zero transfer function even at larger wave number. This complicates the energy transfer mechanism because there is no defined spectral gap. On the contrary, spectral cut-off filter has its simplicity in the wavenumber space and has been used sucessfully by different authors [15], [57], [21] and others. The sharp spectral filter gives a sharp spectral gap between large and small scale motion and hence the transfer of energy from different scales are clearly realized. From the transfer function of the spectral filter it can be shown that $\grave{G}(\mathbf{k}) = \grave{G}(\mathbf{k})^2 \rightarrow \widehat{\mathbf{u}'} = 0$, that is the Reynolds assumption is exactly satisfied. Hence the spectral cut-off function leads to the RANS solution from definition. Further the model coefficient for subgrid stress model should

Table 4.1: One-dimensional Filter and transfer functions

Name	Filter function	Transfer function
	$G(r)$	$\grave{G}(k) \equiv \int_{-\infty}^{\infty} e^{ikr} G(r)\, dr$
Box	$\frac{1}{\Delta} H\left(\frac{1}{2}\Delta - \lvert r\rvert\right)$ 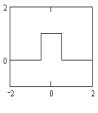	$\frac{sin\left(\frac{1}{2}k\Delta\right)}{\frac{1}{2}k\Delta}$ 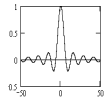
Gaussian	$\left(\frac{6}{\pi\Delta^2}\right)^{1/2} exp\left(-\frac{6r^2}{\Delta^2}\right)$ 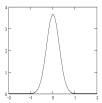	$exp\left(-\frac{k^2\Delta^2}{24}\right)$ 
Sharp spectral	$\frac{sin(\pi r/\Delta)}{\pi r}$ 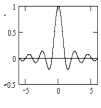	$H\left(\frac{\pi}{\Delta} - \lvert k\rvert\right)$ 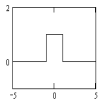
Cauchy	$\frac{\frac{\pi}{24}}{\pi\Delta\left[(r/\Delta)^2 + (\pi/24)^2\right]}$ 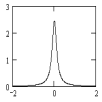	$exp\left(-\frac{\pi\Delta\lvert k\rvert}{24}\right)$ 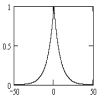
Pao		$exp\left(-\frac{\pi^{2/3}}{24}\left[\Delta\lvert k\rvert\right]^{4/3}\right)$ 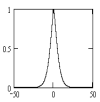
Pade		$\frac{[1-cos(\pi/\Delta)][1+cos(k)]}{2[1-cos(\pi/\Delta)cos(k)]}$

not be obtained based on the spectral filter. Moreover the spectral filter in physical space causes non-local oscillatory behavior. The resulting stress tensors don't follow realizibility condition of the quantity τ_{kk} which relates to the SGS kinetic energy. Gaussian filter is an intermediate of the two filter function and overcomes the disadvantages of the above filter functions in both the physical and wavenumber space. For the Gaussian filter we can define a cut-off wave number, k_{LES}, which can be related to the grid filter and thus the transfer of energy between different scales can be obtained as is done for the spectral cut-off filter. The other filters are used mostly in the wave number space and find their use mostly in theoretical sense. Pade filters has been discussed in detail by Pruett *et al.* [47].

Random data is generated and then filtering operation is applied to look graphically into some of the aspects of the filter functions Figure 4.1. Then the Fourier transformation is taken which enables us to reflect on their nature in wavenumber space. It must be observed that the average of the fluctuating data is non-zero for the Gaussian and box filter, Figure 4.2. For the sharp spectral filter it must have been zero but shows an oscillatory behavior across the zero axis. This is due to the fact that in the finite domain the integral of the filter is not exactly equal to one. The spectral decomposition of the filtered data are nearly the same for all the filters in lower wave number, but at higher wave number (which represents the energy contained in subgrid scale motion) sharp spectral and Gaussian filter both have no components but they still exsists for the box filter, Figures 4.4, 4.5, 4.3 .

The important property of the filter function is the moment of the filter, which has been computed in the Appendix A.3 for all the three filters. We can also derive some important relationships about the small and large scale motion from the Taylor's series expansion as discussed in Appendix A.4.

4.2 Navier-Stokes Equation in Wave Number space

Taking the Fourier transform of the continuity equation and momentum equation we get the equations in the wavenumber space as

$$\begin{aligned} k_i \grave{u}_i(\mathbf{k},t) &= 0 \\ \left(\frac{\partial}{\partial t} + \nu k^2\right) \grave{u}_i(\mathbf{k},t) &= -ik_i P_{kj}(\mathbf{k}) \int_{\mathbf{k}=\mathbf{k}'+\mathbf{k}''} \grave{u}_i(\mathbf{k}')\, \grave{u}_j(\mathbf{k}'')\, d\mathbf{k}' \end{aligned} \tag{4.8}$$

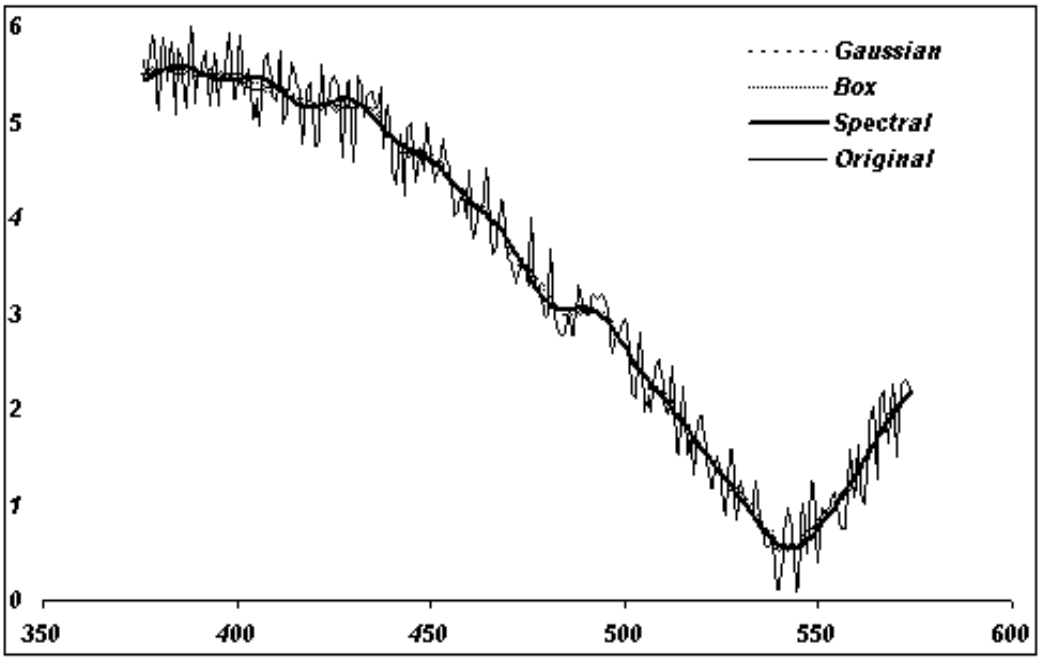

Figure 4.1: The random data and filtered data

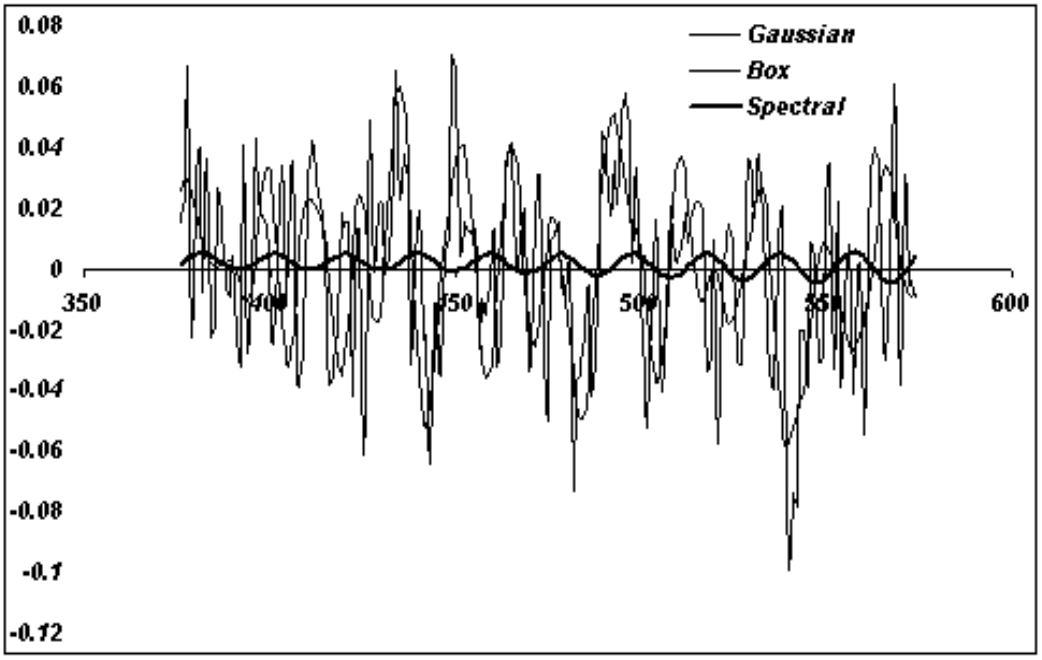

Figure 4.2: The averaged fluctuation data

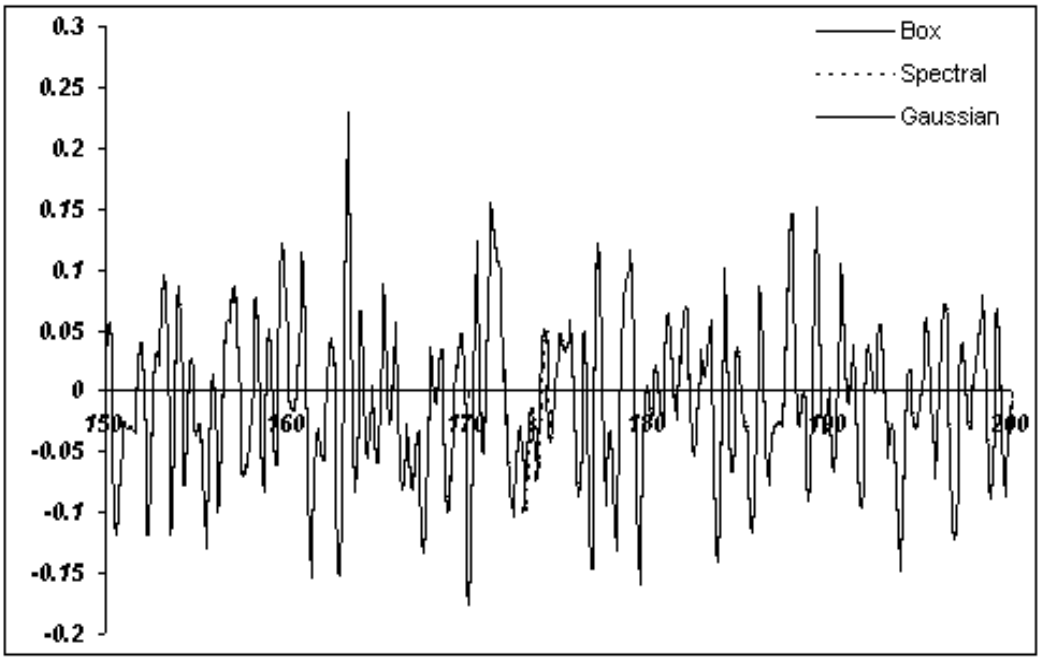

Figure 4.3: The spectral decomposition of the fluctuating component of the data

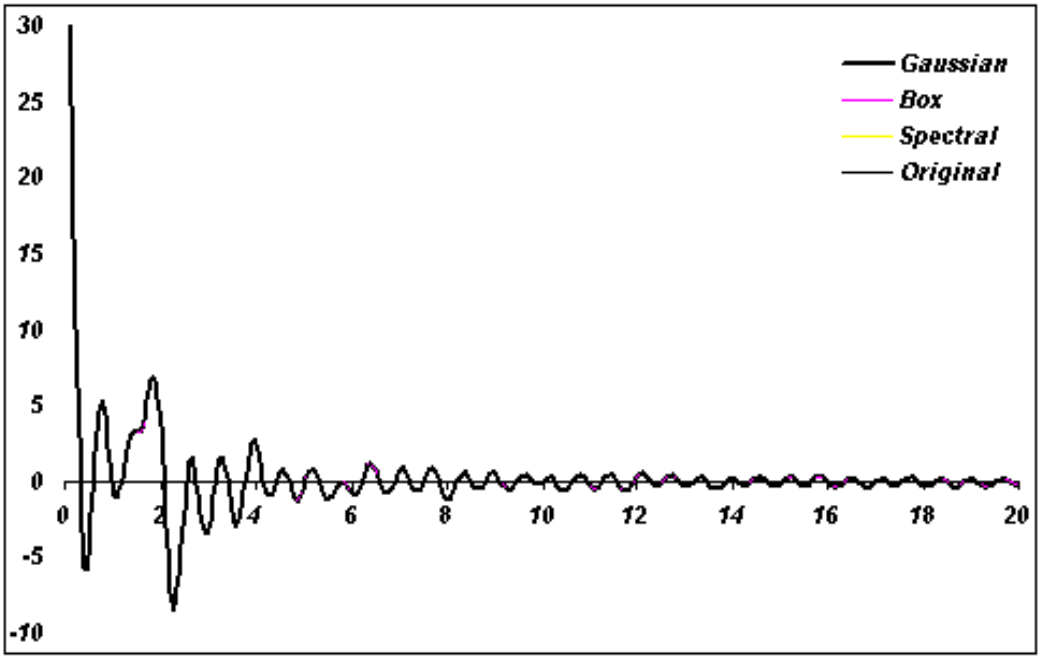

Figure 4.4: The spectral decomposition, lower wave number or resolved scale component

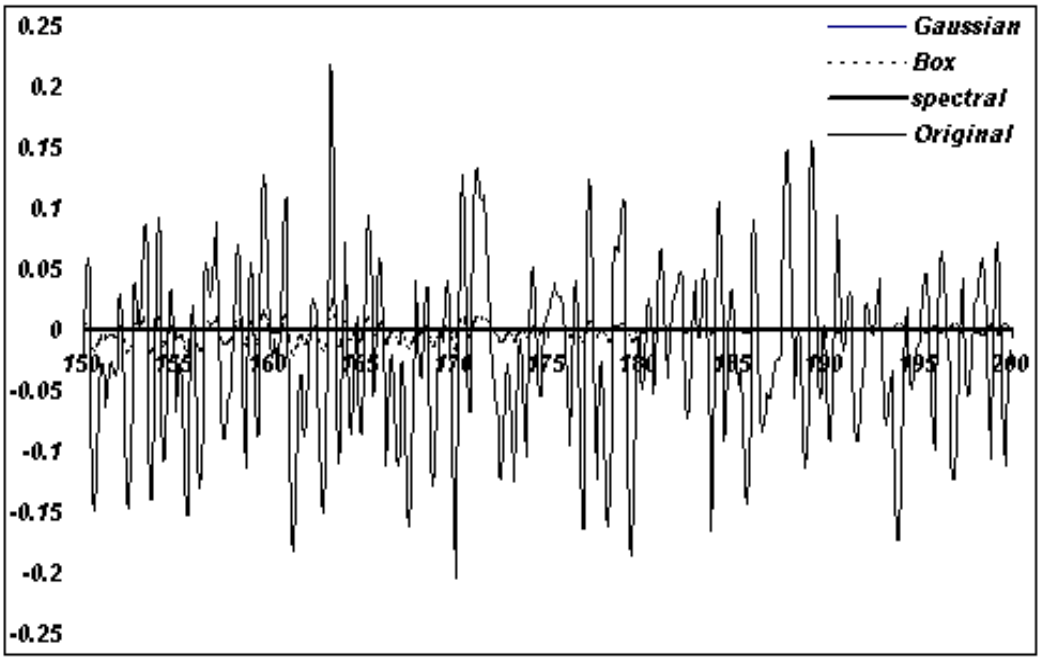

Figure 4.5: The spectral decomposition, higher wave number or subgrid scale component

From the continuity equation we find that $\grave{\mathbf{u}}$ is in the plane perpendicular to $\mathbf{k}$, on the contrary $\grave{p}$ is parallel to $\mathbf{k}$. Introducing the tensor

$$P_{ij}(\mathbf{k}) = \delta_{ij} - \frac{k_i k_j}{k^2}$$

gives us the transformed momentum equation. The filtered equation can be obtained by multiplying the equation by the Fourier component of the filter (the convolution appears as product in Fourier space) as

$$\left(\frac{\partial}{\partial t} + \nu k^2\right) \grave{\hat{u}}_i(\mathbf{k}, t) = -ik_i P_{kj}(\mathbf{k}) \grave{G}(\mathbf{k}) \int_{\mathbf{k}=\mathbf{k}'+\mathbf{k}''} \grave{u}_i(\mathbf{k}') \grave{u}_j(\mathbf{k}'') \, d\mathbf{k}' \tag{4.9}$$

The integral on the right hand side can be decomposed into two parts, one of which is

$$F_{ij}(\mathbf{k}) = \int_{\mathbf{k}=\mathbf{k}'+\mathbf{k}''} \grave{G}(\mathbf{k}') \grave{u}_i(\mathbf{k}') \grave{G}(\mathbf{k}'') \grave{u}_j(\mathbf{k}'') \, d\mathbf{k}' = \int_{\mathbf{k}=\mathbf{k}'+\mathbf{k}''} \grave{\hat{u}}_i(\mathbf{k}') \grave{\hat{u}}_j(\mathbf{k}'') \, d\mathbf{k}'$$

which represents the interaction of the large/resolved scale components with each other and can be computed exactly. The other component represents the subgrid scale components, which

appears as the subgrid stresses in the physical space.

$$\grave{\tau}_{ij}(\mathbf{k}) = \grave{G}(\mathbf{k}) \int_{\mathbf{k}=\mathbf{k}'+\mathbf{k}''} \grave{u}(\mathbf{k}')\,\grave{u}(\mathbf{k}'')\,d\mathbf{k}' - \int_{\mathbf{k}=\mathbf{k}'+\mathbf{k}''} \grave{G}(\mathbf{k}')\,\grave{u}(\mathbf{k}')\,\grave{G}(\mathbf{k}'')\,\grave{u}(\mathbf{k}'')\,d\mathbf{k}'$$

The decomposition of the above triadic interaction can be obtained in terms of Leonard, cross and Reynolds term as shown in Appendix A.2. The equation of the resolved scale energy (compare with its physical conterpart Eq. 2.5),

$$\grave{K}_r(\mathbf{k}) = \frac{1}{2}\grave{\hat{u}}_k \grave{\hat{u}}_k^*$$

where $\grave{\hat{u}}_k^*$ is the complex conjugate of the velocity spectra, can be obtained as

$$\frac{\partial \grave{K}_r}{\partial t} = -2\nu k^2 \grave{K}_r + T_f + T_r \tag{4.10}$$

where $T_f(k,t)$ and $T_r(k,t)$ are the transfer of energy to the wavenumber k from the other modes due to the triadic interactions. The first term on the right is the dissipation by molecular viscosity from the resolved scale motion, and is always negative. The term $T_f(k)$ is the rate of transfer of energy to wavenumber k from the resolved scale motion. The total energy is conserved in such interactions. Thus this term vanishes over all resolved scale modes

$$\sum_{\mathbf{k}} T_f(\mathbf{k}) = 0$$

The second term $T_r(\mathbf{k})$ represents the transfer of energy by the subgrid stress term. This represents the transfer of energy from the subgrid scale components to the large scale. The transfer occurs through various triadic interactions as discussed in Appendix A.1, Figure A.1. The positive value ($T_r > 0$)corresponds to *backscatter* of energy. On the other hand positive value represents the *forward scatter*. The expected transfer of energy to the residual motion is

$$\langle \mathcal{P}_r \rangle = -\langle \sum_{\mathbf{k}} T_r(\mathbf{k}) \rangle$$

The above term is predominantly positive, but can be decomposed into positive and negative parts where the negative component is estimated from the Eddy Damped Quasi Normal Markovian Theory (EDQNM) theory.

4.3 Estimating Backscatter coefficient from EDQNM theory

The transfer of energy from the subgrid scale (large wave number) to resolved scale (smaller scale) results in the backscatter of energy and appears as a negative dissipation in the equation of subgrid scale energy transport equation. The estimation of the amount of backscatter (B) is done with help of EDQNM theory. Here we discuss the estimation of backscatter as a fraction of the total dissipation, as $B = c_b\epsilon$, which will be used in the calculation of the model coefficients. For a complete analysis refer to Lesieur[57]. Here we present only the results from the literature.

$$\begin{aligned} c_b &= 1.37 - 1.4 \text{ for spectral cut-off filter [15]}, \ c_{b\theta} = 0.45 \\ &= 0.43 - 0.489 \text{ for top hat filter [15]}, \ c_{b\theta} = 0.33 \\ &= 0.34 \text{ for Gaussian filter [15]} \\ &= 0.176 \text{ for smooth filter [55]}, \quad c_{b\theta} = 0.077 \end{aligned} \tag{4.11}$$

We also try to relate the backscatter terms to the subgrid scale terms. These subgrid backscatter of energy lead to the stochastic fluctuations in the subgrid stresses. This renders the resolved scale velocity to be unpredictable in time. The undeterministic nature of the flow field is not respected by the dissipative model such as the Smagorinsky model or the mixed model with fixed coefficients. The estimation of the backscatter coefficient and modeling it properly may help us to overcome the problem. Non-local expansion which computes the backscatter of energy assumes

$$k \ll k_{LES} \ , \quad k' = k'' > k_{LES} \tag{4.12}$$

This range of wave number is a component of the Reynolds stress and thus the backscatter estimated by the EDQMN theory comes from the Reynolds stress term of the subgrid stress and gives rise to the k^4 spectrum for the small wave number. The near local expansion which exists

in the wave number range of

$$k \sim k_{LES}, \quad k' \text{ or } k'' > k_{LES} \text{ and } k'' \text{ or } k' < k_{LES} \tag{4.13}$$

In this range of wavenumber, which comes from the cross stresses, gives a sharp rise in backscatter of energy in the near the cut-off wave number. The local expansion shows that the forward and backward scatter of energy for this type of interaction is cancelled exactly. Hence, the net transfer of energy due to these interaction is zero. Although these interactions effect the evolution of resolved scale but do not directly change the energy of these scales.

4.3.1 Non-Local Expansion

Non-local expansion estimates the forward (P) and backscatter (B) of the energy in the limit of the wave number such that

$$\begin{aligned} P &= \int_0^\infty 2k^2 E(k)\,\eta(k)\,dk \\ B &= \int_0^\infty F(k)\,dk \end{aligned} \tag{4.14}$$

where,

$$\begin{aligned} \eta(k) &= \frac{1}{15}\int_{k_c}^\infty \vartheta_{0k'k'}\left(5E(k') + k'\frac{\partial E(k')}{\partial k'}\right)dk' \\ F(k) &= \frac{14}{15}k^4\int_{k_c}^\infty \vartheta_{0k'k'}\frac{E(k')^2}{k'^2}dk' \end{aligned} \tag{4.15}$$

and the energy spectrum $E(k)$ is taken from the inertial subrange. Further the time scale θ_{kpq} for the fully developed flow can be written as

$$\begin{aligned} \vartheta_{kpq} &= \left[\mu_{kpq} + \nu\left(k^2+p^2+q^2\right)\right]^{-1} \\ \mu_{kpq} &= \mu_k + \mu_p + \mu_q \\ \mu_k &= 0.19C_K^{3/2}\left[k^3E(k)\right]^{1/2} \end{aligned} \tag{4.16}$$

In all the above equations the time dependence has been neglected. The integral given by Eq. (4.14) can be evaluated in the inertial subrange but requires the relation between Kolmogorov's

length scale and grid scale. From the dissipation relation in the inertial subrange we get $\Delta = 5.77\eta$ and $= 5.8966\eta$ for sharp spectral and Gaussian filter respectively. The integrals thus are computed to obtain the forward (c_f) and backscatter (c_b) coefficients

$$\begin{aligned} c_b &= \frac{14}{0.38 \times 75}\pi^5 I_1 = 0.042 \\ c_f &= \frac{1}{0.38 \times 3}\pi^{4/3} I_2 = 0.198 \end{aligned} \tag{4.17}$$

where the integrals are:

$$\begin{aligned} I_1 &= \int_\pi^\infty \frac{t^{-22/3}}{a + t^{-4/3}} dt \\ I_2 &= \int_\pi^\infty \frac{t^{-11/3}}{a + t^{-4/3}} dt \end{aligned} \tag{4.18}$$

where $a = 0.22603$. The integrals are evaluated numerically to obtain the forward and backward scatter coefficients. Since in the above computation the grid scale is of the order of the dissipation length scale, which does not hold for the LES, the values cannot be accepted. The computation carried out by Leslie and Quarani [15], Schumann [55] uses a simpler definition of the time scale $\vartheta_{kpq} = [\mu_{kpq}]^{-1}$, so that viscosity effect is neglected in comparision to the grid scale dissipation (holds for LES), and gives us the value of the coefficients as, $c_b = 0.098$ and $c_f = 0.658$. If for the time being if we assume that most of the backscatter of the energy is obtained from the non-local term then the total dissipation by different stress components are

$$\begin{array}{ccccccc} \epsilon & = & \epsilon_{\mathcal{L}} & + & \epsilon_{\mathcal{C}} & + & \epsilon_{\mathcal{R}} \\ & & [0.44\epsilon] & & [X] & & [(0.66 - 0.1)\,\epsilon] \end{array} \tag{4.19}$$

which shows that $X \to 0$. Henceforth the forward and backward scatter of energy from the cross term will be assumed to be zero. This result is supported by the numerical results as the $\eta(k)$ and $F(k)$ balance each other at the cut-off wave number. The above computations can also be interpreted as

$$\int_0^{k_c} (P - B)\, dk = 0.56\epsilon$$

Since the non-local approximation gives only an approximate result, there are still regions in the Reynolds stress zone which neither form a part of near local or the non-local approximation. Schumann [55] in an attempt to compute the total backscatter applied the local equilibrium such that

$$\int_0^{k_c} (P - B)\, dk = \epsilon \tag{4.20}$$

and obtained the value of $c_b = 0.176$, which will be used in the model.

For the diffusion of the passive scalar, θ, the non-local expansion can be extended as discussed by Lesieur [57], Herring *et al.* [68]. The forward and backward transfer of energy can be estimated similar to that of the turbulent kinetic energy.

$$\begin{aligned} P_\theta &= \int_0^\infty 2k^2 E_\theta(k)\, \eta_\theta(k)\, dk \\ B_\theta &= \int_0^\infty F_\theta(k)\, dk \end{aligned} \tag{4.21}$$

where,

$$\begin{aligned} \eta_\theta(k) &= \frac{2}{3}\int_{k_c}^\infty \vartheta^\theta_{0k'k'} E(k')\, dk' \\ F_\theta(k) &= \frac{4}{3}k^4 \int_{k_c}^\infty \vartheta^\theta_{0k'k'} \frac{E(k')\, E_\theta(k')}{k'^2} dk' \end{aligned} \tag{4.22}$$

Time scale appearing in the above equation can be obtained from the ratio of the time scale which can be expressed as a constant.

$$\frac{\vartheta^\theta_{0k'k'}}{\vartheta_{0k'k'}} = \frac{1}{3Pr}$$

The above value has been suggested by Lesieur [57] and was used by Mason and Thompson [24] for computing the backscatter for scalar quantity. For any scalar other than temperature Prandtl number, Pr, can be replaced by Schmidt number, Sc. Herring *et al.* [68] estimated it to lie in the range 0.56-1, further Schumann [55] assumed its value to be 0.73. Performing the integration for the backward and forward scatter, the backward scatter of the scalar flux can be related to the backscatter of the turbulent kinetic energy, $\frac{c_{b\theta}}{c_b} = \frac{10}{7}\frac{\beta}{C_k}\frac{1}{3Pr}$. Further Schumann recalculated the

time scale ratio and obtained the backscatter coefficient ratio, which he expressed as the subgrid scale Prandtl number.

$$\frac{c_{b\theta}}{c_b} = 0.44 = Pr_{sgs}$$

The above value of the backward scatter for scalar quantity will be used in the determination of model coefficient for scalar fluxes.

CHAPTER V

GOVERNING EQUATIONS

In the hierarchy of methods for the solution of turbulent fluid flow the LES (Large Eddy Simulation) occupies an intermediate position between DNS (Direct numerical simulation) and RANS (Reynolds-averaged Navier-Stokes equations) and is motivated by the limitations of the either methods. The LES finds its use exhaustively in the atmospheric flows or mesoscale calculations, where the horizontal scales of motion are of the order 10-100 kilometers. For such length scales DNS simulation requirement exceeds the capabilies of the exsisting computational facility. On the other hand the RANS simulation can be obtained on the grid sizes which are of the order of the largest eddies (large scales). Since we are most interested in the effects of intermediate and small scales motions,a better resolution of these flows are required. LES being the intermediate of DNS and RANS (grid size requirement) serves the purpose. Apart from the atmospheric flow LES is also more reliable and accurate than RANS for flow over bluff bodies, which involves vortex shedding and unsteady separation. RANS models fails for the flow phenomenon in which large scale unsteadiness is significant. We have simulated the mesoscale flow as the application of the new nonlinear model as developed in later chapters.

The Environmental Fluid Dynamic Computer (EFDC) [27] code used in this study solves the simplified equation for mesoscale flow. The basic assumptions involved in the mesoscale flow have been described here and thereby the simplified equations are derived. For the mesoscale atmospheric model the basic governing equation are the conservation equation of mass, momentum, heat and vapor pressure. The basic governing equations for fluid flow are the Navier-Stokes equations.

Continuity equation:

$$\frac{\partial \rho}{\partial t} + div\,(\rho \mathbf{u}) = 0$$

Momentum Equation:

$$\frac{\partial \rho \mathbf{u}}{\partial t} + div\,(\rho \mathbf{u}\mathbf{u}) + f \times \mathbf{u} = \rho \mathbf{f} - grad\,(p) + div\,(\boldsymbol{\sigma})$$

Temperature equation:

$$\frac{\partial \rho T}{\partial t} + div\,(\rho T \mathbf{u}) = \frac{Dp}{Dt} + \boldsymbol{\sigma} : \mathbf{D} + div\,(\kappa grad\ T)$$

Conservation of any scalar quantity e.g., water vapor for atmospheric flow or salinity for oceanographic flow or any other concentrations is

$$\frac{\partial \rho c}{\partial t} + div\,(\rho c \mathbf{u}) = div\,(\nu_c grad\ c) + S_c$$

In the momentum equation $f = (f_1, f_2, f_3)$ is the Coriolis vector related to the speed of earth's rotation (Ω), latitude (φ) and angle made with east direction (β), as $f_1 = 2\Omega cos\varphi cos\beta$, $f_1 = 2\Omega cos\varphi sin\beta$ and $f_3 = 2\Omega sin\varphi$. Further $\boldsymbol{\sigma}$ is the stress tensor and is defined as $\lambda\,(div\mathbf{u})\,\mathbf{I} + 2\mu\mathbf{D}$ where $\mathbf{D}$ is the rate-of-strain-tensor. The vector $\mathbf{f} = (0, 0, g)$ is the body force body force term and has only one component in vertical direction, κ is the fluid's thermal conductivity and ν_c is molecular diffusivity of scalar quantity 'c'. S_c is the body source term for the processes that are not considered in the equation. These terms may arise from the chemical reaction, phase change etc, discussed in details by Stull [69] and others [70][71]. The above conservation equations can be simplified for the mesoscale meteorological flow by estimating the order of magnitude of each term by scale analysis. The smaller order terms are thus neglected to get the simplified equation.

5.1 Definition of Mesoscale flow

The atmospheric flow phenomenon are scale dependent and can best be categorized by three basic scales: macro (space scales of more than 1000m and time scale of order of weeks), meso and micro (space scale of meters and time scale of minutes). The mesoscale is intermediate between micro and macro scale. Many of the phenomenon of the atmospheric flow lie in this scale range such as sea and land breezes, mountain-valley winds, air flow around rough terrain, urban circulation, frontal circulation and tropical cyclones. Orlanski [72] further classified eight

horizontal space and time subdivisions. These scales are important because of the assumptions valid for these scales, namely, Boussinesq approximation, anelastic equation, shallow convection etc.

5.2 Density variation effect on atmospheric flow

The density stratification in the atmospheric is prominent because of the temperature, water vapor and other scalar variables variation on which the density varies according to the equation of state. This variation of density effects the flow except in steady parallel motion where this effect can be realized as the inertia effect. The variation of density also effect the body force term. For the atmospheric flow the body force comes into picture as a consequence of gravitation. The interplay of the inertia as well as gravity effect of density is the most intriguing aspect of the atmospheric flow. These effects are in turn dependent on the scale of flow being considered. The main effort of the simplification of the governing equation is to separate out these effects for the specific scale flow.

5.3 Equation of state

The equation of state for an ideal gas which is valid for mesoscale flow is

$$p = \rho RT \tag{5.1}$$

where T is the absolute temperature. We further introduce the spliting of the mesoscale therodynamic variables (ϕ) such that

$$\phi = \phi_0 + \phi'$$

where ϕ_0 is the synoptic scale quantity and ϕ' is the mesoscale perturbation. Introducing the above spliting in the mesoscale equation of state Eq. (5.1) and neglecting the higher order terms we get the equation of state for the synoptic scale quantities as

$$p_0 = \rho_0 RT_0 \tag{5.2}$$

The equation of the perturbation quantities can be obtained by subtracting the two equations Eq. (5.1) and (5.2). Further dividing the perturbation equation by the synptic scale equation and neglecting still higher order terms the linearized perturbation ideal gas law is obtained as

$$\frac{p'}{p_0} = \frac{\rho'}{\rho_0} + \frac{T'}{T_0} \tag{5.3}$$

Making the shallow convection approximation and thereby neglecting the pressure term we get

$$\frac{\rho'}{\rho_0} = -\frac{T'}{T_0} \tag{5.4}$$

5.3.1 Coefficient of thermal expansion

If density is assumed to be a function of pressure p and temperature T then the small change in density $\delta\rho$ can be related to the changes in pressure, δp and temperature, δT as

$$\delta\rho = \left(\frac{\partial\rho}{\partial p}\right)_T \delta p + \left(\frac{\partial\rho}{\partial T}\right)_p \delta T \tag{5.5}$$

Dividing both sides by ρ we get

$$\frac{\rho'}{\rho_0} \sim \frac{\delta\rho}{\rho} = \left(\frac{\partial ln\rho}{\partial p}\right)_T \delta p + \left(\frac{\partial ln\rho}{\partial T}\right)_p \delta T \tag{5.6}$$

The reciprocal of the coefficient of the first term is called the *bulk modulus* E while the negative of the coefficient of second term is the *coefficient of thermal expansion* β which has a value of $1.53 \times 10^{-4}\ K^{-1}$ for water and $3.5 \times 10^{-3}\ K^{-1}$ for air. If the ideal gas law is valid then

$$\beta = -\left(\frac{\partial ln\rho}{\partial T}\right)_p = \frac{1}{T_0} \tag{5.7}$$

where the ideal gas for synoptic scale quantity has been used. The above form of β also yields to the same relation between density and temperature Eq. (5.4) from Eq. (5.6).

5.4 Conservation of mass

Spilting the state variables into synoptic scale and perturbation quantities we get the continuity equation as

$$\frac{D\left(\rho_0+\rho'\right)}{Dt}+\left(\rho_0+\rho'\right) div\ \mathbf{u}=0$$

where ρ_0 is the synoptic scale reference density and $\acute{\rho}$ is its perturbation. We assume that the $|\rho'/\rho_0| \ll 1$. It has been assumed that the rate of change of synoptic state quantities are small in comparison to the perturbation quantity and the horizontal synoptic gradient be much less than the mesoscale gradients.

$$|\ \frac{\partial\rho_0}{\partial t}\ |\ll|\ \frac{\partial\rho'}{\partial t}\ |\ ,\ |\ \frac{\partial\rho_0}{\partial x}\ |\ll|\ \frac{\partial\rho'}{\partial x}\ |\quad \text{and}\ |\ \frac{\partial\rho_0}{\partial y}\ |\ll|\ \frac{\partial\rho'}{\partial y}\ |$$

Hence the continuity equation under these assumptions can be simplified as

$$\frac{\partial\rho'}{\partial t}+\left(\mathbf{u}\cdot grad\right)\rho'+w\frac{\partial\rho_0}{\partial z}+\rho_0 div\ \mathbf{u}=0$$

The method of scale analysis can be used further to eliminate the remaining terms

$$\begin{aligned}
|\ \frac{\partial\rho'}{\partial t}\ | \quad &\sim \quad \frac{\rho'}{t_\rho}\ ,\ |\ u\frac{\partial\rho'}{\partial x}\ |\sim\ U\frac{\rho'}{L_x}\ ,\ |\ v\frac{\partial\rho'}{\partial y}\ |\sim\ V\frac{\rho'}{L_y}\ ,\ |\ w\frac{\partial\rho'}{\partial z}\ |\sim\ W\frac{\rho'}{L_z}\\
|\ w\frac{\partial\rho_0}{\partial z}\ | \quad &\sim \quad W\frac{\rho_0}{L_z}\ ,\ |\ \rho_0\frac{\partial u}{\partial x}\ |\sim\ \rho_0\frac{U}{L_x}\ ,\ |\ \rho_0\frac{\partial v}{\partial y}\ |\sim\ \rho_0\frac{V}{L_y}\ ,\ |\ \rho_0\frac{\partial w}{\partial z}\ |\sim\ \rho_0\frac{W}{L_z}
\end{aligned} \tag{5.8}$$

where t_ρ^{-1} are the characteristic frequency of variation in density on mesoscale, U,V and W are the representative velocities and L_x, L_y and L_z are the spatial scales of the mesoscale disturbance. We further define the *density-scaled height*, H_ρ as

$$H_\rho=-\frac{1}{\rho_0}\frac{\partial\rho_0}{\partial z}$$

This height is approximately 8 km in the earths troposphere and will be further related to the Brunt-Vaisala frequency of the atmospheric flow. The continuity equation can be further obtained by neglecting the lower order terms, the order of the terms will be compared with the term which is expected to remaim.

5.4.1 Deep continuity equation

Comparing the order of magnitude of other terms with respect to $w\frac{\partial \rho_0}{\partial z}$ and under the assumption $|\rho'/\rho_0| \ll 1$ the equation can be further simplified as

$$w\frac{\partial \rho_0}{\partial z} + \rho_0 div\ \mathbf{u} = 0$$

provided

$$L_z \sim H_\rho\ ,\ \frac{U}{W}\frac{H_\rho}{L_x} \sim 1\ ,\ \frac{V}{W}\frac{H_\rho}{L_y} \sim 1\ ,\ \frac{H_\rho}{Wt_\rho} \sim 1$$

since L_z is approximately equal to H_ρ the second and third condition imply that $\frac{U}{L_x} \sim \frac{V}{L_y} \sim \frac{W}{L_z}$, which can be interpreted that if the length scales in the horizontal plane is larger than that in the vertical plane then vertical velocity is smaller than the plane velocity. If in the continuity equation above we include the spatial variation of velocity then the equation of mass can be written concisely as

$$div\ (\rho_0 \mathbf{u}) = 0 \tag{5.9}$$

This the the *deep convection continuity equation* as the vertical depth of circulation is the same order of the density scaled depth.

5.4.2 Shallow continuity equation

Contrary to the above assumption, the *shallow convection continuity equation* is obtained under the assumption that $L_z \ll H_\rho$ along with the earlier assumption of $\frac{U}{L_x} \sim \frac{V}{L_y} \sim \frac{W}{L_z}$. Under these assumptions the magnitudes of each term can be estimated with respect to $\rho_0\frac{\partial w}{\partial z}$ thereby the shallow continuity equation is obtained as

$$div\ \mathbf{u} = 0 \tag{5.10}$$

which is often referred as the *incompressibility assumption.* Hence for the incompressibility effect to be applicable the order of length scales should be $L_z \ll L_x \sim L_y$. Hence the velocity component W in the 'z' direction is small in comparision to the other two velocity components.

5.5 Momentum Equation

We will deduce the conservation of momentum for the shallow convection case. We will be using the Boussinesq assumption which defines Boussinesq Flow as: "*Motion in which (mesoscale and turbulent) perturbation density may be ignored, except in buoyancy term, where it is the linear sum of mesoscale pressure and temperature perturbations*". We have already shown from the equation of state that the pressure perturbation are small as compared to the temperature hence will be replaced with temperature perturbations only. Hence the synoptic scale momentum equation can be written as

$$\frac{D\mathbf{u}}{Dt} + f \times \mathbf{u} = \mathbf{f} - \frac{1}{\rho_0} grad\ p + \nu \nabla^2 \mathbf{u} \tag{5.11}$$

It is beneficial to decompose the equations in component form since the gravitational acceleration is present only in the vertical direction.

5.5.1 Vertical equation of motion

The equation of motion in the vertical direction is obtained as

$$\frac{Dw}{Dt} + f_1 v - f_2 u = \left(1 + \frac{\rho'}{\rho_0}\right) g - \frac{1}{\rho_0} \frac{\partial}{\partial z} (p_0 + p') + \nu \frac{\partial^2 w}{\partial z^2}$$

Further assuming that the synoptic scale is in *hydrostatic equilibrium* so that

$$\frac{\partial p_0}{\partial z} = -\rho_0 g$$

Carrying out order of analysis for the above equation it can be shown that magnitude of vertical acceleration is much smaller that the magnitude of pressure gradient [70]. The Coriolis component can also be neglected as compared to the gravity effect. The equation of motion thus reduces to

$$\frac{\partial p'}{\partial z} = -\rho' g \tag{5.12}$$

The superscript $(.')$ will be neglected from here onwards and the density, ρ, and pressure, p, will represent the mesoscale perturbation quantities. This will help us to make room for the filtering of the equation to obtain the equation of motion of turbulent flow.

5.5.2 Horizontal equation of motion

From the shallow convection equation it has been established that the vertical velocity is small compared to the horizontal velocity hence will be neglected from the Coriolis component. The mesoscale pressure is a function of the vertical coordinate only, hence will not appear in the horizontal equation of motion. It must be noted that this is true only for the orthogonal coordinates, in curvilinear coordinate system pressure gradient will have components along each direction. The momentum equations become

$$\begin{aligned} \frac{Du}{Dt} - fv &= -\frac{1}{\rho_0}\frac{\partial p_0}{\partial x} + \nu\frac{\partial^2 u}{\partial z^2} \\ \frac{Dv}{Dt} + fu &= -\frac{1}{\rho_0}\frac{\partial p_0}{\partial y} + \nu\frac{\partial^2 v}{\partial z^2} \end{aligned} \tag{5.13}$$

where $f = 2\Omega sin\varphi$. The synoptic scale pressure variation in the horizontal plane can be obtained from the geostrophic wind.

5.6 Geostrophic Winds

Geostrophic wind is the simple atmospheric motion when the air moves horizontally without the change of velocity and direction of motion under the external force of gravity. The vertical velocity component is assumed to be small with respect to horizontal velocity component and in the vertical direction the force of gravity dominates so that the Coriolis component can be neglected. The governing equation thus can be simplified as

$$\begin{aligned} -fv &= -\frac{1}{\rho_0}\frac{\partial p_0}{\partial x} \\ fu &= -\frac{1}{\rho_0}\frac{\partial p_0}{\partial y} \\ g &= -\frac{1}{\rho_0}\frac{\partial p_0}{\partial z} \end{aligned} \tag{5.14}$$

From the above equations the geostrophic wind are defined in terms of pressure gradient as

$$U_g = -\frac{1}{\rho f}\frac{\partial p_0}{\partial y} \quad \text{and} \quad V_g = \frac{1}{\rho f}\frac{\partial p_0}{\partial x} \tag{5.15}$$

Introcucing the synoptic scale pressure gradient in terms of geostrophic wind velocities, EQ. (5.15) in the Eqs. (5.12) and (5.13), the equation of the momentum for the mesoscale flow can be written as

$$\begin{aligned} \frac{\partial u_i}{\partial t} + u_j \frac{\partial u_i}{\partial x_j} &= -e_{ij3} f \left(U_{gj} - u_j\right) - \frac{1}{\rho_0}\frac{\partial p}{\partial x_i} + \nu \frac{\partial^2 u_i}{\partial x_j \partial x_j} \quad \text{for } i = 1, 2 \\ \frac{\partial p}{\partial x_i} &= -\rho g \quad \text{for } i = 3 \end{aligned} \tag{5.16}$$

where e_{ijk} is the permulation symbol. For constant diffusivity the conservation equation of heat and scalar quantity is obtained as:

$$\begin{aligned} \frac{DT}{Dt} &= 2\frac{\nu}{C_v}\mathbf{D} : \mathbf{D} + \kappa \nabla^2 T \\ \frac{Dc}{Dt} &= \nu_c \nabla^2 c + S_c \end{aligned} \tag{5.17}$$

where C_v is the specific heat at constant volume and other source terms such as radiation, phase change etc have been neglected.

5.7 Equation of motion of filtered variable in a turbulent flow

For the turbulent flow the equation of motion can be obtained by filtering the equation of *shallow continuity* such that $\phi = \hat{\phi} + \phi'$ where ϕ is any dependent flow variable we get filtered synoptic scale conservation equation.

$$div\ \hat{\mathbf{u}} = 0 \tag{5.18}$$

Applying the filtering in the momentum equation we get the filtered momentum equation as

$$\begin{aligned} \frac{\partial \hat{u}_i}{\partial t} + \hat{u}_j \frac{\partial \hat{u}_i}{\partial x_j} &= -e_{ij3} f \left(\hat{U}_{gj} - \hat{u}_j\right) - \frac{1}{\rho_0}\frac{\partial \hat{p}}{\partial x_i} + \nu \frac{\partial^2 \hat{u}_i}{\partial x_j \partial x_j} - \frac{\partial}{\partial x_j}\left(\widehat{u_i u_j} - \hat{u}_i \hat{u}_j\right) \quad \text{for } i = 1, 2 \\ \frac{\partial \hat{p}}{\partial x_i} &= -\hat{\rho} g \quad \text{for } i = 3 \end{aligned} \tag{5.19}$$

From the above equations we see that only six components of stresses appear, i.e., τ_{1j} and τ_{2j} for $j = 1-3$. Since we have considered shallow equations so the length scales in the vertical direction

are much smaller that the horizontal length scales so the stresses along the vertical direction, τ_{13}, τ_{23}, can be computed using Reynolds' stresses where as the stresses in the horizontal plane, $\tau_{11}, \tau_{22}, \tau_{12}$, are computed using subgrid scale turbulence as suggested by Blumberg and Mellor [73]. Neglecting the viscous dissipation in the temperature equation and the source term due to other processes in the scalar transport equation we get the filtered equation as:

$$\begin{aligned} \frac{\partial \hat{T}}{\partial t} + \hat{u}_j \frac{\partial \hat{T}}{\partial x_j} &= \kappa \nabla^2 \hat{T} - \frac{\partial}{\partial x_j}\left(\widehat{T u_j} - \hat{T}\hat{u}_j\right) \\ \frac{\partial \hat{c}}{\partial t} + \hat{u}_j \frac{\partial \hat{c}}{\partial x_j} &= \nu_c \nabla^2 \hat{c} - \frac{\partial}{\partial x_j}\left(\widehat{c u_j} - \hat{c}\hat{u}_j\right) \end{aligned} \tag{5.20}$$

The scalar diffusion ($\mathbf{H}_\theta$) in the temperature (T) and scalar (c) equation will be modeled in the same manner as for the momentum equation. The scalar diffusion quantities H_{T3} and H_{c3} will be modeled based on the Reynolds' stresses where as $H_{T1}, H_{T2}, H_{c1}, H_{c2}$ will be modeled as the subgrid scale turbulence.

5.8 Reynolds stress closure

Mellor and Yamada [26] have developed various levels of Reynolds' stress modeling, one of which is named by them as $2\frac{1}{2}$ level which has been used here. It converges to the one-equation model when the buoyancy term is neglected; this model was further modified by Galperin *et al.* [74]. The closure obtained by this model is

$$\begin{aligned} \sigma_{xz} &= \nu_T \frac{\partial \hat{u}}{\partial z} \\ \sigma_{yz} &= \nu_T \frac{\partial \hat{v}}{\partial z} \\ H_{Tz} &= \frac{1}{Pr} \nu_T \frac{\partial \hat{T}}{\partial z} \end{aligned} \tag{5.21}$$

where Pr is the Prandlt number whose value is approximated as 0.7. ν_T is the vertical turbulent viscosity and is modeled as

$$\nu_T = lqS_M$$

where l is the length scale and q^2 is the turbulent kinetic energy. The empirical formulae for the unknown S_M is obtained as

$$S_M = A_1 \frac{1 - 3C_1 - \left(\frac{6A_1}{B_1}\right) - 2A_2 G_H \left[(B_2 - 3A_2)\left(1 - \frac{6A_1}{B_1}\right) - 2C_1 (B_2 + 6A_1)\right]}{[1 - 3A_2 (6A_1 + B_2)](1 - 9A_1 A_2 G_H)} \tag{5.22}$$

where G_H is the Richardson number of the flow which can be related to the Brunt-Vaisala frequency N of the flow as

$$G_H = \left(\frac{l}{q}\right)^2 N^2$$

where the constants has been obtained as

$$(A_1,\ B_1,\ A_2,\ B_2,\ C_1,\ \lambda_1) \equiv (0.92,\ 16.6,\ 0.74,\ 10.1,\ 0.08,\ 0.12\ )$$

5.9 Logarithmic Layer

The numerical solution is not carried out right from the surface upwards, so near the wall resolution has to be considered. Log-law is considered from the surface to the middle of the first grid. The surface roughness is defined in terms of the *surface roughness height*, z_0. Surface roughness coefficient can be written in terms of the roughness height and hence the roughness of the bottom layer can be computed. From the log law:

$$\frac{\partial \hat{u}}{\partial z} = \frac{u_\tau}{\kappa z} \quad \text{and} \quad \frac{\partial \hat{v}}{\partial z} = \frac{v_\tau}{\kappa z} \tag{5.23}$$

Integrating the above equation from the surface, z_0, to the mid of the first layer, $\frac{\Delta_1}{2}$ we get

$$\hat{u}_1 = \frac{u_\tau}{\kappa} ln\left(\frac{\Delta_1}{2z_0}\right) \quad \text{and} \quad \hat{v}_1 = \frac{v_\tau}{\kappa} ln\left(\frac{\Delta_1}{2z_0}\right)$$

where $\hat{u}_1$ and $\hat{v}_1$ are the velocities of the first layer. Defining

$$U_\tau = \sqrt{u_\tau^2 + v_\tau^2} \quad \text{and} \quad \sigma_w = \sqrt{\sigma_{wx}^2 + \sigma_{wy}^2}$$

From the above definitions we obtain the surface friction coefficient as

$$c_f = \sqrt{\frac{\sigma_w}{\rho_0 U_\tau^2}} = \kappa^2 \left[ln \left(\frac{\Delta_1}{2z_0} \right) \right]^{-2}$$

From the skin friction coefficient the stress at the bottom layer is obtained.

$$\sigma_{xz}|_0 = c_f \sqrt{\hat{u}_1^2 + \hat{v}_1^2}\ \hat{u}_1 \quad \text{and} \quad \sigma_{yz}|_0 = c_f \sqrt{\hat{u}_1^2 + \hat{v}_1^2}\ \hat{v}_1 \tag{5.24}$$

5.10 Transformation of equation

So far the equations of motion have been expressed in terms of orthogonal coordinates. To simulate the mesoscale atmospheric flow we need to transform the equations to a body conforming coordinate system usually called the *terrain following* coordinate system or *sigma* representation. The new generalized coordinate system is

$$\begin{aligned} \xi^1 &= g_1(x) & x &= f\left(\xi^1\right) \\ \xi^2 &= g_2(y) & y &= g\left(\xi^2\right) \\ \xi^3 &= \frac{z + h(x,y)}{\zeta(x,y,t) + h(x,y)} & z &= \left[\zeta\left(\xi^1,\xi^2,t\right) + h\left(\xi^1,\xi^2\right)\right]\xi^3 - h\left(\xi^1,\xi^2\right) \end{aligned} \tag{5.25}$$

where $\zeta(x,y,t) \equiv \zeta\left(\xi^1,\xi^2,t\right)$ is the free surface elevation and $h(x,y)$ is the terrain height. The covariant base vectors are thus obtained as

$$\begin{aligned} \mathbf{a}_i &= \frac{\partial \mathbf{x}}{\partial \xi^i} \\ \mathbf{a}_1 &= h_1\mathbf{i} + \left(\left[h_{\xi^1} + \zeta_{\xi^1}\right]\xi^3 - h_{\xi^1}\right)\mathbf{k} \\ \mathbf{a}_2 &= h_2\mathbf{j} + \left(\left[h_{\xi^2} + \zeta_{\xi^2}\right]\xi^3 - h_{\xi^2}\right)\mathbf{k} \\ \mathbf{a}_3 &= (h+\zeta)\,\mathbf{k} \end{aligned} \tag{5.26}$$

where the variables in the subscript represent the derivative and $\mathbf{i}, \mathbf{j}, \mathbf{k}$ are the unit vectors for the Cartesian frame. Further let $(h + \zeta) = H$, which is the total depth of the fluid as a function is ξ^1, ξ^2, t. The six independent components of the fundamental metric tensor $g_{ij} = \mathbf{a}_i \cdot \mathbf{a}_j$ are

obtained as

$$\begin{aligned} g_{11} &= h_1^2 + \left(H_{\xi^1}\xi^3 - h_{\xi^1}\right)^2 & g_{22} &= h_2^2 + \left(H_{\xi^2}\xi^3 - h_{\xi^2}\right)^2 \\ g_{33} &= H^2 & g_{12} &= \left(H_{\xi^1}\xi^3 - h_{\xi^1}\right)\left(H_{\xi^2}\xi^3 - h_{\xi^2}\right) \\ g_{13} &= H\left(H_{\xi^1}\xi^3 - h_{\xi^1}\right) & g_{23} &= H\left(H_{\xi^2}\xi^3 - h_{\xi^2}\right) \end{aligned} \tag{5.27}$$

Thus the determinant of the fundamental metric tensor $g = det\left(g_{ij}\right) = h_1^2 h_2^2 H^2$. The contravariant base vectors can be obtained from the covariant base vector components.

$$\begin{aligned} \mathbf{a}^i &= \frac{1}{2\sqrt{g}} e^{ijk}\left(\mathbf{a}_j \times \mathbf{a}_k\right) \\ \mathbf{a}^1 &= \frac{1}{h_1}\mathbf{i} \\ \mathbf{a}^2 &= \frac{1}{h_2}\mathbf{j} \\ \mathbf{a}^3 &= -\frac{H_{\xi^1}\xi^3 - h_{\xi^1}}{h_1 H}\mathbf{i} - \frac{H_{\xi^2}\xi_3 - h_{\xi^2}}{h_2 H}\mathbf{j} + \frac{1}{H}\mathbf{k} \end{aligned} \tag{5.28}$$

The contravariant component of the velocity can be obtained from the velocity in the Cartesian frame by $u^i = \mathbf{u} \cdot \mathbf{a}^i$.

$$\begin{aligned} u^1 &= \frac{1}{h_1}u \\ u^2 &= \frac{1}{h_2}v \\ u^3 &= \frac{1}{H h_1}\left[h_{\xi^1} - \xi^3 H_{\xi^1}\right]u + \frac{1}{H h_2}\left[h_{\xi^2} - \xi^3 H_{\xi^2}\right]v + \frac{1}{H}w \end{aligned} \tag{5.29}$$

The coordinate transform discussed so far takes care of the steady part of the transformation, but the new coordinate system is unsteady and so the grid speed $w^i = \frac{\partial \xi^i}{\partial t}$ must be included, and thus the resulting contravariant velocities are defined as $\mathbf{u} = \mathbf{v} - \mathbf{w}$, [23]. For the unsteady coordinate system the time derivative is given by [23]

$$\frac{\partial}{\partial t} = \frac{\partial}{\partial \tau} + \mathbf{w} \cdot \ grad$$

Since the grid speed has only one component, $w^3 = -\frac{\xi^3}{H}\zeta_t$, so that only u^3 is modified. The resulting contravariant velocities are:

$$\begin{aligned} v^1 &= \frac{1}{h_1}u \\ v^2 &= \frac{1}{h_2}v \\ v^3 &= \frac{1}{H}\left[w - \xi^3\left(\zeta_t + uh_1^{-1}h_{\xi^1} + vh_2^{-1}h_{\xi^2}\right) + \left(1-\xi^3\right)\left(uh_1^{-1}\zeta_{\xi^1} + vh_2^{-1}\zeta_{\xi^2}\right)\right] \end{aligned} \tag{5.30}$$

The components if the contravariant metric, $g^{ij} = \mathbf{a}^i \cdot \mathbf{a}^j$ are obtained.

$$\begin{aligned} g^{11} &= \frac{1}{h_1^2} & g^{22} &= \frac{1}{h_2^2} \\ g^{33} &= \left[\frac{\left(h_{\xi^1} - \xi^3 H_{\xi^1}\right)}{Hh_1}\right]^2 + \left[\frac{\left(h_{\xi^2} - \xi^3 H_{\xi^2}\right)}{Hh_2}\right]^2 + \frac{1}{H^2} & g^{12} &= 0 \\ g^{13} &= \frac{1}{h_1^2 H}\left(h_{\xi^1} - \xi^3 H_{\xi^1}\right) & g^{23} &= \frac{1}{h_2^2 H}\left(h_{\xi^2} - \xi^3 H_{\xi^2}\right) \end{aligned} \tag{5.31}$$

Christoffel symbols of first and second kind which are expressed as

$$[ij,k] = \frac{\partial \mathbf{a}_i}{\partial x_j} \cdot \mathbf{a}_k \quad \text{and} \quad \Gamma_{ij}^l = g^{kl}\,[ij,k] \tag{5.32}$$

can be determined. The only non zero coefficients are:

$$\begin{aligned} \Gamma_{11}^1 &= \frac{1}{h_1}h_{1\xi^1} & \Gamma_{22}^2 &= \frac{1}{h_2}h_{2\xi^2} \\ \Gamma_{11}^3 &= \frac{1}{H}\left(H_{\xi^1\xi^1}\xi^3 - h_{\xi^1\xi^1}\right) & \Gamma_{22}^3 &= \frac{1}{H}\left(H_{\xi^2\xi^2}\xi^3 - h_{\xi^2\xi^2}\right) \\ \Gamma_{33}^3 &= 0 & \Gamma_{12}^3 &= \frac{1}{H}\left(H_{\xi^1\xi^2}\xi^3 - h_{\xi^1\xi^2}\right) \\ \Gamma_{13}^3 &= \frac{1}{H}H_{\xi^1} & \Gamma_{23}^3 &= \frac{1}{H}H_{\xi^2} \end{aligned} \tag{5.33}$$

Once the Christoffel symbol of the second kind are obtained, the transformation of the vector ($\mathbf{A}$) and tensor ($\mathbf{T}$) can be obtained as discussed in details by Warsi [23]. Representative covariant derivative of contravariant components are shown below

$$A^i_{,k} = \frac{\partial A^i}{\partial \xi^k} + \Gamma^i_{jk}A^j \quad \text{and} \quad T^{ij}_k = \frac{\partial T^{ij}}{\partial \xi^k} + \Gamma^i_{lk}T^{lj} + \Gamma^j_{lk}T^{il} \tag{5.34}$$

The curvilinear coordinate system is nonsteady but the time dependent term is eliminated under the continuity equation from the *shallow convection approximation.* Because of this assumption the transformation of the equations cannot be obtained exactly. Thus we keep the time term and then obtain the transformed equation and apply the approximation. The transformation of the continuity equation

$$\frac{\partial \rho_0}{\partial t} + div\ (\rho_0 \mathbf{u}) = 0$$

is obtained as

$$\frac{\partial}{\partial \tau}(\rho_0 \sqrt{g}) + \frac{\partial}{\partial \xi^i}\left[\rho_0 \sqrt{g} v^i\right] = 0$$

Now assuming constant density ρ_0 we get the required continuity equation in nonsteady coordinates as

$$\frac{\partial}{\partial \tau}\left[h_1 h_2 \zeta\right] + \frac{\partial}{\partial \xi^1}\left[h_2 H u\right] + \frac{\partial}{\partial \xi^2}\left[h_1 H v\right] + \frac{\partial}{\partial \xi^3}\left[h_1 h_2 H v^3\right] = 0 \tag{5.35}$$

The velocity component v^3 is zero both at the bottom surface and at the free surface. Thus integrating the continuity equation over the fluid depth along ξ^3 we get

$$\frac{\partial}{\partial \tau}\left[h_1 h_2 \zeta\right] + \frac{\partial}{\partial \xi^1}\left[h_2 H \int_0^1 u d\xi^3\right] + \frac{\partial}{\partial \xi^2}\left[h_1 H \int_0^1 v d\xi^3\right] = 0 \tag{5.36}$$

which can be solved to obtain the evolution of free surface.

The convective term

$$\frac{\partial \mathbf{u}}{\partial t} + div\,(\mathbf{u}\mathbf{u})$$

in transformed coordinates is

$$\frac{1}{\sqrt{g}} \frac{\partial\left(\sqrt{g} u^i \mathbf{a}_i\right)}{\partial \tau} + \left(u^i v^k\right)_{,k} \mathbf{a}_i \quad \text{where} \quad \left(u^i v^k\right)_{,k} = \frac{\partial u^i v^k}{\partial \xi_k} + \Gamma^i_{lk} u^l v^k + \Gamma^k_{lk} u^i v^l$$

From the above relation and the values of Γ^i_{jk} obtained above the coefficients of the base vectors $\mathbf{a}_1$ and $\mathbf{a}_2$ respectively are

$$\begin{aligned}
&\frac{1}{\sqrt{g}}\left[\frac{\partial}{\partial\tau}\left(h_1h_2Hu\right)+\frac{\partial}{\partial\xi^1}\left(h_2Huu\right)+\frac{\partial}{\partial\xi^2}\left(h_1Hvu\right)+\frac{\partial}{\partial\xi^3}\left(h_1h_2Hu^3u\right)\right] \quad , \\
&\frac{1}{\sqrt{g}}\left[\frac{\partial}{\partial\tau}\left(h_1h_2Hv\right)+\frac{\partial}{\partial\xi^1}\left(h_2Huv\right)+\frac{\partial}{\partial\xi^2}\left(h_1Hvv\right)+\frac{\partial}{\partial\xi^3}\left(h_1h_2Hu^3v\right)\right]
\end{aligned} \tag{5.37}$$

The coefficient of $\mathbf{a}_3$ will form the third equation, but the convective term for the third equation has been neglected because of the hydrostatic assumption so they will not be considered any further. The third momentum equation has the pressure term and thus we now consider the components of the pressure term (including the body force term due to free surface elevation) in the new coordinate system, which gives

$$grad\ \left(p+g\zeta\right)=g^{ik}\frac{\partial}{\partial\xi^i}\left(p+g\zeta\right)\mathbf{a}_k$$

Thus the components of the pressures along the three directions $\mathbf{a}_1$, $\mathbf{a}_2$ and $\mathbf{a}_3$ respectively are

$$\begin{aligned}
&\frac{1}{h_1^2}\frac{\partial}{\partial\xi^1}\left(p+g\zeta\right)+\frac{1}{h_1^2H}\left[h_{\xi^1}-\xi_3H_{\xi^1}\right]\frac{\partial p}{\partial\xi^3} \quad , \\
&\frac{1}{h_2^2}\frac{\partial}{\partial\xi^2}\left(p+g\zeta\right)+\frac{1}{h_2^2H}\left[h_{\xi^2}-\xi^3H_{\xi^2}\right]\frac{\partial p}{\partial\xi^3} \quad , \\
&\frac{1}{H}\frac{\partial p}{\partial\xi^3}
\end{aligned} \tag{5.38}$$

From the above considerations the third momentum equation is simply

$$\frac{\partial p}{\partial\xi^3}=-gH\frac{\rho}{\rho_0} \tag{5.39}$$

We have the stress term in the momentum equation appearing in the form $div\ \boldsymbol{\sigma}$ as the isotropic component is absorbed along with the pressure term. The corresponding $\mathbf{a}_1$ and $\mathbf{a}_2$ components in the new coordinate system respectively are

$$\begin{aligned}
&\frac{1}{h_1^2h_2H}\left[\frac{\partial}{\partial\xi^1}\left[h_2H\left(h_1^2\sigma^{11}\right)\right]+\frac{\partial}{\partial\xi^2}\left[h_1H\left(h_1h_2\sigma^{12}\right)\right]+H\frac{\partial}{\partial\xi^3}\left[h_2H\left(h_1^2\sigma^{13}\right)\right]\right] \quad , \\
&\frac{1}{h_1h_2^2H}\left[\frac{\partial}{\partial\xi^2}\left[h_1H\left(h_2^2\sigma^{22}\right)\right]+\frac{\partial}{\partial\xi^1}\left[h_2H\left(h_1h_2\sigma^{21}\right)\right]+H\frac{\partial}{\partial\xi^3}\left[h_1H\left(h_2^2\sigma^{23}\right)\right]\right]
\end{aligned} \tag{5.40}$$

The contravariant components of the stresses can be obtained from the modeled stresses. The vertical components of the stresses (scalar fluxes) have been modeled as:

$$\boldsymbol{\sigma} = -A_v grad\ \mathbf{u} \quad \text{and} \quad \mathbf{H} = -\frac{A_v}{Pr} grad\ \theta$$

from which the contravariant components σ^{13} and σ^{23} are obtained as

$$\sigma^{13} = -A_v \left[g^{13} \frac{\partial u^1}{\partial \xi^1} + g^{23} \frac{\partial u^1}{\partial \xi^2} + g^{33} \frac{\partial u^1}{\partial \xi^3} \right] \tag{5.41}$$

Since it has been assumed that [70]

$$\frac{\partial z}{\partial \xi^1} \sim \frac{\partial z}{\partial \xi^2} \ll \frac{\partial z}{\partial \xi^3}$$

the separation of flux into vertical and horizontal component is desirable, hence the vertical stress components can be approximated as below.

$$\sigma^{13} \approx -A_v \frac{1}{H^2} \frac{\partial u^1}{\partial \xi^3} \quad \text{and} \quad \sigma^{23} \approx -A_v \frac{1}{H^2} \frac{\partial u^2}{\partial \xi^3} \tag{5.42}$$

From the tensor form of the new-nonlinear model we get the contravariant components of the stresses as

$$\begin{aligned} T^{11} \;=\; & h_1^2 \sigma^{11} = -\alpha_0 K_{sgs}^{1/2} \Delta \frac{1}{h_1} \frac{\partial u}{\partial \xi^1} \\ & + \alpha_1 \Delta^2 \left[\frac{1}{h_1^2} \left(\frac{\partial u}{\partial \xi^1} \right)^2 + \frac{1}{h_2^2} \left(\frac{\partial u}{\partial \xi^2} \right)^2 - \frac{1}{3} \left[\frac{1}{h_1^2} \left(\frac{\partial u}{\partial \xi^1} \right)^2 + \frac{1}{h_2^2} \left(\frac{\partial v}{\partial \xi^2} \right)^2 + \frac{1}{h_2^2} \left(\frac{\partial u}{\partial \xi^2} \right)^2 + \frac{1}{h_1^2} \left(\frac{\partial v}{\partial \xi^1} \right)^2 \right] \right] \\ & - \alpha_2 \Delta^2 \left[\frac{1}{h_1^2} \left(\frac{\partial u}{\partial \xi^1} \right)^2 + \frac{1}{h_1^2} \left(\frac{\partial v}{\partial \xi^1} \right)^2 - \frac{1}{3} \left[\frac{1}{h_1^2} \left(\frac{\partial u}{\partial \xi^1} \right)^2 + \frac{1}{h_2^2} \left(\frac{\partial v}{\partial \xi^2} \right)^2 + \frac{1}{h_2^2} \left(\frac{\partial u}{\partial \xi^2} \right)^2 + \frac{1}{h_1^2} \left(\frac{\partial v}{\partial \xi^1} \right)^2 \right] \right] \end{aligned} \tag{5.43}$$

Similarly other components can be determined. The only term left to be transformed is the viscous diffusion term which is expressed as $\nu div\,(grad\ \mathbf{u})$. Although the viscosity term is considerably small in comparison to the turbulent viscosity for high Reynolds number flow, its effect can be retained with the turbulent viscosity term. It can be shown that its effect modifies the vertical viscosity to $A_v + \nu$ and in the plane adds up to the first term, $\nu + \alpha_0 K_{sgs}^{1/2} \Delta$. The

final transformed equation of motion is

$$\begin{aligned}
&\frac{\partial}{\partial t}\left(h_1h_2Hu\right)+\frac{\partial}{\partial\xi^1}\left(h_2Huu\right)+\frac{\partial}{\partial\xi^2}\left(h_1Hvu\right)+\frac{\partial}{\partial\xi^3}\left(h_1h_2Hv^3u\right)+h_1h_2H\left(V_g-v\right)\\
&=-h_2H\frac{\partial(p+g\zeta)}{\partial\xi^1}-h_2\left[h_{\xi^1}-\xi^3H_{\xi^1}\right]\frac{\partial p}{\partial\xi^3}+\frac{\partial}{\partial\xi^3}\left[\left(A_v+\nu\right)\frac{h_1h_2}{H}\frac{\partial u}{\partial\xi^3}\right]-\left[\frac{\partial}{\partial\xi^1}\left(h_2HT^{11}\right)+\frac{\partial}{\partial\xi^2}\left(h_1HT^{12}\right)\right]\\
&\frac{\partial}{\partial t}\left(h_1h_2Hv\right)+\frac{\partial}{\partial\xi^1}\left(h_2Huv\right)+\frac{\partial}{\partial\xi^2}\left(h_1Hvv\right)+\frac{\partial}{\partial\xi^3}\left(h_1h_2Hv^3v\right)-h_1h_2H\left(U_g-u\right)\\
&=-h_1H\frac{\partial(p+g\zeta)}{\partial\xi^2}-h_1\left[h_{\xi^2}-\xi^3H_{\xi^2}\right]\frac{\partial p}{\partial\xi^3}+\frac{\partial}{\partial\xi^3}\left[\left(A_v+\nu\right)\frac{h_1h_2}{H}\frac{\partial v}{\partial\xi^3}\right]-\left[\frac{\partial}{\partial\xi^1}\left(h_1HT^{21}\right)+\frac{\partial}{\partial\xi^2}\left(h_2HT^{22}\right)\right]\\
&\frac{\partial p}{\partial\xi^3}=-gH\frac{\rho}{\rho_0}
\end{aligned}\tag{5.44}$$

These transormed equation with the equation of continuity Eq. (5.35) and (5.36) form the equations of motion. The conservation equation of the temperature and scalar quantities can be obtained similarly as

$$\begin{aligned}
&\frac{\partial}{\partial t}\left(h_1h_2H\theta\right)+\frac{\partial}{\partial\xi^1}\left(h_2Hu\theta\right)+\frac{\partial}{\partial\xi^2}\left(h_1Hv\theta\right)+\frac{\partial}{\partial\xi^3}\left(h_1h_2Hv^3\theta\right)=\\
&\frac{\partial}{\partial\xi^3}\left[\frac{\left(A_v+\nu\right)}{Pr}\frac{h_1h_2}{H}\frac{\partial\theta}{\partial\xi^3}\right]+\left[\frac{\partial}{\partial\xi^1}\left(h_2HT^1\right)+\frac{\partial}{\partial\xi^2}\left(h_1HT^2\right)\right]
\end{aligned}\tag{5.45}$$

where the terms T^1 and T^2 represents the subgrid fluxes and the diffusion terms. Upon transformation the terms can be written as:

$$\begin{aligned}
T^1 \quad = \quad & h_1H^1=\frac{\nu+\alpha_0K_{sgs}^{1/2}\Delta}{Pr}\frac{1}{h_1}\frac{\partial\theta}{\partial\xi^1}-\alpha_1\Delta^2\left[\frac{1}{h_1^2}\frac{\partial\theta}{\partial\xi^1}\frac{\partial u}{\partial\xi^1}+\frac{1}{h_2^2}\frac{\partial\theta}{\partial\xi^2}\frac{\partial u}{\partial\xi^2}\right]+\\
& \alpha_2\Delta^2\left[\frac{1}{h_1^2}\frac{\partial\theta}{\partial\xi^1}\frac{\partial u}{\partial\xi^1}+\frac{1}{h_1h_2}\frac{\partial\theta}{\partial\xi^2}\frac{\partial u}{\partial\xi^1}\right]
\end{aligned}\tag{5.46}$$

similarly T^2 can be expressed. For any other scalar transport other than temperature Prandtl number is replaced by Schmidt number. Vinokur [75] and Hamrick [76] also obtained the transformed equations of motion and can be consulted for further generalization.

5.11 Numerical method

The equations of motions are solved over a six faced cell in three dimensional curvilinear space. The variables are defined on the grid as suggested by Arkawa and Lamb [27] called the staggered grid location or the MAC grid. The variables are defined such that the velocities in the plane are assumed constant over the vertical cell layer and the vertical velocity is defined at

the interface such that it varies linearly over the layer. The vertical discretization is considered first by integrating the equations over the cell layer. The computational scheme solves the layer averaged equations of motion by splitting them into external-internal modes. This splitting of equation into these modes helps us to run the code for larger time steps [77]. More insight into this aspect can be obtained from the linearized equations which helps to separate out the internal and external gravity wave motions. The simplified form of the cell averaged equations of motion in the k^{th} layer can be written as

$$\begin{aligned}
&\frac{\partial \zeta}{\partial t} + \frac{\partial u_k}{\partial x} + \frac{\partial v_k}{\partial y} + w_{k+1} - w_k = 0 \\
&\frac{\partial u_k}{\partial t} + f\left(V_g - v_k\right) = -g\frac{\partial \zeta}{\partial x} - \frac{1}{\rho_0}\frac{\partial p'}{\partial x} + \text{source term} \\
&\frac{\partial v_k}{\partial t} - f\left(U_g - u_k\right) = -g\frac{\partial \zeta}{\partial y} - \frac{1}{\rho_0}\frac{\partial p'}{\partial y} + \text{source terms}
\end{aligned} \tag{5.47}$$

where the *source terms* include the convective, viscous and stress terms. The momentum equation can be intergrated over the entire depth of the fluid to obtain the averaged equation of motion.

$$\begin{aligned}
&\frac{\partial \zeta}{\partial t} + \frac{\partial [u]}{\partial x} + \frac{\partial [v]}{\partial y} = 0 \\
&\frac{\partial [u]}{\partial t} + f\left(V_g - [v]\right) = -gH\frac{\partial \zeta}{\partial x} - \frac{1}{\rho_0}\frac{\partial [p']}{\partial x} + [\text{source terms}] \\
&\frac{\partial [v]}{\partial t} - f\left(U_g - [u]\right) = -gH\frac{\partial \zeta}{\partial y} - \frac{1}{\rho_0}\frac{\partial [p']}{\partial y} + [\text{source terms}]
\end{aligned} \tag{5.48}$$

The above equations represents the equations of the motion of a single *homogeneous fluid* with free surface [70]. If the Coriolis forces are neglected, the pressure due to the baroclinicity of the fluid, i.e the density variation is kept as the source term and further assuming that the free surface elevation is very small in comparision to the magnitude of the total depth then the above equations can be expressed in linearized form which gives the gravity wave.

$$\begin{aligned}
\frac{\partial \zeta}{\partial t} &= -\frac{\partial [u]}{\partial x} - \frac{\partial [v]}{\partial y} \\
\frac{\partial [u]}{\partial t} &= -gH\frac{\partial \zeta}{\partial x} \\
\frac{\partial [v]}{\partial t} &= -gH\frac{\partial \zeta}{\partial y}
\end{aligned} \tag{5.49}$$

The above equations when solved gives wave motion called the gravity wave, as it is a consequence of gravity effect, and has phase velocity, $c = \sqrt{gH}$. They are also called the *external gravity mode* or the *barotropic mode*. The external mode equation for the transformed equation can be obtained similarly.

The internal mode equations can be obtained by various methods, here we will form the equation of the velocity deviation from the depth averaged velocity. Subtracting the cell averaged and depth averaged equation we get the perturbation equation in generalized form as

$$\begin{aligned}
&w_{k+1} - w_k + \frac{\partial u'_k}{\partial x} + \frac{\partial v'_k}{\partial y} = 0 \\
&\frac{\partial u'_k}{\partial t} - f\left(v'_k\right) = -\frac{1}{\rho_0}\frac{\partial p'}{\partial x} + \text{source term} - [\text{source terms}] \\
&\frac{\partial v'_k}{\partial t} - f\left(u'_k\right) = -\frac{1}{\rho_0}\frac{\partial p'}{\partial y} + \text{source term} - [\text{source terms}] \\
&\frac{\partial p'}{\partial z} = -\rho g
\end{aligned} \tag{5.50}$$

If the Coriolis force is neglected as before, the linearized form of the above equation represents the gravity wave existing at the interface of the two fluids. In the simplified *two-layered fluid* model described by Pielke [70] the equations can be expressed in terms of the interface height h, assuming the interface to be a material surface such that $w = \frac{Dh}{Dt}$ we have

$$\begin{aligned}
\frac{\partial h}{\partial t} &= -h_0\frac{\partial u'}{\partial x} - h_0\frac{\partial v'}{\partial y} \\
\frac{\partial u'}{\partial t} &= -g\frac{\rho}{\rho_0}\frac{\partial h}{\partial x} \\
\frac{\partial v'}{\partial t} &= -g\frac{\rho}{\rho_0}\frac{\partial h}{\partial y}
\end{aligned} \tag{5.51}$$

The above equation gives the *internal gravity mode* or the *baroclinic mode* and has a phase velocity, $c = \sqrt{\frac{\rho}{\rho_0}gh_0}$, where h_0 is the layer depth. It is evident from the above analysis that the external mode is associated with the high speed gravity wave and internal mode equation are associated with slow moving baroclinic waves. If the Coriolis force is also retained the linearized equation gives another set of wave motion called *Rossby wave* discussed by Pielke [70]. From the Von-Neumann analysis [78] it can be shown that the CFL number for the linerized wave equation

is given as

$$\text{CFL} = c\frac{\Delta t}{\Delta x}$$

Hence the external mode equation has to be solved for smaller time step whereas the internal mode equation can be solved for larger time steps. Hence if the equations of motion are solved without splitting, then it has to be run for smaller time steps. Since the requirement is to run the code for larger time step, hence splitting the equations in external-internal mode is beneficial. The internal and external mode equations for the transformed equation of motion is given in details by Hamrick [27].

The external mode is solved using semi-implicit three time level scheme with a periodic two time level correction step using trapezoidal scheme. The advective term in the momentum equation is computed by central difference approximation or by upwind advection. The equation for the free surface displacement is formed which is a discrete Helmholtz type elliptic equation which is solved using *conjugate gradient scheme*. The momentum equations are then solved substituting the free surface displacement at the new time step obtaining the velocities. The correction steps re-evaluates the free surface evolution and velocities at the new time level. The stability criteria for the semi-implicit scheme and the *trapezoidal scheme* is discussed by Hamrick.

Internal mode solution is obtained using fractional step scheme combining implicit step for the vertical shear and explicit for other terms. In the implicit step for the vertical shear requires the specification of bottom and surface stresses. The bottom stresses are expressed from the logarithmic boundary layer discussed above. The surface stresses are zero for free surface. In the program provisions are also available for prescribing the surface stress from the wind speed over the ocean surface. The vertical velocity can be obtained finally satisfying the perturbation continuity equation. Numerical solution of transport equation is solved using three time level *fractional step method*.

CHAPTER VI

FLOW OVER BACKWARD FACING STEP

Flow over a backward facing step is a widely used benchmark problem to evaluate the performance of models in the prediction of separated flows. Among the several features that contribute to its interest are geometrical similarity, fixed separation point, inherent nonlinearities, separation, reattachment and several recirculation regions. The separation-reattachment process is a complex interaction between the separated shear layer and adjacent flow and depends on the flow regime at separation and reattachment. Three different flow regimes are possible: (i)Laminar-laminar, Re 50-1200 [2],[79], (ii)Transition , Re 1200-6600 Karniadakis *et al.* [22], (iii)Turbulent-turbulent, Re 6600-above [80],[6],[81]. We will be considering the third flow regime where the flow before and after is turbulent. Apart from the flow regime there are several other parameters that effect the reattachment length and in fact the recirculation zones.

6.1 Parameters

A comprehensive list of the parameters on which the flow over a backward facing step depends is yet to be formulated. Here we will be discussing a few of the parameters which helps us to understand the physics of the problem and also to comprehend the results which are the expansion ratio, top surface boundary condition and the near wall treatment when the solution is not obtained up to the wall.

6.1.1 Expansion Ratio

Expansion ratio ($E = h_s/H$) is expressed as the ratio of step height (h_s) and channel height (H). For the free surface the expansion ratio is defined for the initial fluid depths i.e at time t=0. In the limit $E \to 0$, fully developed channel flow is obtained, whereas for $E \to 1$ flow characteristics are similar to that of wall jet. For negative expansion ratio we obtain the forward

facing step. Presently we will be considering expansion ratio, $E \sim 0.5$. Thangam and Knight [2] considered laminar flow for expansion ratio in the range 0.25-0.75 and rigid lid boundary condition, Figure 6.1. The reattachment length were computed for varying Reynolds number and expansion ratio and it was concluded that the reattachment length of the primary vortex increases with the increase of expansion ratio. Barton [79] studied both rigid lid and free surface boundary condition to study the effect of the expansion ratio on reattachment length for laminar flow. He concluded that the reattachment length for both the cases are same until the recirculation zones on the upper boundary is formed for rigid lid case. The reattachment length continues to increase with expansion ratio for free surface case. Eaton and Johnston [1] plotted some results for both double-sided expansion and rigid lid case for turbulent flow and concluded that the reattachment length increases with expansion ratio. Although it wasn't a exhaustive study, only expansion ratio up to 0.45 was studied, but gives a trend, Figure 6.2.

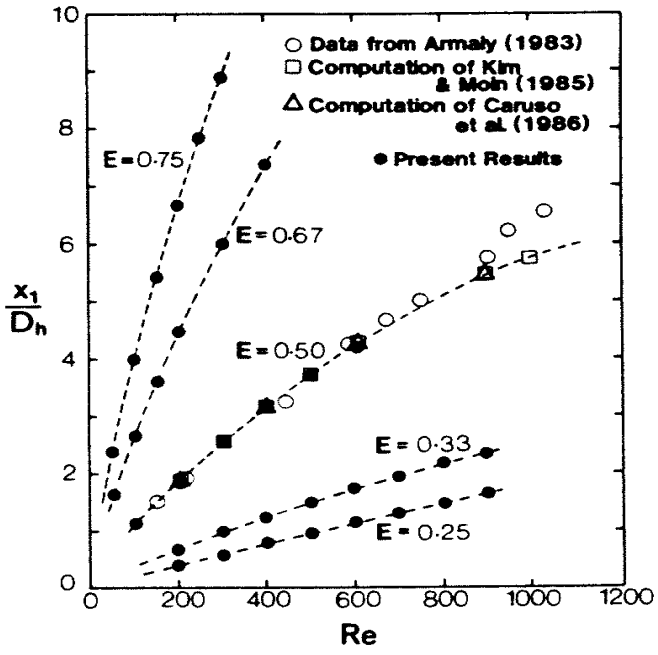

Figure 6.1: Variation of Reattachment length for varying Re and E, Thangam and Knight [2]

6.1.2 Top Boundary Condition

Other more important factor to be considered is the top boundary condition. Numerical solution for the above flow field can be carried out with various top boundary conditions (a)

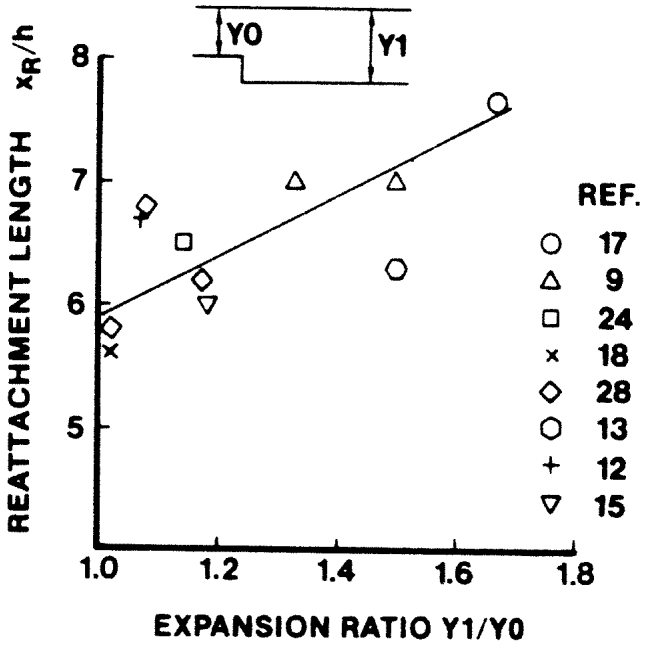

Figure 6.2: Variation of Reattachment length with E, Eaton and Johnston [1]

rigid lid with free slip (b) rigid lid with no slip (c) free surface. The boundary condition of the first type can be used if one wants to replicate the experimental data for symmetric channel flow, or the double sided expansion. Rigid lid condition with no slip replicates the experimental results with single sided step. We will be considering free surface over the top boundary, which is the most relevant case for the atmospheric flow. The number of recirculation zones and the reattachment length varies with the upper boundary condition. From the literature available we compile some of the results over wide range of Reynolds number and different top boundary condition, Figure 6.3.

The recirculation zone 1 is the secondary recirculation zone observed near the step corner. It must be observed that the direction of the vortex is opposite to the vortex in zone 2. Although not much literature is available where this secondary recirculation zone is observed, but its presence has been acknowledged for both transitional and turbulent flow [1],[82],[83]. Although Rabbitt [82] performed numerical experiment for asymmetric flow, it has been referred only for the understanding the physical behavior of the flow. The presence of secondary vortex for laminar flow has not been reported so far. The secondary vortex can be captured if the grid resolves the corner of the step such that the logarithmic layer is resolved [84].

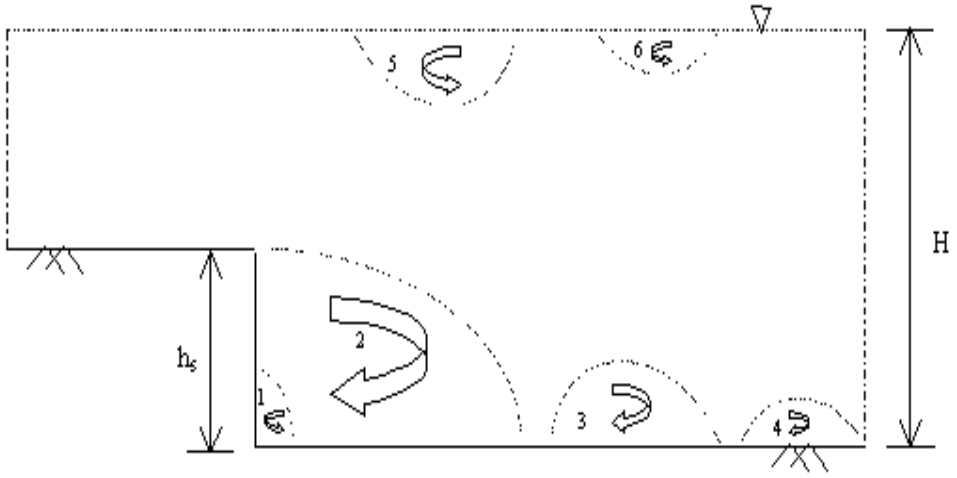

Figure 6.3: Recirculation zones behind formed for flow over backward facing step

The formation of the recirculation zone 5 has been reported only for rigid lid, no slip boundary condition for both laminar [85],[86], [81] and transitional flow. Barton [79] studied the effect of the upper recirculation region which causes the flow retardation and decrease in the reattachment length. Armlay *et al.* [3] experimentally measured and concluded that the upper recirculation zone disappears for $Re > 6600$, which marks the transition of flow to turbulent. The recirculation zone 6 has been reported for the stratified flow [83] which starts appearing in the transitional flow regime Figure 6.4.

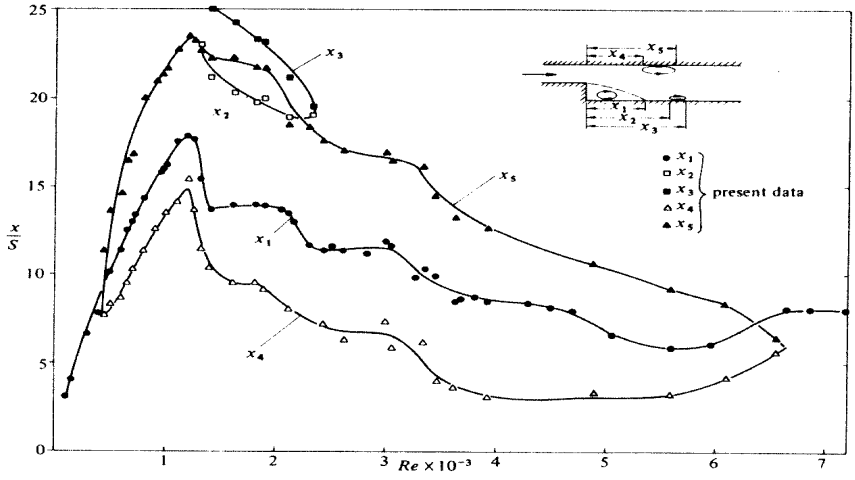

Figure 6.4: Recirculation zone variation with Re, Armlay *et al.* [3]

The presence of recirculation zone 4 has been reported for the free surface flow in the Laminar flow regime [87] at high Froude number. The recirculation zone 3 has been reported for rigid-lid boundary conditions too for laminar flow [2], [3]. Armlay concluded from his experiment that the appearance of recirculation zone 3 marks the start of transition zone and disappears for $Re > 2300$, Figure 6.4.

Table 6.1: Recirculation Zones

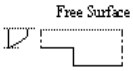	Laminar Flow	Zones 2,3,4 appear depending upon the Froude number of the flow.
	Transitional flow	
	Turbulent flow	Zones 1 and 2.
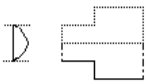	Laminar Flow	Zones 2 and 3
	Transitional flow	Zones 1 and 2
	Turbulent flow	Zones 1 and 2
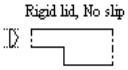	Laminar Flow	Zones 2 and 5
	Transitional flow	Zone 2 ,5 and Zone 3 when Re<2300 Occurance of zone 1 and 6 is reported for stratified flow.
	Turbulent flow	Zone 1,2

From the numerical and experimental data above we conclude that in the turbulent flow regime we can observe only the recirculation zone 1 and 2. Since the grid we have considered is does not resolves the corner and also the logarithmic boundary layer is not resolved recirculation zone 1 will not be captured. The recirculation zones that are formed for different upper boundary conditions and flow regime are shown in table 6.1.

6.1.3 Effect of Skin Friction

The treatment of the boundary conditions at the wall plays an important role in the resolution of internal as well as external flow structure. If turbulence model is used such that the solution can be obtained all the way up to the wall then the best results can be obtained, which in return requires fine grid resolution near the surface and corners. This may be computationally expensive. The alternative is the use of some wall function. We have considered that the

logarithmic boundary layer extends from the wall to the mid-point of the first layer. The stresses at the first layer is obtained from the surface coefficient assumed to be constant for a surface [4]. The surface stress coefficient is obtained as:

$$c_f = \kappa^2 \left(ln \left(\Delta_1 / 2 z_0 \right)^{-2} \right) \tag{6.1}$$

where Δ_1 is the thickness of the first layer and z_0 is the surface roughness height. For a surface of constant roughness height, c_f is constant throughout.

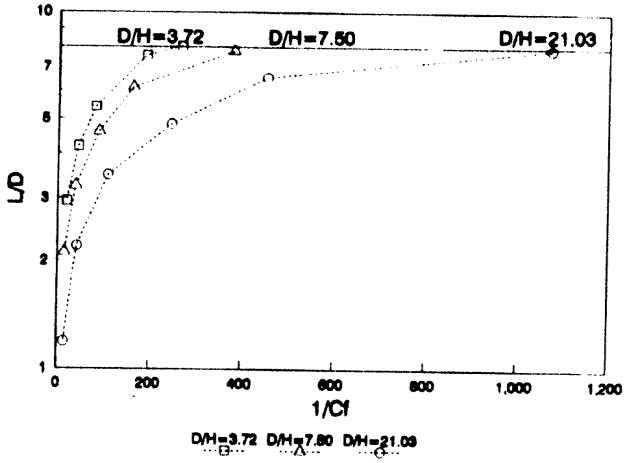

Figure 6.5: Variation of reattachment length with surface friction coefficient, Li and Yu [4]

Jovic and Driver [5] experimentally computed the skin friction coefficient. They used double sided expansion step for varying Reynolds number in turbulent regime. The skin friction coefficient varied along the step Figure 6.6. Numerical simulation of Akselvoll and Moin [88] show good agreement with experimental data. Li [4] plotted the variation of reattachment length with varying skin friction and aspect ratio (domain width: step height) Figure 6.5. Hwang and Peng [84] carried out numerical simulation for turbulent flow using $k - \epsilon$ model using both near wall treatment and modified two layer model valid up to wall. The near wall treatment yielded separation length of 4.2 whereas two layer model yielded 5.2. It is apparent that near wall treatment effects the reattachment length.

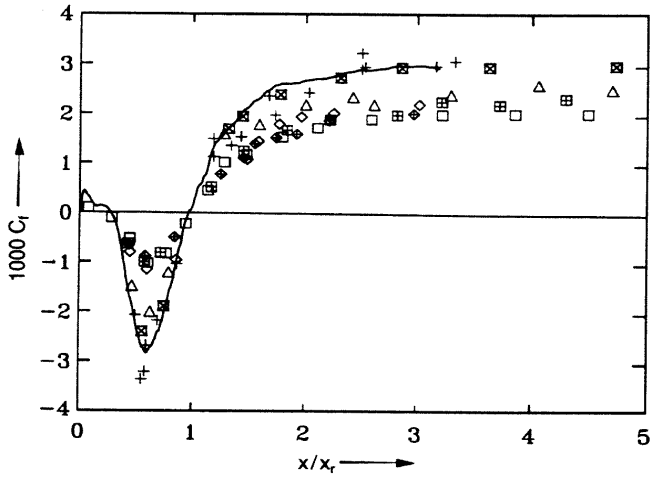

Figure 6.6: Variation of surface friction coefficient along the flow, Jovic and Driver [5]

6.2 Model setup

The simulation is carried out over $40 \times 20 \times 100$ grid points in I,J and K direction respectively. The grid points are packed exponentially near the step along I direction and uniformly along J direction. The spacing of the grid lines increases exponentially normal to the surface. The thickness of the first layer is few millimeter. The step height is 0.3 m and the domain depth is assumed to be three times the step height $H/h_S = 3$. The downstream boundary is present at approximately $20h_s$. The step is located $5h_S$ from the upstream boundary. The Reynolds number at which the simulation has been performed is $Re = 5 \times 10^4$. The width of domain is $6.5h_S$ which is sufficient enough to maintain the two-dimensionality of the flow.

As discussed above top boundary is assumed to be free surface and on either side radiation boundary condition is applied. On downstream boundary pressure boundary condition is applied such that the surface elevation is zero. Radiation boundary prevents the gravity wave, Rossby wave etc , due to the free surface to move out of the domain without reflection. Coriolis force is neglected for the flow simulation hence Rossby wave wouldn't appear.

6.2.1 Inflow Boundary

For rigid lid, no slip top boundary condition the inflow velocity profile is obtained from the fully developed channel flow, whereas for the free slip condition half the channel flow profile is prescribed as it represents the double expansion flow. Since we are simulating the free surface

flow the turbulent velocity profile for flow over a flat plate is used, which is approximated as ([23] eqn 6.251):

$$\frac{\hat{u}(\eta)}{\hat{u}_e} = Atan^{-1}(\Gamma\eta) + B\left(1 - e^{-\Gamma^2\eta^2}\right)[tanh(b\eta^a)]^{1/2} + \Gamma_1\eta^2 e^{-\Gamma\eta/\alpha_0^1.2} \tag{6.2}$$

where, $\eta = \frac{z}{\theta}$, θ is the momentum thickness of the turbulent boundary layer; $\Gamma = \alpha_0^2 R_\theta [c_f/2]^{1/2}$, R_θ is the Reynolds number based on momentum thickness; $A = R_\theta c_f/2\Gamma$; $B = 1 - A\pi/2$; $\alpha_0 = 0.3$. The velocity profile can be computed for zero pressure gradient flow over flat plate. The fluid depth is assumed to be the momentum thickness and the free surface evolves as the edge of the shear layer.

6.3 Results

This numerical simulation is performed to evaluate the performance or the new nonlinear model. The model is tested by both *a priori* and *a posteriori* analysis. Piomelli *et al.* [89] coined these terms for evaluating the performance of the subgrid stress model. In *a priori* analysis the stresses are computed by the different models using the DNS data and the results are compared. Hence there is no direct LES required and insight can be obtained about the physics of the different models. The *a posteriori* analysis is used to compare the stresses obtained from the subgrid scale model, after it has been implemented in a LES, with the DNS or the experimental data. This test is the ultimate test of model performance, but it incorporates other sources of error such as numerical method, grid discretization, averaging etc, so the detailed physics of the problem or model is not captured. Here we present both the test for the new nonlinear model.

6.3.1 A Priori Test

An *a priori* test is performed using the DNS data, because of the unavailability of the DNS data here the a priori analysis is performed with the velocity data obtained from the LES simulation using Smagorinsky model. The stresses from the Smagorinsky, mixed nonlinear and new nonlinear model has been compared. Although it is not exactly an *a priori* analysis which uses the DNS solution to compare the results, the results presented below gives some insight into the model behavior. The normal stress τ_{xx} comparison shows significant correlation between new-nonlinear model and Smagorinsky, Figure 6.7,6.8. However, the nature of distribution of

stress is same as that of the mixed-nonlinear model. The new-nonlinear model gives larger shear stress τ_{xy} than the Smagorinsky model, whereas mixed-nonlinear gives smaller value. The peak of the stress for new-nonlinear and Smagorinsky model are nearly at the same location, Figure 6.9, 6.10.

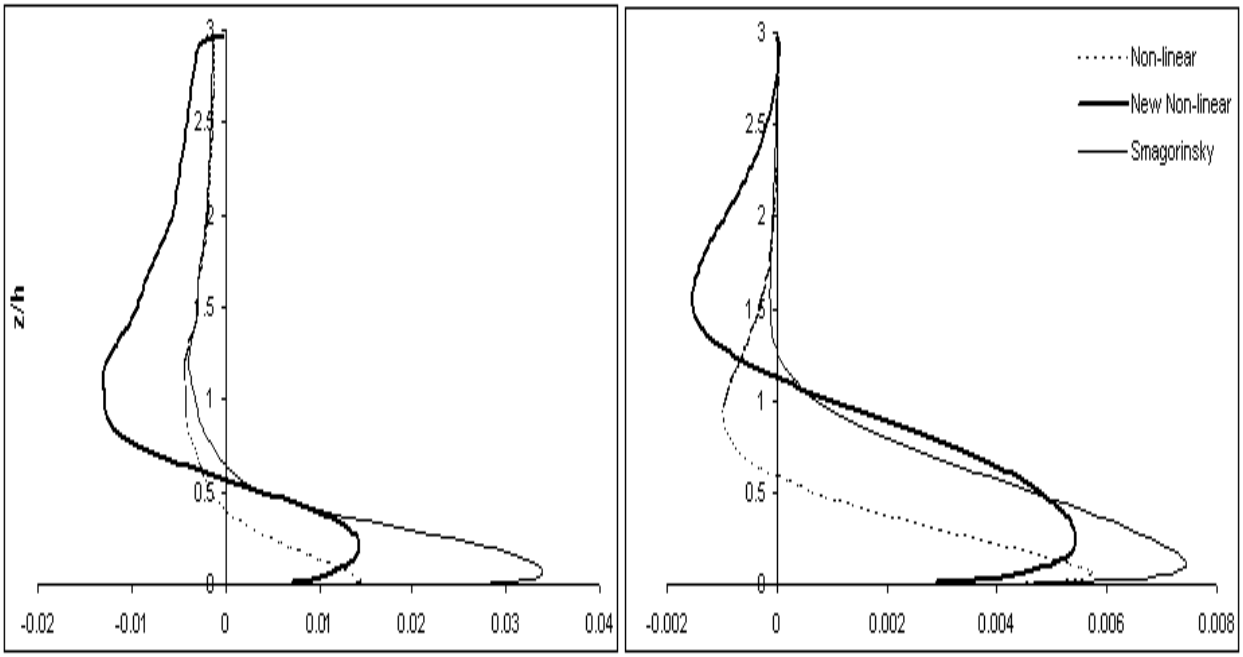

Figure 6.7: τ_{xx} compared for different subgrid stress models at various locations

6.3.2 A Posteriori Test

The new nonlinear model is implemented in the code and clipping is performed so that deterministic solution is obtained. The reattachment point obtained from this simulation is nearly at $x_R/h_S = 5.2$. Which is underprediction as compared to other model simulation, 5.7 by using $K-\epsilon$ model by Speziale [7], 6.4 as reported by Murali [81], 6.7 by Ghosal et al [20] as well as experimental result [6] who obtained $x_R/h_S = 7 \pm 1$. The reattachment length obtained by different for different upper boundaries in turbulent flow regime has been presented in table 6.2. We have added some recent results to the data set of Eaton and Johnston. The reattachment length varies from 4.5 to 8. Free surface data so far available are in transition-turbulent zone hence no definite conclusion can be drawn. But it is apparent that presence of free surface decreases the reattachment length. Other important parameter which effects the reattachment

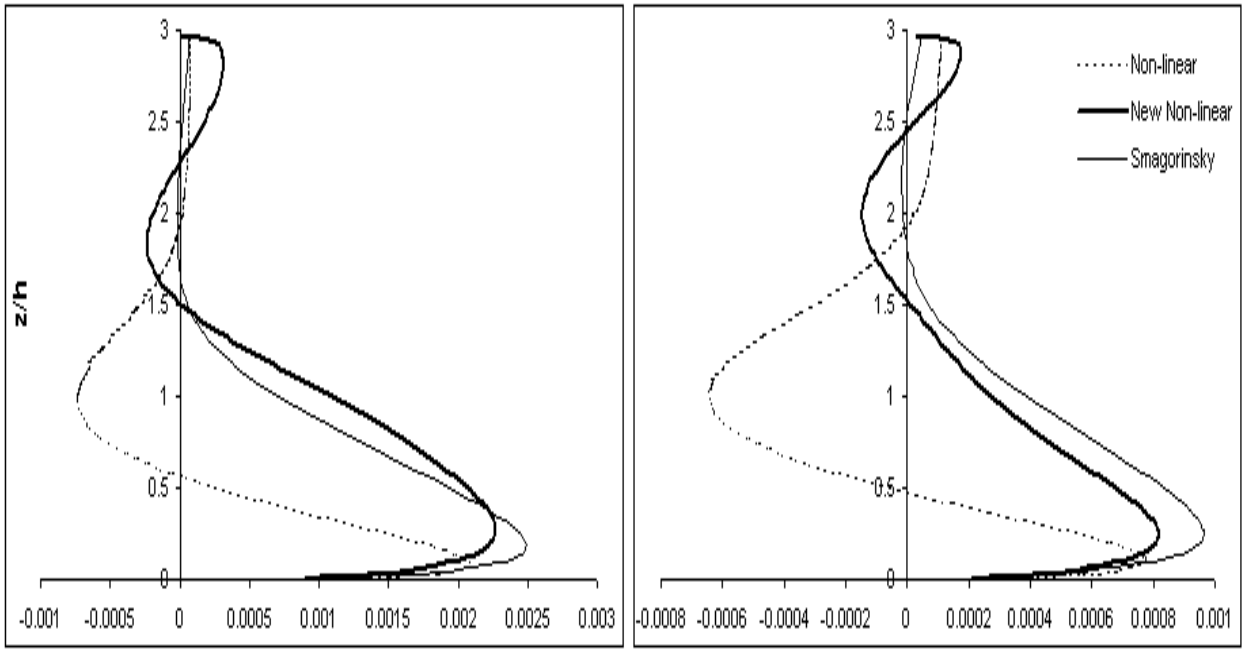

Figure 6.8: τ_{xx} compared for different subgrid stress models at various locations

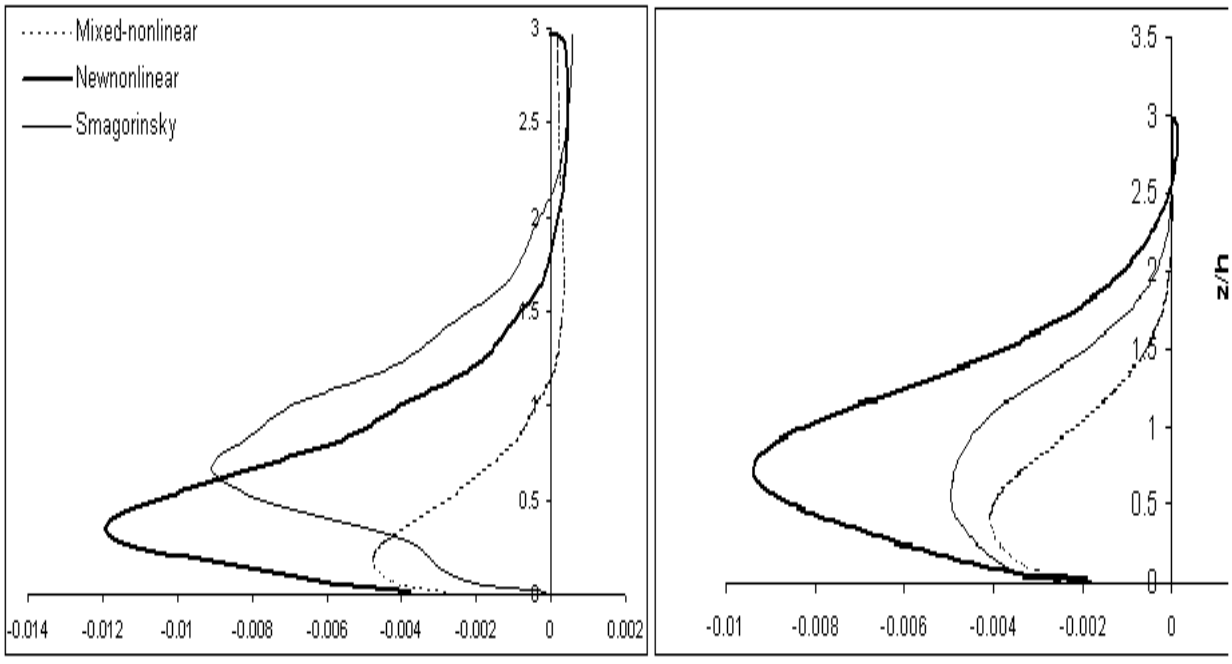

Figure 6.9: τ_{xy} compared for different subgrid stress models at various locations

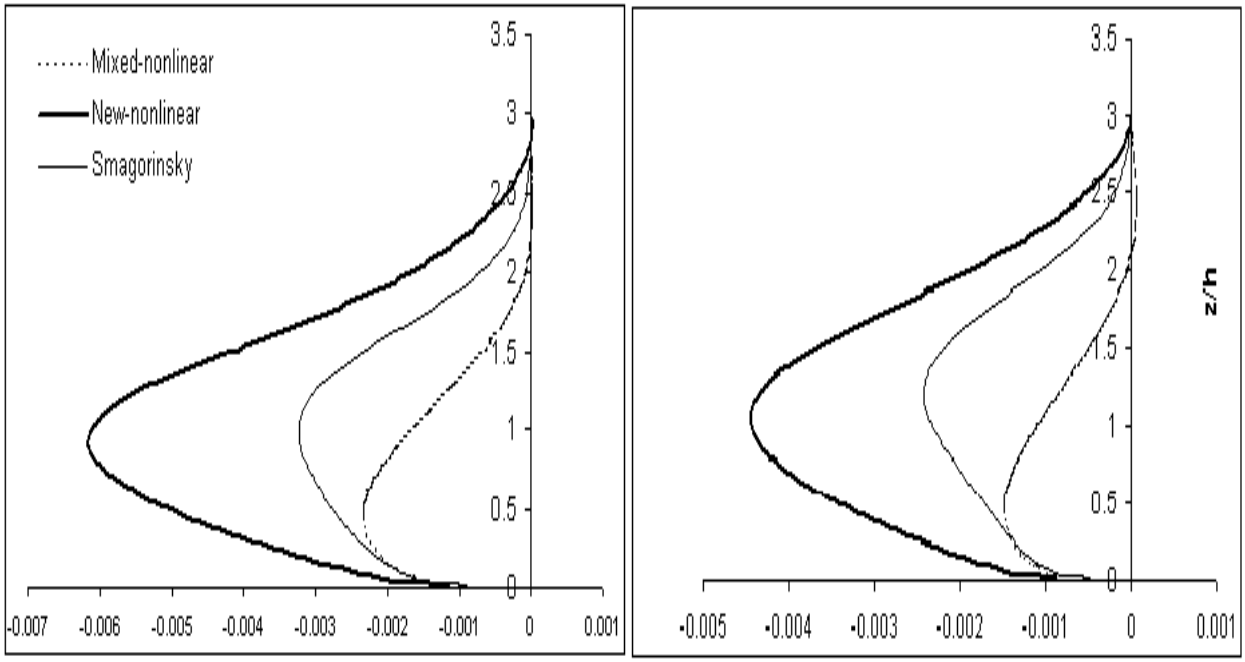

Figure 6.10: τ_{xy} compared for different subgrid stress models at various locations

length is near wall treatment [84]. This inference can be supported by a double-layer use in log wall region by Avva *et al.* [7] which gives larger separation than that of Speziale's simulation [7]. The separation length also varies depending on the fineness of grid [90]. Moreover the governing equations are hydrostatic which may cause discrepancy in the result.

Velocity profile and TKE is compared with the experimental result (velocity profile data extracted from Kim *et al.* [6] and TKE data is taken from Speziale [7]) and show very good match. It can be observed that the turbulent velocity profile is not recovered completely even far away from the step which may be because of the boundary condition. TKE distribution shows a good comparison.

The production dissipation balance has been shown in Figures 6.20. The production due to subgrid stresses in the horizontal stresses is small and their nature is shown in Figure 6.22.

The normal stresses τ_{xx} and τ_{yy} plots at locations situated downstream are shown in Figures 6.24, 6.25. It is evident that the magnitude of stresses decreases as we move downstream. It must be observed that the the normal stresses are absolutely positive contrary to the *a priori* analysis. The change in stress distribution (τ_{xy}) nature can be observed when the flow is in recirculating, attaching and far downstream regions from the Figures 6.26, 6.27.

Table 6.2: Reattachment length, * data from Eaton and Johnston [1]

Author	***Re***	**Boundary**	**Numerical scheme**		X_R/h_s
Present	5×10^4	Free surface	LES, New nonlinear model		5.2
Akselvoll & Moin	5.1×10^3	No slip	LES, dynamic localization model		6.1
Driver *et al.*	3.7×10^4		Experiment		5.3-6.8
Neto *et al.*	3.8×10^4	No slip	LES, Smagorinsky type model with Kraichnan's spectral eddy viscosity		8.1
Jaw and Hwang	3×10^4	Free slip	Two-scale low-*Re*		4.5
Hwang *et al.*	3.7×10^4	Free slip	Second-order Reynold's stress closure with near wall resolution		6.1
	5.4×10^4				7.0
Kim *et al.*	$(4\text{-}5.5)\times10^4$	No slip	Experimental		7±1
Zienkiewicz *et al.*	3×10^3	No slip	Split characteristic based semi-implicit scheme		5.6-5.7
Bellucci and Bruno	3×10^5	No slip	Incompressible flow with combustion, k-ε model		5.1
Ilinca *et al.*	5×10^4	No slip	Adaptive unstructured grid, k-ε model	Coarse mesh	5.63
				Fine mesh	6.2
Denaro	6×10^4	No slip	Local average DNS		8.0
Etheridge &Kemp		Free surface	Experiment		4.2
Ross&Larock	4.7×10^4	No slip	Alebraic stress method		6.6
Murali & Warsi	6.6×10^3	No slip	Fractional time stepping		6.4
Abott & Kline	$2\text{-}5\times10^4$	Free slip	*		7±1
Avva *et al.*	1×10^5	No slip	Fine mesh, double –layer log wall region		6.3
Speziale	1×10^5	No slip	k-ε model		5.7

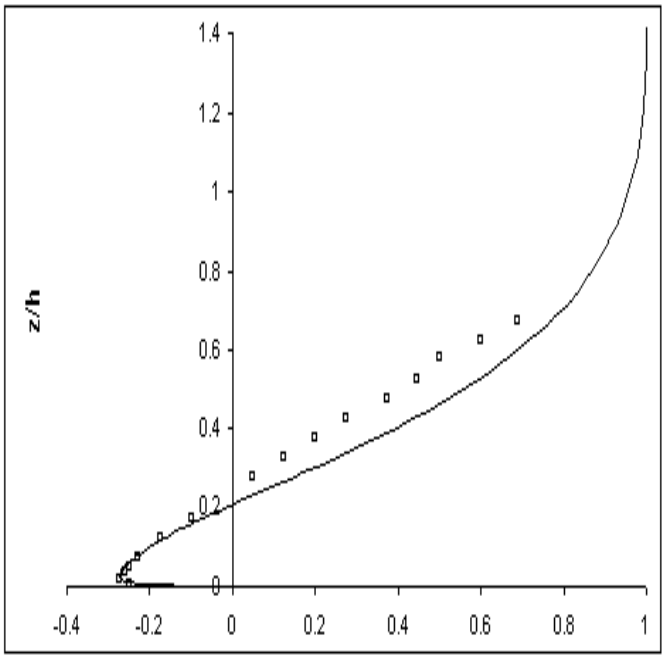

Figure 6.11: U velocity compared with experimental data [6] at $x/h_S = 5.33$

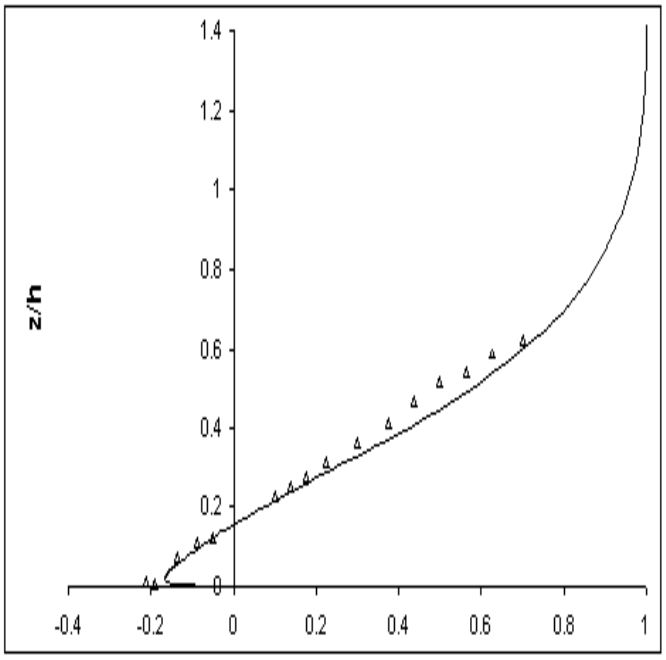

Figure 6.12: U velocity compared with experimental data [6] at $x/h_S = 6.22$

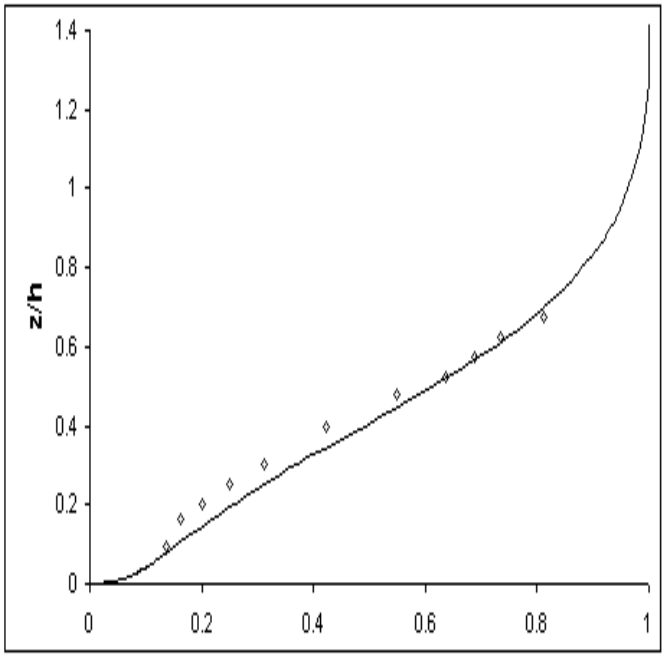

Figure 6.13: U velocity compared with experimental data [6] at $x/h_S = 7.11$

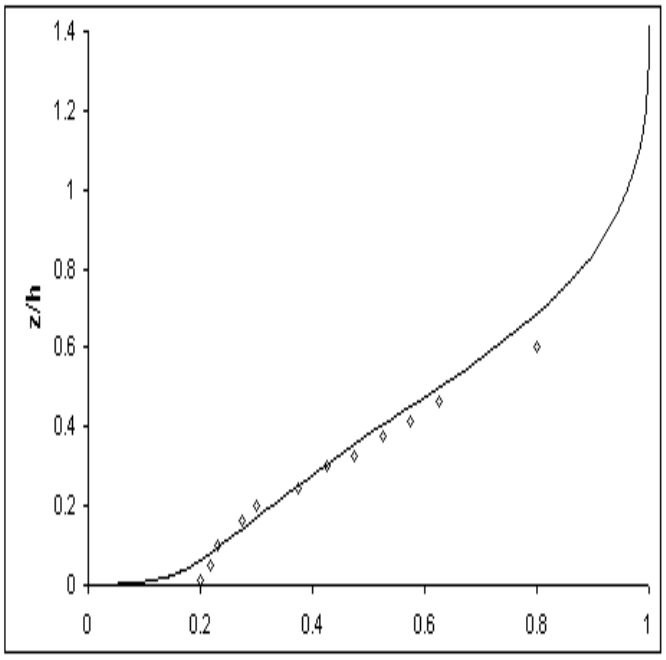

Figure 6.14: U velocity compared with experimental data [6] at $x/h_S = 8.0$

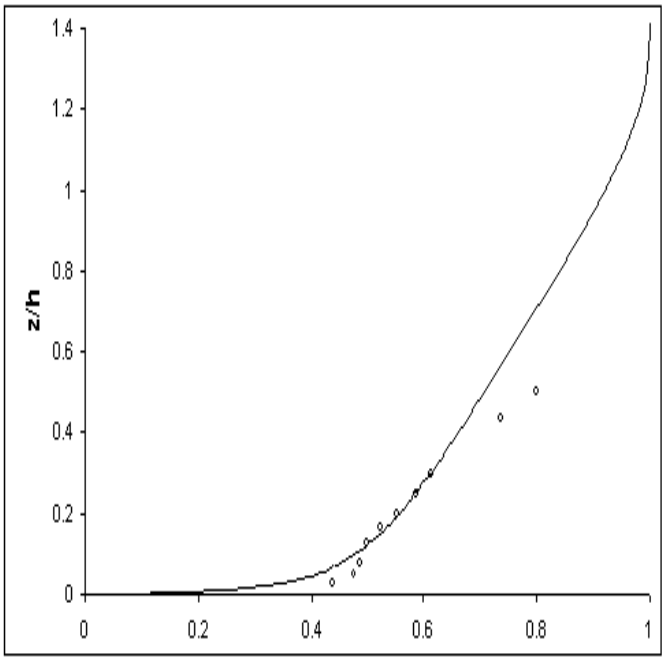

Figure 6.15: U velocity compared with experimental data [6] at $x/h_S = 10.67$

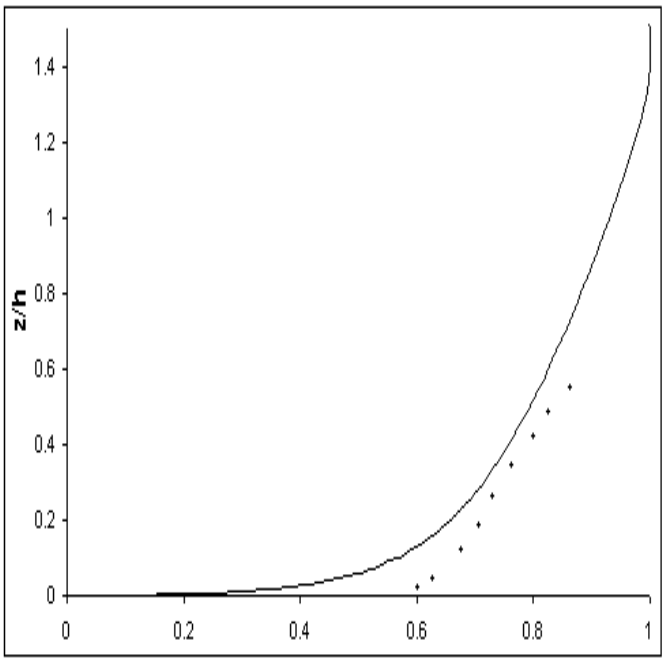

Figure 6.16: U velocity compared with experimental data [6] at $x/h_S = 16.0$

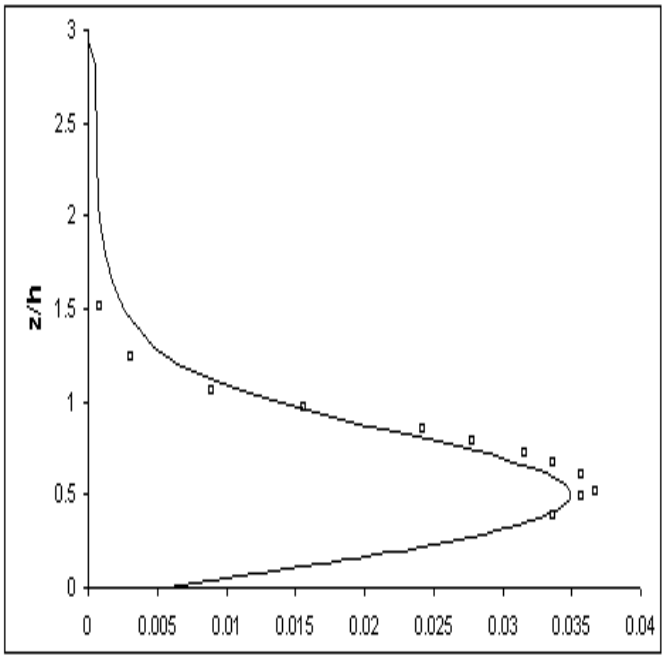

Figure 6.17: K/U^2 compared with experimental data [7] at $x/h_S = 7.667$

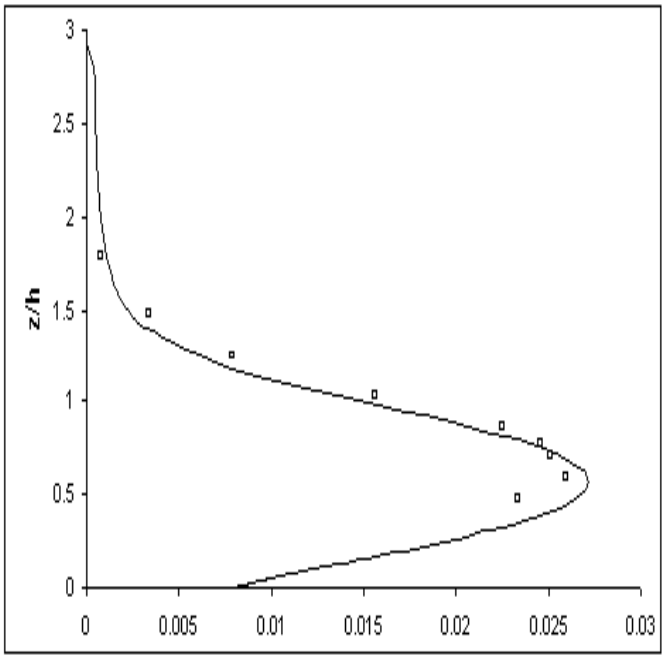

Figure 6.18: K/U^2 compared with experimental data [7] at $x/h_S = 8.533$

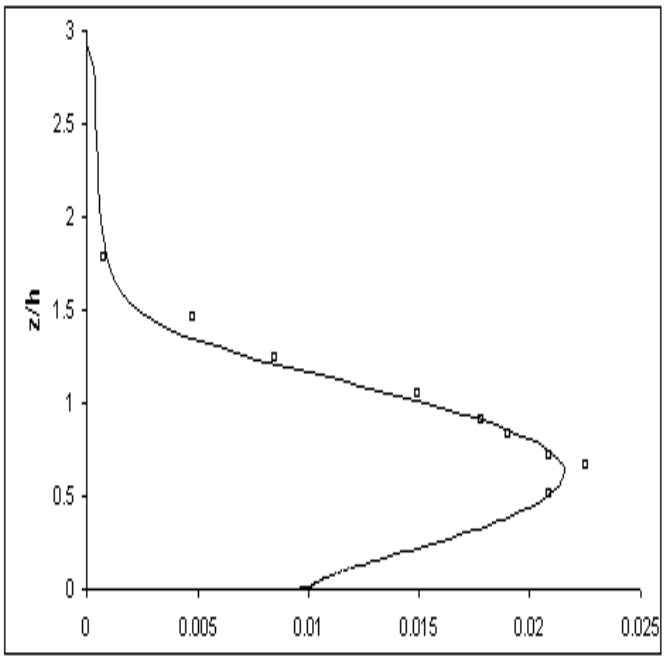

Figure 6.19: K/U^2 compared with experimental data [7] at $x/h_S = 10.33$

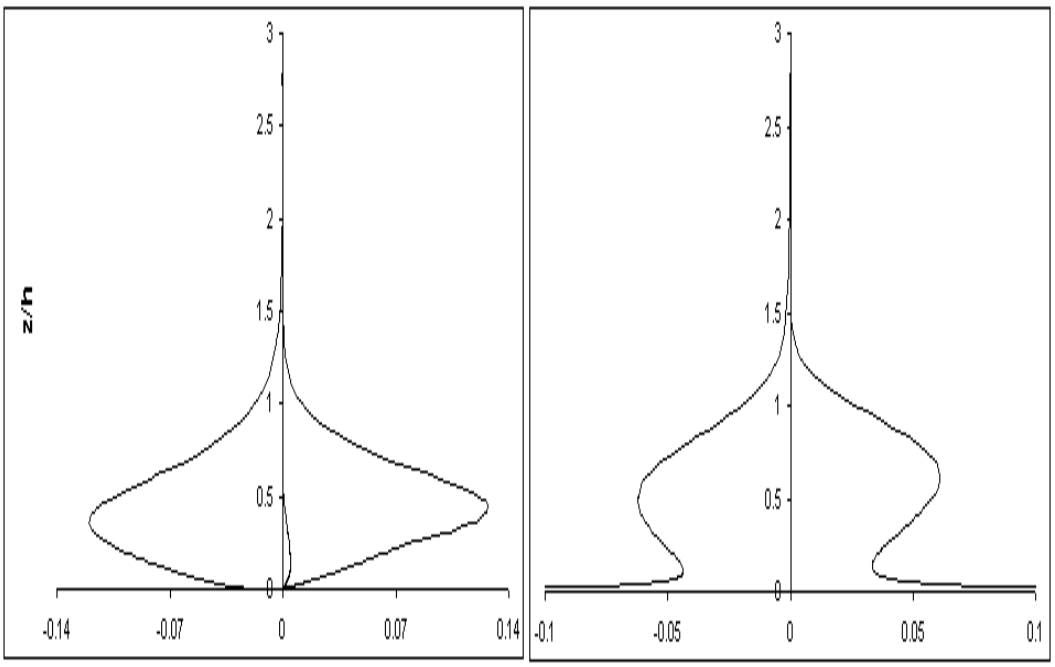

Figure 6.20: The production-disspation balance at different locations

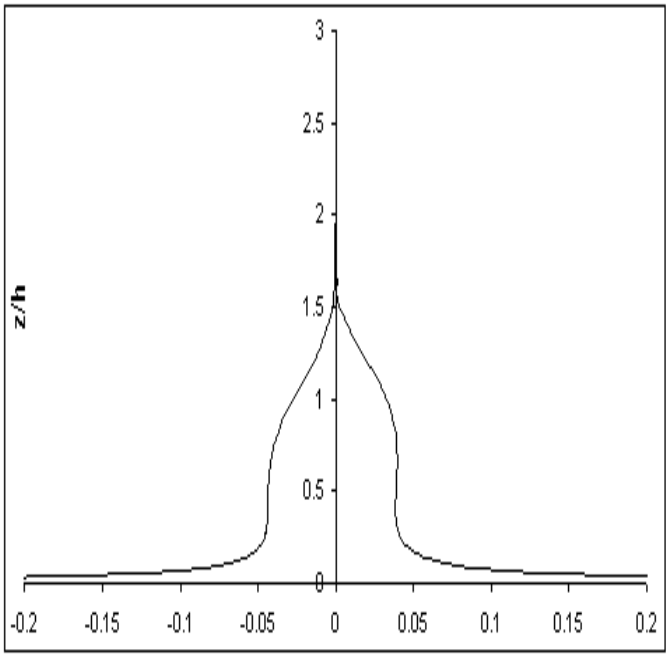

Figure 6.21: The production-disspation balance at different locations

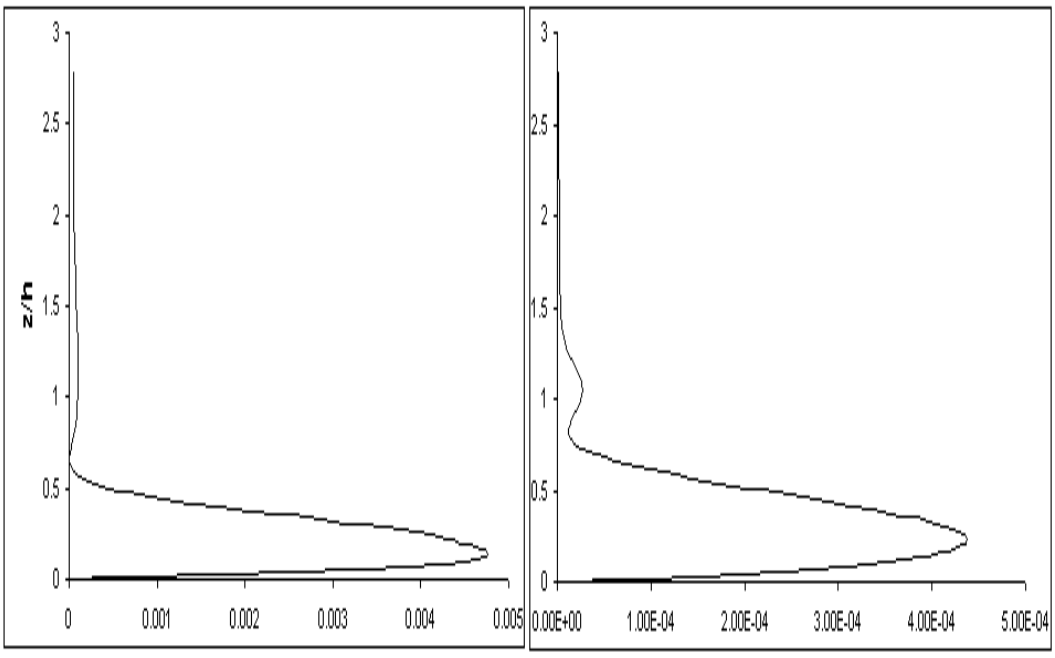

Figure 6.22: Production term due to subgrid stresses at different locations

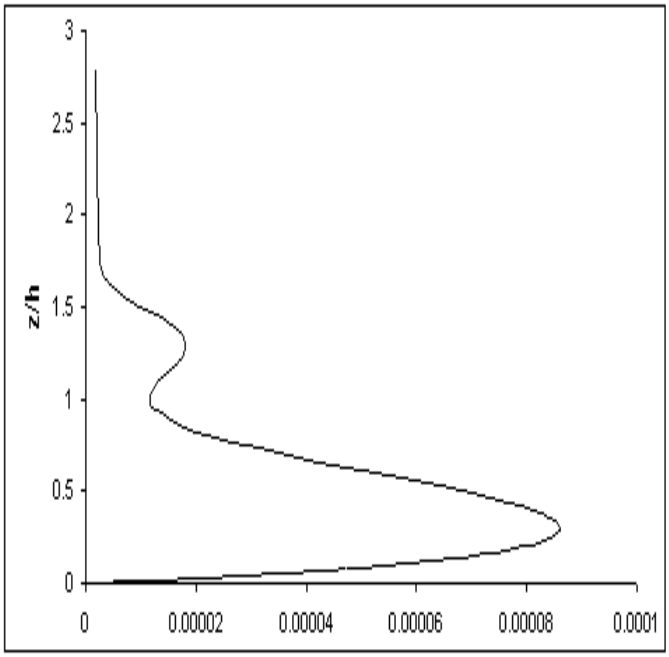

Figure 6.23: Production term due to subgrid stresses at different locations

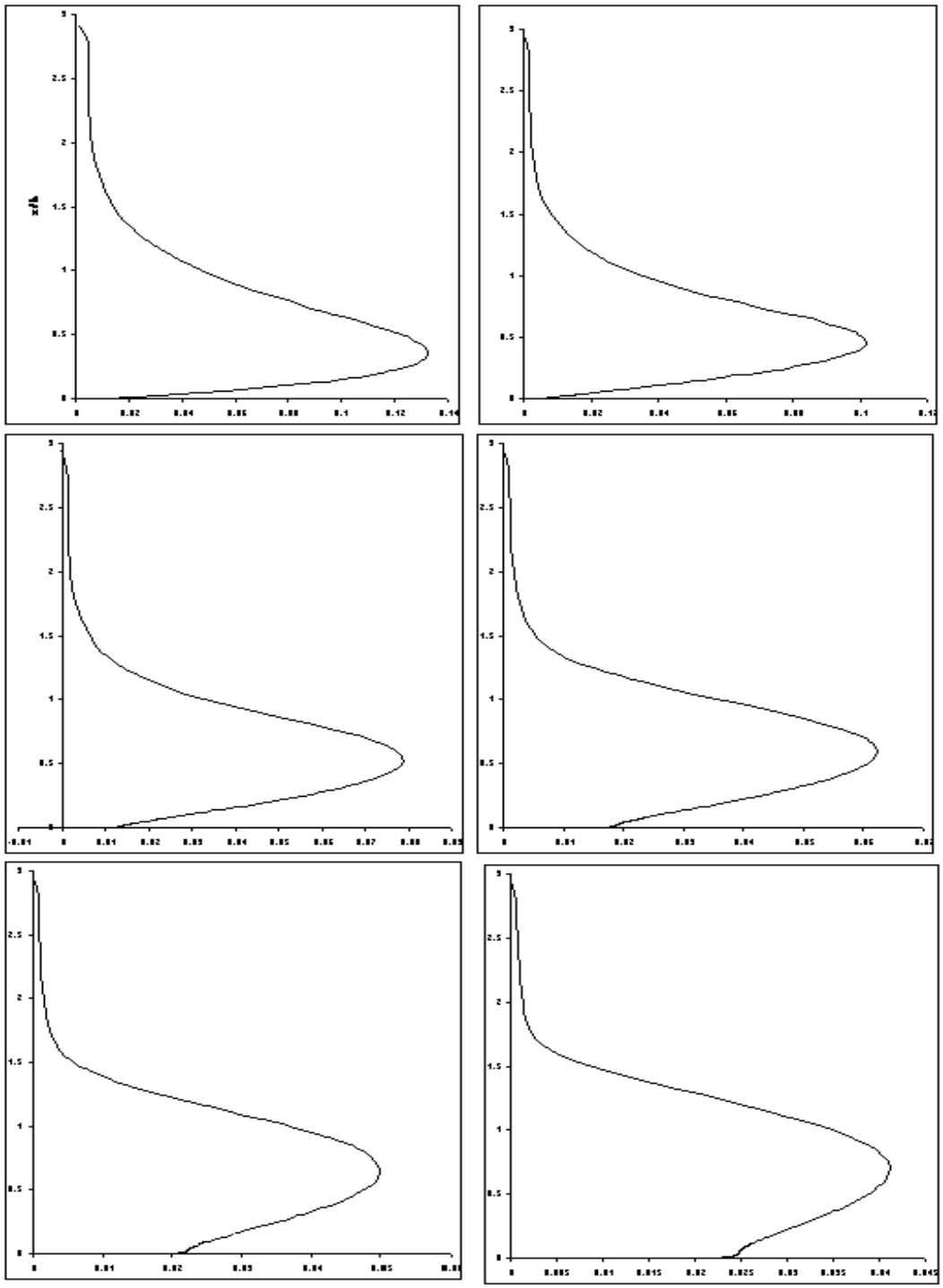

Figure 6.24: τ_{xx} plot at different locations

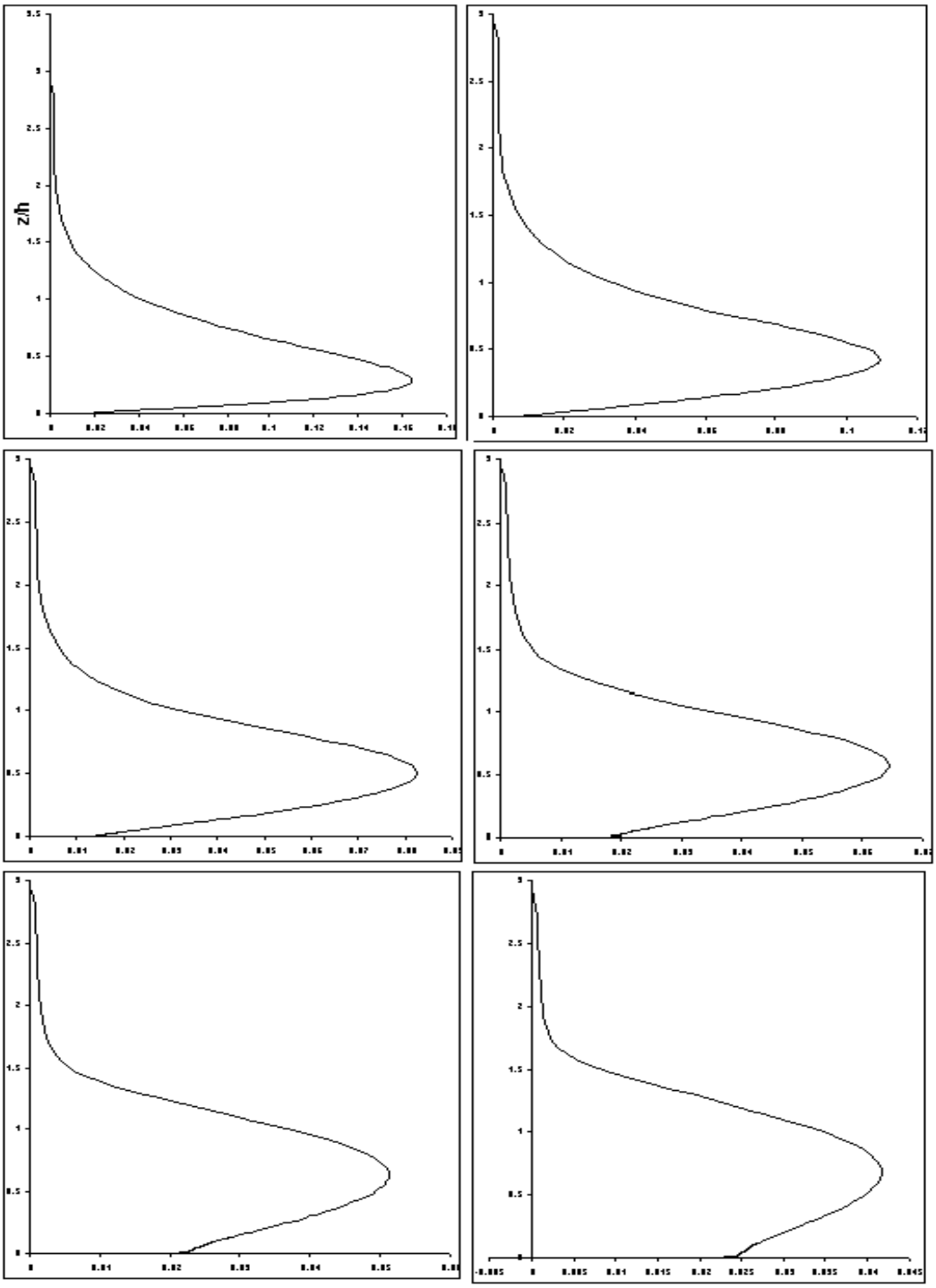

Figure 6.25: τ_{yy} plot at different locations

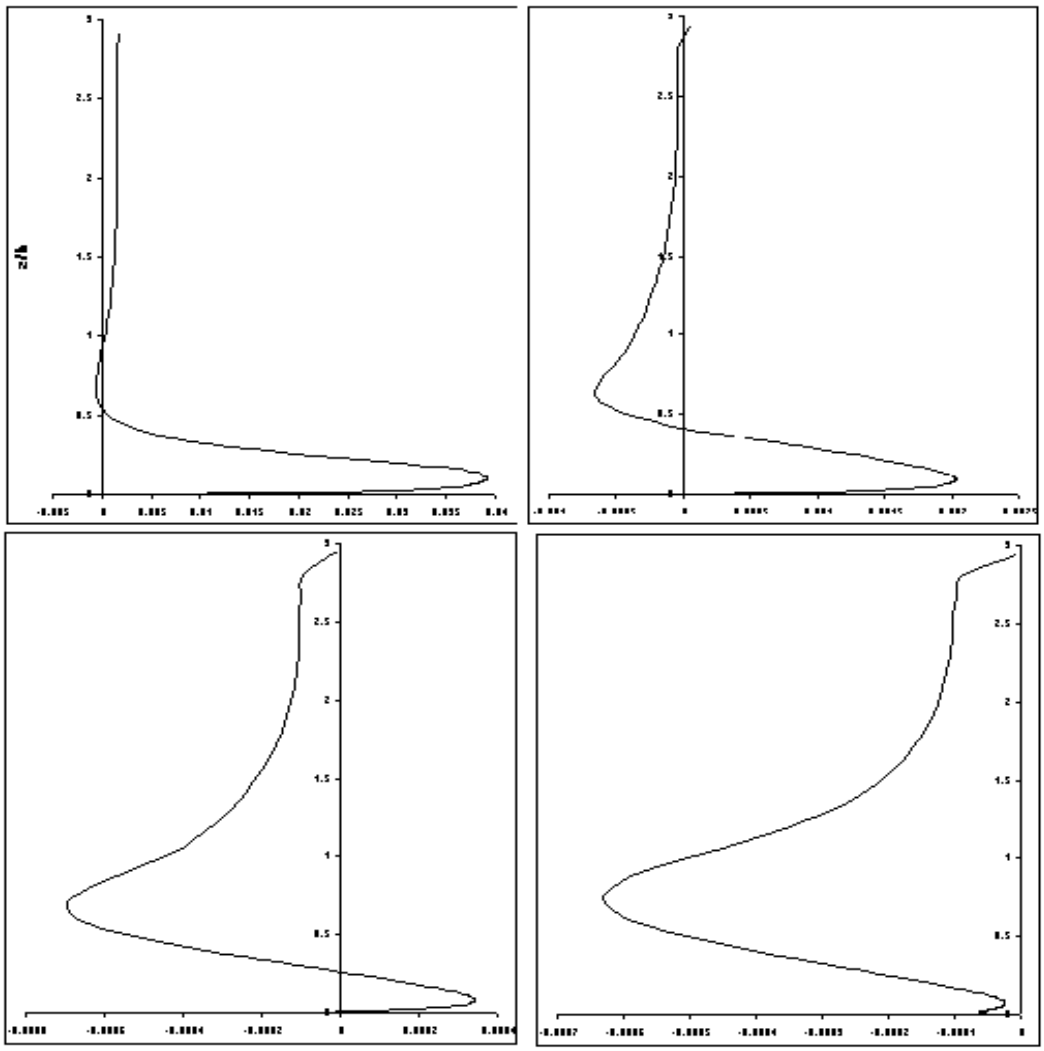

Figure 6.26: τ_{xy} plot at different locations, A

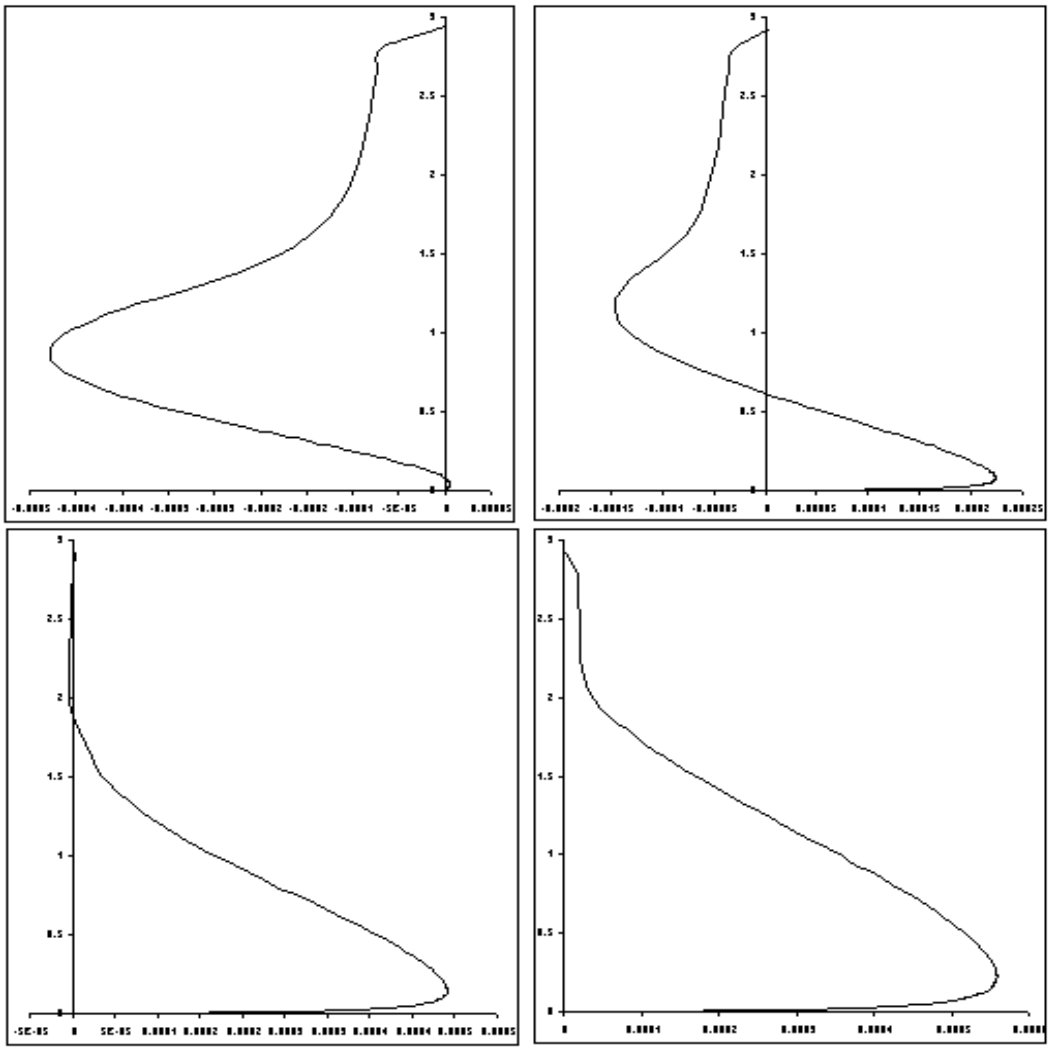

Figure 6.27: τ_{xy} plot at different locations, B

CHAPTER VII

FLOW OVER AN ELLIPTIC MOUNTAIN RIDGE

Stratified flow over an elliptic mountain ridge forms an important hydrodynamic flow of geophysical application. This flow has been studied extensively theoretically by linear gravity wave theory [91][92] for $Fr \gg 1$ and by potential theory [93] valid for $Fr \ll 1$. But when $Fr \sim O(1)$ the approximations are no longer valid and hence the analytical solution can not be obtained. Hence numerical simulation has to be performed to study such flow. Various authors have studied different aspect of the flow such as Olfasson and Bougeault [94] studied the nonlinear flow over three-dimensional elliptic mountain for varying Froude number, Afanasyev and Peltier [95] studied the flow over two-dimensional ridge whereas Bauer *et al.* [96] studied the effect of aspect ratio on the flow field. Vosper [97] studied the three-dimensional flow field over circular mountain. There has been efforts by other authors too to study the effect of stratified flow [98], [99], [100]. But little effort has been done to study the effect of the turbulence in such flow fields. Usually the physics of the turbulent flow is lost in presence of other effects such as baroclinic effect. Here we study only the turbulence effect on stratified flow over two-dimensional elliptic mountain ridge. The density stratification is assumed to be constant in time such that the baroclinic instability is eliminated. Hence the solution of the temperature equation is not required and the stability does not change in the flow interior. The vortex generation mechanism in such flow field is studied through the Mean Square Vorticity Fluctuation (MSVF) rate equation, which has been modeled to get more insight.

The hydrostatic equation, as discussed earlier, is used to solve the flow. The flow phenomenon is studied with respect to the lee wave/lee vortices generation and upstream blocking effect. The new nonlinear model has been implemented in the simulation and the flow has been studied for varying Froude number in the range, $Fr \sim 1$. For the stratified flow the Froude number is defined as $Fr = \frac{Nh_M}{U}$, where U is the inflow velocity which is assumed constant throughout the fluid depth, h_M is the mountain height and N is the Brunt-Vaisala frequency. Brunt-Vaisala

frequency is the parameter which describes the stratified flow. The other parameter which is important for the flow considered here is Richardson number, Ri, which describes the interaction of the buoyancy effect and turbulent flow. The flow considered here depend on these parameters and has been defined in the following section.

7.1 Brunt-Vaisala frequency

The variation of density effects the incompressible flow through inertia and gravity effect. The interplay of both these parameters are the most intriguing aspect of Stratified flow [101]. The simulation here is under the hydrostatic assumption which includes the density variation with respect to gravity effect and the inertia effect is neglected. The stratified flow is described in terms of a few dominant parameters, one of which is Brunt-Vaisala or Buoyancy frequency. Let a small fluid volume δV is displaced by a small distance δz in a stable atmosphere, which is characterized by a negative density gradient. Then the fluid volume in the new location has higher density than the surrounding and hence the buoyancy force acts on the volume in the downward direction. Similarly when the fluid volume is displaced downwards then the buoyancy force acts upwards so that the effect of buoyancy is to direct the flow toward the starting position, hence buoyancy acts as a restoring force. From the Newton's second law of motion we have $F_i = ma_i$ which gives

$$\begin{aligned} \rho_0 \epsilon z g \delta V &= \rho_0 \delta V \frac{d^2 z}{dt^2} \\ \frac{d^2 z}{dt^2} + \epsilon g z &= 0 \end{aligned} \tag{7.1}$$

where ϵ is the density gradient $-\frac{1}{\rho_0}\frac{\partial \rho}{\partial z}$. The above equation can be identified with the one dimensional simple harmonic motion, which characterizes the wave motion. This wave motion can be identified with gravity wave which can exist only in stable atmosphere. The eigen frequency of the motion is thus,

$$N^2 = -\frac{g}{\rho_0}\frac{\partial \rho}{\partial z} \tag{7.2}$$

The above parameter is called the Brunt-Vaisala frequency and governs the gravity wave. Long [102] developed a linear model which gives a valid steady state solution up to the point of

overturning. The hydrostatic form of Long's equation is

$$\delta_{zz} + \frac{N^2}{U_0^2}\delta = 0 \tag{7.3}$$

where $\delta(x, z)$ is the field of vertical displacement from which the velocity field $u(x, z)$ and $w(x, z)$ can be determined:

$$\begin{aligned} u &= U_0(1 - \delta_z) \\ w &= U_0\delta_x \end{aligned} \tag{7.4}$$

The solution of the above linearized equations show the presence of waves in the stratified flow called the lee waves [101]. These equations form the basis of the mountain waves and significant research has been done to simulate the other complex phenomenon such as flow splitting, wave breaking, flow reversal, three dimensional effects etc.

7.2 Richardson Number

In a statistically stable environment the turbulent vertical velocity motion acts against the force of gravity. The effect of the density is to suppress turbulence while the shearing stresses tend to generate turbulence mechanically [69]. The Richardson number is conventionally defined as the ratio of negative buoyant production to the shear production

$$R_f = -\frac{P_b}{P_s} \equiv \frac{\beta g \overline{\acute{w}\acute{T}}}{\overline{\acute{u}\acute{w}}\frac{\partial \overline{u}}{\partial z} + \overline{\acute{v}\acute{w}}\frac{\partial \overline{v}}{\partial z}} \tag{7.5}$$

Further, using the modeling for the stress terms we obtain the gradient Richardson number which is physically more plausible.

$$R_i = \frac{\beta g \frac{\partial \overline{T}}{\partial z}}{\left(\frac{\partial \overline{u}}{\partial z}\right)^2 + \left(\frac{\partial \overline{v}}{\partial z}\right)^2} \tag{7.6}$$

The above parameters can be expressed in terms of the buoyancy gradient which can be related to the temperature gradient. The coefficient of the eddy viscosity for temperature flux can be

related to the eddy viscosity of the vertical shear stress through the Prandlt number, Pr.

$$\kappa_T = \frac{\nu_T}{Pr}$$

It is fairly well established experimentally that $0.7 < Pr < 0.85$

7.3 Lee Vortices

Atmospheric observations have indicated the existence of alternately ascending and descending air currents above a mountain range and stationary waves at various heights on the lee side of the mountain called lee waves. The mechanism for the production of these vortices has been investigated thoroughly by many authors, [103],[104]. It has been well established that the isentropes bends causing an inversion of the density stratification locally producing the vortices. More insight can be obtained from the conservation of the potential-vorticity. For the inviscid flow the vorticity equation can be written as:

$$\frac{D\boldsymbol{\omega}}{Dt} = (\boldsymbol{\omega} \cdot grad)\,\mathbf{u} + \frac{1}{\rho^2}\,(grad\ \rho \times grad\ p) \tag{7.7}$$

The first term on the right hand side represents the rate of change of ω due to stretching and turning of the vortex lines and the second term the creation of vorticity by baroclinic effect. For two-dimensional flow the baroclinic effect is responsible for the generation of the vorticity. For the three-dimensional flow the vortex stretching term cause the vortex in the plane to produce vortex in the vertical plane [105]. Most of the geophysical application observe the baroclinically produced vorticity mostly and has been studied extensively. But the effect of turbulence on such flow phenomenon has been discarded this far in all studies. Here we are studying the turbulence generated vortex phenomenon. The baroclinic effect has be ignored by assuming gradient of density and pressure to be parallel. Numerical experiment has been carried out for stable, neutral and unstable boundary layer. The most important governing parameter in our simulation is Richardson number which can be related to the buoyancy frequency. The mean vorticity equation is written as

$$\frac{\overline{D}\overline{\boldsymbol{\omega}}}{Dt} = (grad\ \overline{\mathbf{u}}) \cdot \overline{\boldsymbol{\omega}} + \nu\nabla^2\overline{\boldsymbol{\omega}} + div\left(\overline{\acute{\mathbf{u}}\acute{\boldsymbol{\omega}}} - \overline{\acute{\boldsymbol{\omega}}\acute{\mathbf{u}}}\right) \tag{7.8}$$

The buoyancy effect does not appear in the mean vorticity transport equation but appears in the vorticity generation mechanism. The transport equation for Mean Square Vorticity Fluctuation (MSVF) can be thought analogous to the Turbulent kinetic equation and hence the correlation terms can be defined as production, dissipation and transport [23]. The transport equation of MSVF ($\phi = \frac{1}{2}\overline{\acute{\boldsymbol{\omega}} \cdot \acute{\boldsymbol{\omega}}}$) is obtained as

$$\frac{\partial \phi}{\partial t} + \overline{u}_j \frac{\partial \phi}{\partial x_j} = -\overline{\acute{\omega}_i \acute{u}_j} \frac{\partial \overline{\omega_i}}{\partial x_j} - \frac{\partial}{\partial x_j}\left(\overline{\acute{u}_j \psi}\right) + \overline{\acute{\omega}_i \acute{\omega}_j \acute{D}_{ij}}$$
$$+\overline{\acute{\omega}_i \acute{\omega}_j}\ \overline{D}_{ij} + \overline{\omega}_j \overline{\acute{\omega}_i \frac{\partial \acute{u}_i}{\partial x_j}} + \nu \nabla^2 \phi - \nu \overline{\left(\frac{\partial \acute{\omega}_i}{\partial x_j}\right)^2} + \beta g \left(\overline{\acute{\omega}_1 \frac{\partial \acute{T}}{\partial x_1}} - \overline{\acute{\omega}_2 \frac{\partial \acute{T}}{\partial x_2}} \right) \tag{7.9}$$

where, $\psi = \frac{1}{2}\acute{\boldsymbol{\omega}} \cdot \acute{\boldsymbol{\omega}}$ and the physical interpretation of the terms are

$$P^{\omega} = -\overline{\acute{\omega}_i \acute{u}_j} \frac{\partial \overline{\omega_i}}{\partial x_j} + \overline{\acute{\omega}_i \acute{\omega}_j \acute{D}_{ij}} + \overline{\acute{\omega}_i \acute{\omega}_j}\ \overline{D}_{ij}$$

The above terms represent the production of vorticity by different mechanism such as shear, turbulent stretching, stretching/squeezing of vorticity by mean rate-of-strain and mixed production respectively. For the two dimensional flow only one vortex term exists and the vortex stretching terms are zero.

$$P^{b\omega} = \beta g \left(\overline{\acute{\omega}_1 \frac{\partial \acute{T}}{\partial x}} - \overline{\acute{\omega}_2 \frac{\partial \acute{T}}{\partial y}} \right)$$

This term represents the stretching of vorticity by buoyancy. For the two-dimensional case as only one component of density/ potential temperature variation exist, which is along 'z' direction, so the production due to the above term is zero.

$$F^{\omega} = \frac{\partial}{\partial x_j}\left(\overline{\acute{u}_j \acute{\omega}_i \acute{\omega}_i}\right)$$

The term is the turbulent diffusion of the vorticity, while the term

$$\epsilon^{\omega} = \nu \overline{\left(\frac{\partial \acute{\omega}_i}{\partial x_j}\right)^2}$$

is the dissipation of vorticity. Thus the equation of MSVF can be written as :

$$\frac{\partial \phi}{\partial t} + \overline{u}_j \frac{\partial \phi}{\partial x_j} = P^{\omega} + P^{b\omega} + F^{\omega} - \epsilon^{\omega} + \nu \nabla^2 \phi \tag{7.10}$$

These terms can be modeled analogous to the turbulent kinetic energy terms. Defining turbulent viscosity coeffient for vorticity acoording to the one-equation model as

$$\nu_T^{\omega} = C_{\omega} l^2 \phi^{1/2} \quad \text{and} \quad \epsilon^{\omega} = D^{\omega} \phi^{3/2}$$

where length scale is obtained from the turbulent kinetic energy and dissipation, $l = b_3 \frac{K^{3/2}}{\epsilon}$. For the two-dimensional flow mixed production term is absent hence only the shear production is present. The effect of the buoyancy term does not appear in the MSVF equation so far. To capture the physics of the problem we assume the production term $-\overline{\acute{\omega}_i \acute{u}_j} \frac{\partial \overline{\omega_i}}{\partial x_j}$ to consist of two terms one due to shear production and other due to buoyancy. Only one component of the temperature (or density gradient) is present so the buoyant production will have only one component. Production and diffusion terms are modeled as

$$P^{\omega} = A^{\omega} \left(\overline{D}_{ij} \overline{D}_{ij} \right) \phi^{1/2} - \beta g \; B^{\omega} \frac{\partial \overline{T}}{\partial z} \phi^{1/2} \quad \text{and} \quad F^{\omega} = \nu^{\omega} \frac{\partial^2 \phi}{\partial {x_j}^2}$$

The coefficients appearing above can be estimated for the isotropic turbulence. Hence the modeled MSVP transport takes the form

$$\frac{\partial \phi}{\partial t} + \overline{u}_j \frac{\partial \phi}{\partial x_j} = A^{\omega} \left(\overline{D}_{ij} \overline{D}_{ij} \right) \phi^{1/2} - \beta g \; B^{\omega} \frac{\partial \overline{T}}{\partial z} \phi^{1/2} + \left(\nu_T^{\omega} + \nu \right) \nabla^2 \phi - D^{\omega} \phi^{3/2} \tag{7.11}$$

Using the definition of Richardson's number, the same form is obtained from the vorticity equation. The Richardson number governs the flow in the present simulation. Further since we have considered constantly stratified flow the Richardson number can be linearly related to the Froude number ($\frac{Nh}{U}$). Henceforth results will be discussed for varying Froude number.

7.4 Upstream Blocking

This another aspect of mesoscale flow which is observed in highly stratified flow when the vortex is formed on the windward side of the ridge. This phenomenon occurs when the fluids

kinetic energy is not able to overcome the potential barrier of the mountain. This hypothesis was first laid by Sheppard [106]. Simple criterion for upstream blocking can be obtained by Sheppard's theory for continuously stratified fluid.

$$\frac{1}{2}\rho_0 U^2 < g\int_0^h (h-z)\left(-\frac{d\rho}{dz}\right)dz \tag{7.12}$$

Introducing the definition of Brunt-Vaisala frequency above (assuming N being constant with height) we get the criterion of blocking as: $\frac{Nh}{U} > 1$. However studies by Smolarkiewicz and Rotunno [105] contrasts with the phenomenon and suggests that the upstream blocking occurs with the propagation of columnar motion which moves upstream. The columnar disturbances are basically the very long waves in the system. When these disturbances alters the density stratification sufficiently then the upstream blocking is observed. This phenomenon permanently alters the density stratification upstream. Hence study of blocking due to this phenomenon requires that the upstream boundary conditions be adjusted so that the wave are allowed to leave the domain without reflection. The above hypothesis suggests that the lee vortices generation instigates the upstream blocking phenomenon, but laboratory observations suggest upstream motions may appear without lee-ward overturning as studied by Baines [107]. The upstream blocking phenomenon observed in the present study occurs without the leeward vortices and occurs according to the Shepphard's hypothesis. The columnar motion is absent as the density stratification is assumed to be constant throughout the domain as no isentrope bending is present.

7.5 Model Setup

The mountain shape considered in the following simulation is

$$h\,(x,y) = \frac{h_M}{\left[1+(x/L)^2+(y/\beta L)^2\right]^n} \tag{7.13}$$

where β is the aspect ratio, and $\beta \to \infty$ for two-dimensional mountain ; $n = 3/2$; L is the mountain width and h_M is the height of the mountain ridge. The height of the mountain (h_M) is taken to be 200 m. The width of the mountain(L) is taken to be 100 m so that a steeper mountain is obtained. Terrain following vertical coordinate system is used. The horizontal grid used is uniformly distributed with grid length of 25 m in X-direction and 50 m in the Y-direction.

The domain size considered in the numerical simulation is $60 \times 20 \times 100$. The total depth of the domain in the Z-direction is taken to be 1 Km. The grid lines in the vertical direction is stretched exponentially such that the distance between the surface layer and center of the first grid point is the logarithmic layer. The top most boundary is sufficiently far away such that there is no reflection from the upper boundary. Some of the authors have used damping region in upper layers so that the upward propagation of the wave energy is dissipated [108]. Experiment has been carried out with $H/h_M = 3$ which shows significant boundary effect for highly stratified flow. These effects never showed up for $H/h_M = 5$. The grid size in X and Y direction were taken sufficiently large so that the hydrostatic assumption of $\Delta X/\Delta Z \ll 1$ is satisfied and the shallow convection condition is valid. Moreover the modeling of the stress components as Reynolds stress in vertical direction and subgrid stresses in the plane is also supported. The domain length in the X-direction is about 7 times the mountain height in either direction and 5 times along Y-direction. Under these conditions the two-dimensionality of the flow is maintained to a good extent and upstream and downstream are sufficiently far away so that pressure boundary condition is applied on all open boundaries. Pressure boundary condition forces free surface elevation to zero. The inflow conditions is uniform inflow velocity. In most of the numerical experiment inflow velocity is considered to be 5 m/s except for the stable atmosphere flow where input flow velocity is changed. For stable and unstable flow the $Re \sim 1 \times 10^8$. The density stratification is assumed constant for a given specific simulation and assumed to vary linearly.

7.6 Results

The flow is simulated for the model discussed above for neutral, stable and unstable atmosphere. The density is specified in the flow domain varying linearly over the fluid depth such that Brunt-Vaisala frequency is constant over the flow field. In the real atmospheric flow the density becomes constant after certain height and the gravity effect fades out. As the gravity effect has been retained throughout the depth the free stream velocity is not obtained far enough in the vertical direction. It must be noted that in all the countour plots shown below the flow is from left to right.

7.6.1 Neutral atmosphere

If the density is assumed to be constant throughout the domain, i.e the fluid is homogeneous, buoyant production term is zero hence the flow is governed purely by the Reynolds' number of the flow. Turbulent shear is the only production mechanism and the mountain acts as the trigger mechanism for vorticity. Numerical simulation has been performed for varying Reynolds number. When $Re = 1 \times 10^8$ the production term is not sufficiently large to produce vorticity. The production and dissipation balance is shown in Figure 7.1 in the lee of the mountain. The production due to subgrid scale stresses in horizontal plane is small compared to the production by vertical stresses shown in Figure 7.2.

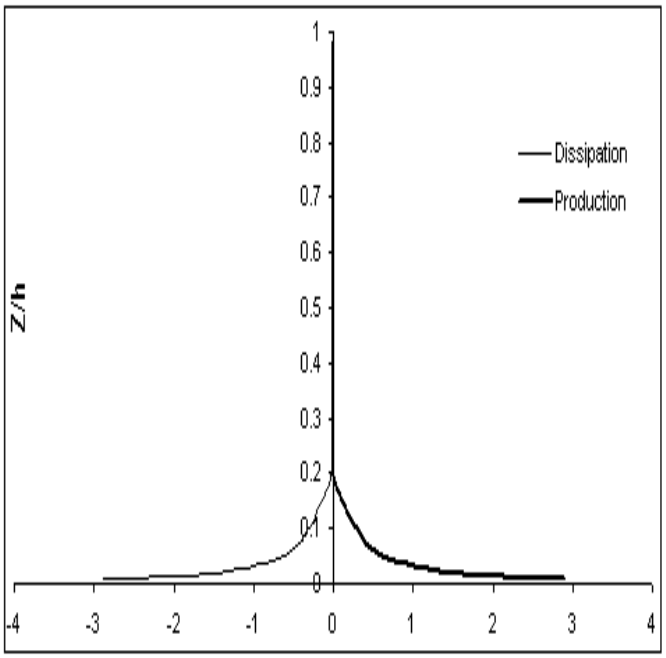

Figure 7.1: Production and Dissipation balance for neutral atmosphere, $10^4 m^2/s^3$

The vorticity generation conditions can also be obtained from the turbulent kinetic energy equation [69] as the production mechanism for vorticity and TKE are the same. Thus concentration of turbulent kinetic energy one of the criteria for wave breaking [94]. When the Reynolds' number is increased to 2×10^8 there is still no vortex in the domain, but concentration of turbulent kinetic energy (TKE) is observed in the lee of the mountain Figure 7.4, 7.6. When the Reynolds' number is further increased to 4×10^8 lee vortices are obtained Figure 7.7, negative

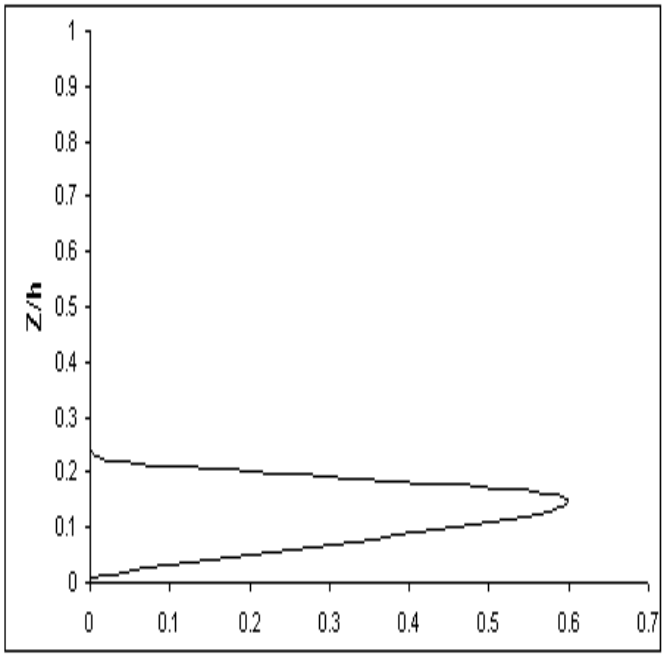

Figure 7.2: Production from subgrid stresses in neutral atmosphere, $10^3 m^2/s^3$

'U' velocity represented by dashed line represents presence of streamline bending. Concentration of the TKE is also observed in the lee of mountain Figure 7.8 .

7.6.2 Stable atmosphere

Stable atmosphere, as discussed above, is defined for which the density gradient is negative or the density decreases as we move upwards. The relation between density gradient and potential temperature gradient can be determined from the *linearized perturbation ideal gas law* for the *shallow convection approximation.* Using the *Poisson's relationship* we get

$$\frac{\acute{\rho}}{\overline{\rho}} = -\frac{\acute{T}}{\overline{T}} \tag{7.14}$$

which concludes that density gradient and temperature gradient are opposite in nature. Hence for stable atmosphere the potential temperature gradient is positive. This implies that the production of vorticity due to buoyancy term is negative hence the buoyancy term dissipates the vorticity, Figure 7.11. So only the turbulent shear leads to the production mechanism. The

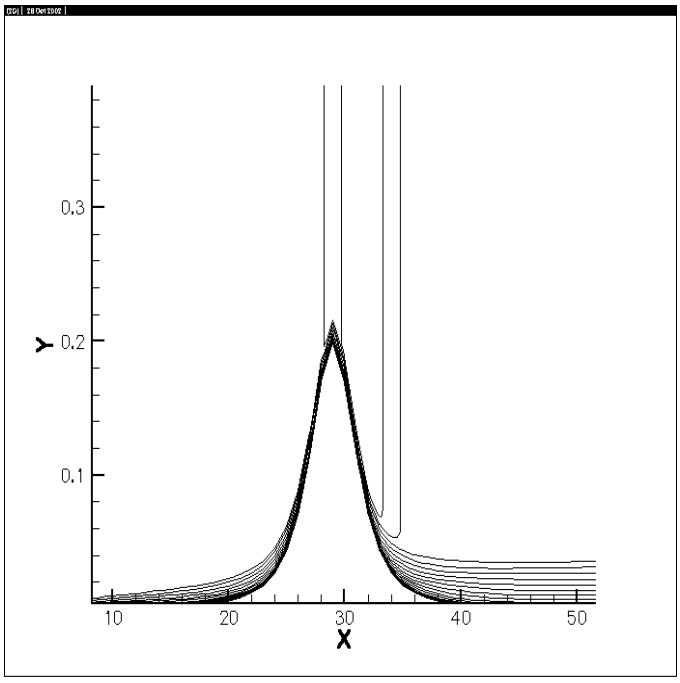

Figure 7.3: U velocity contour for $Re = 1 \times 10^8$, Neutral Atmosphere

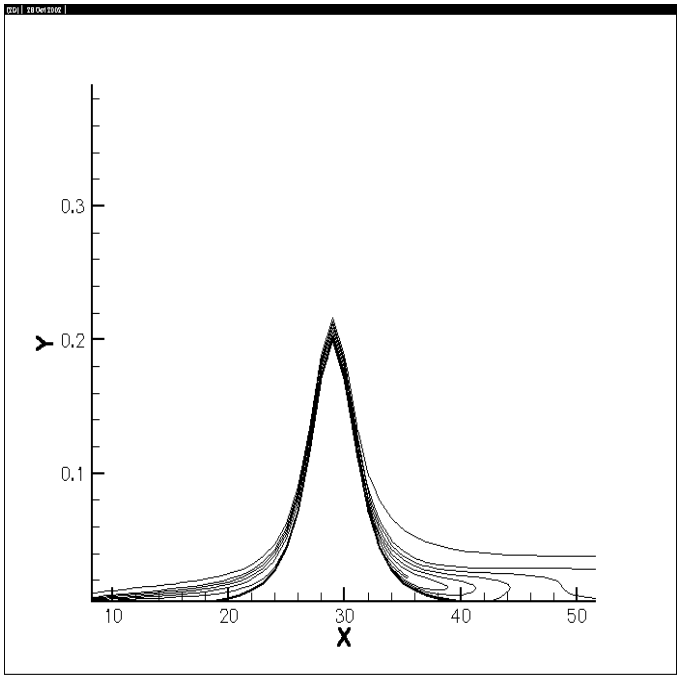

Figure 7.4: TKE contour for $Re = 1 \times 10^8$, Neutral Atmosphere

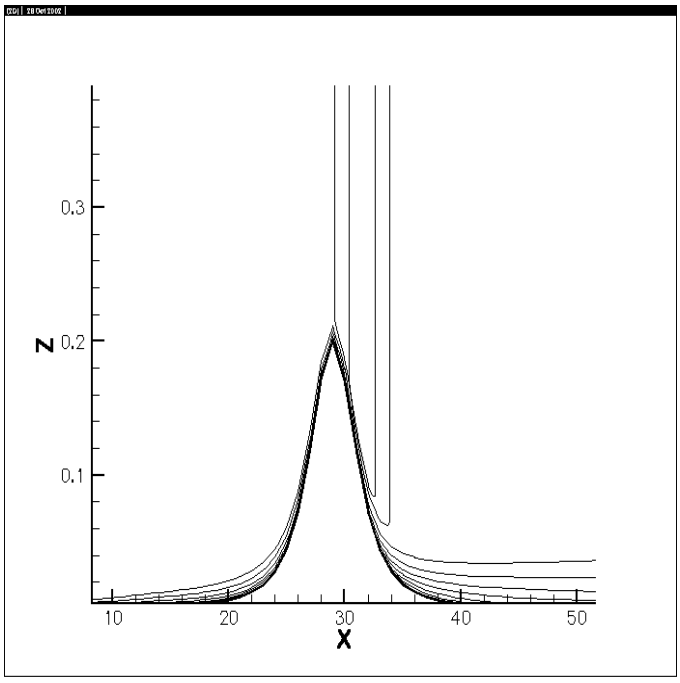

Figure 7.5: U velocity contour for $Re = 2 \times 10^8$, Neutral Atmosphere

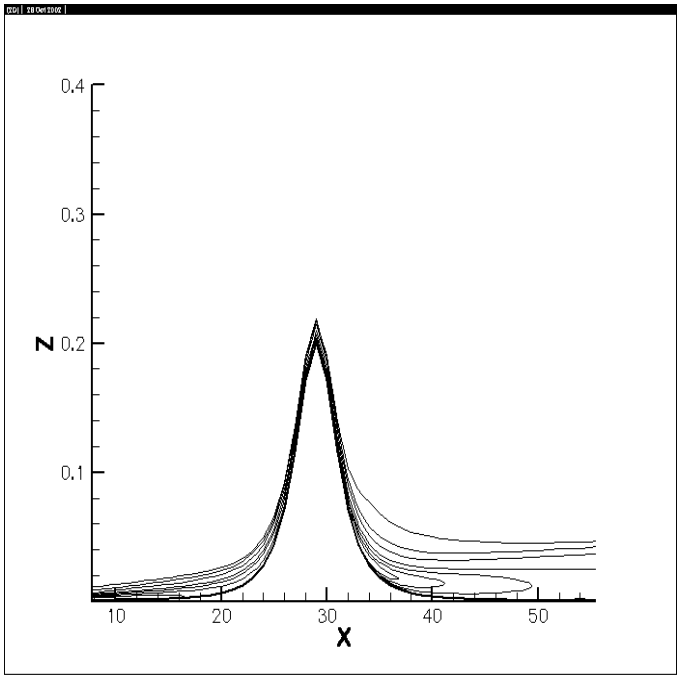

Figure 7.6: TKE contour for $Re = 2 \times 10^8$, Neutral Atmosphere

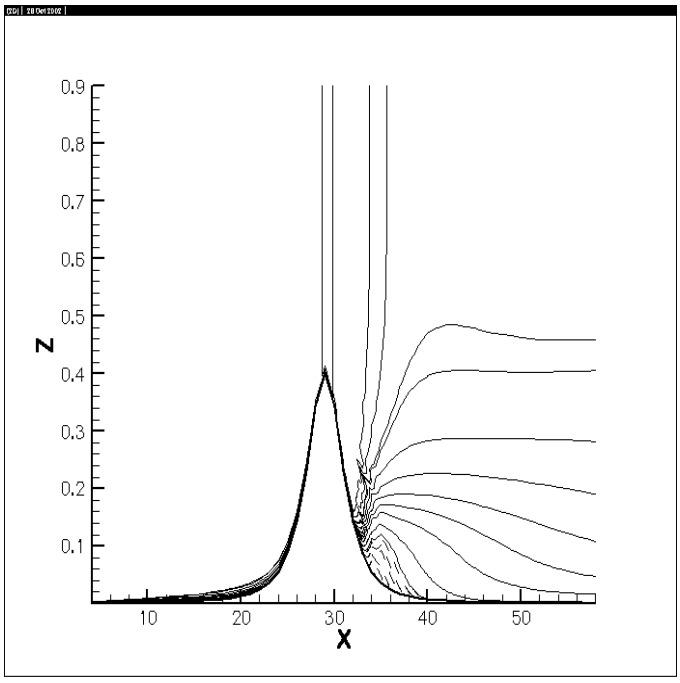

Figure 7.7: U velocity contour for $Re = 4 \times 10^8$, Neutral Atmosphere

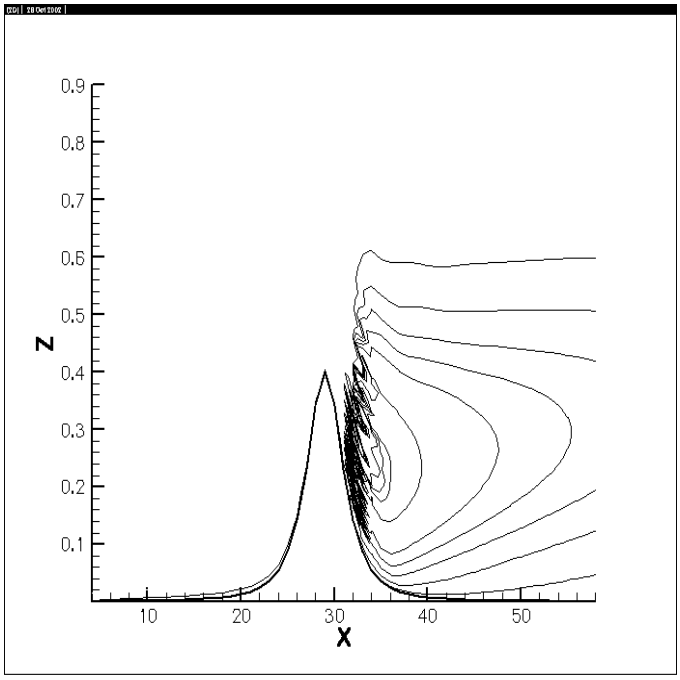

Figure 7.8: TKE contour for $Re = 4 \times 10^8$, Neutral Atmosphere

production due to the horizontal subgrid stress is small compared to these stresses shown in Figure 7.9, 7.10.

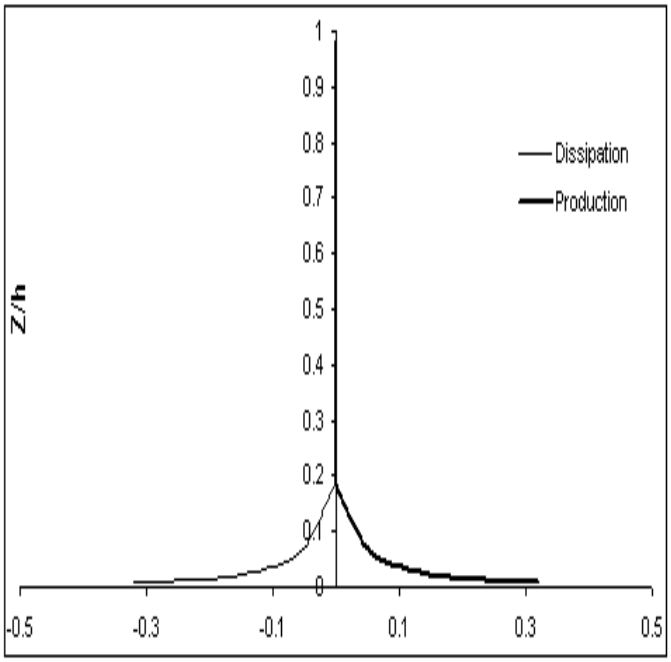

Figure 7.9: Production and Dissipation balance for stable atmosphere, $10^4 m^2/s^3$

As the shear production is not sufficient enough to produce lee vortices for $Re = 1 \times 10^8$, evident from the neutrally stable simulation. Moreover, dissipation of the vorticity is more that the previous case, so lee vortices cannot be observed for this stratification. The results have been presented for $N = 0.0175$ in Figure 7.12,7.13 which do not show any sign of TKE concentration of negative U velocity in the lee of the mountain as expected. However if the density gradient is made more steeper (highly stratified flow) upstream blocking effect is observed. The closer look at the TKE contour for $N = 0.0575$ shows concentration of the TKE near the peak of the mountain on the upwind side Figure 7.15. Upstream blocking effect is observed first when $Fr \cong 2$ which agrees closely to the value 2.14 by Olfasson [94] for elliptic mountain ridge. Baines obtained upstream blocking for $Fr > 1.5$ (Gaussian shaped mountain) ; $Fr > 1.75$ (Witch-of-Angesi shape). The upstream blocking effect become more prominent and negative 'U' velocity can be seen for the highly stratified flow. The vortex moves upwind and is situated at the foot of the mountain Figure 7.16,7.17. However, it must be remembered that the upstream blocking effects observed here are mainly because of Sheppard's hypothesis and not as a consequence of

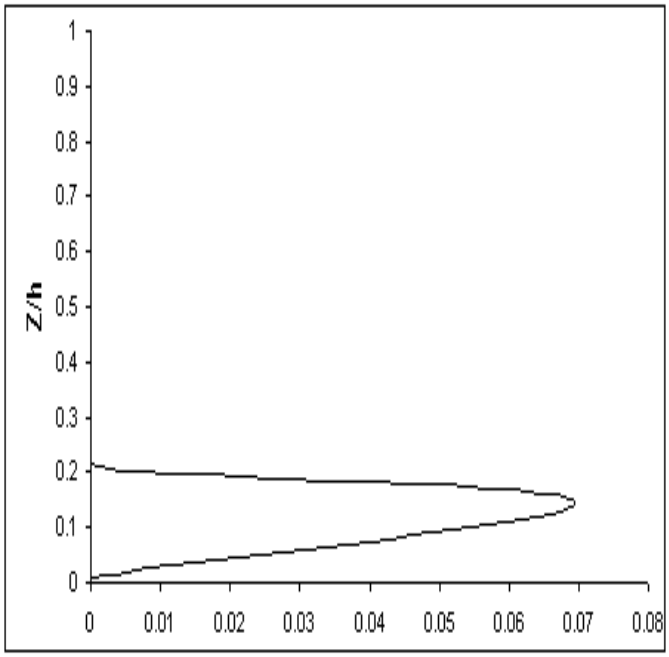

Figure 7.10: Production from subgrid stresses in stable atmosphere, $10^3 m^2/s^3$

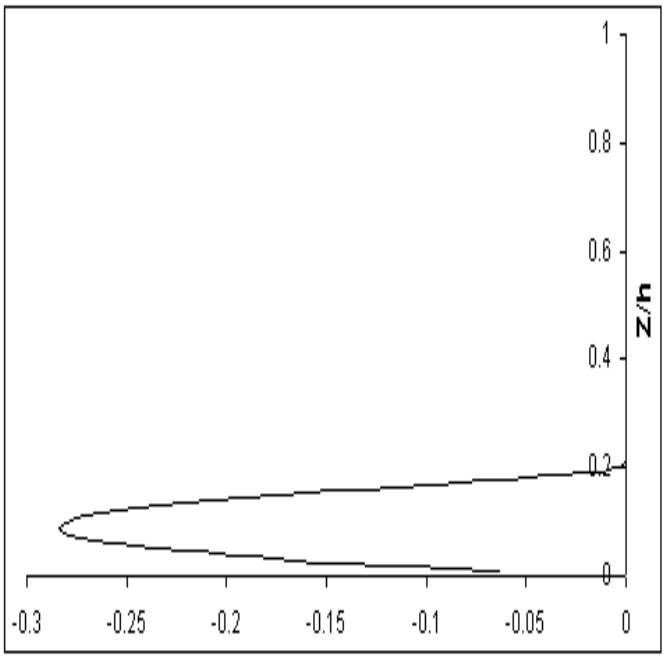

Figure 7.11: Production by buoyancy term in stable atmosphere, $10^3 m^2/s^3$

columnar modes. This phenomenon can be best understood from the momentum equation rather than from the vorticity equation.

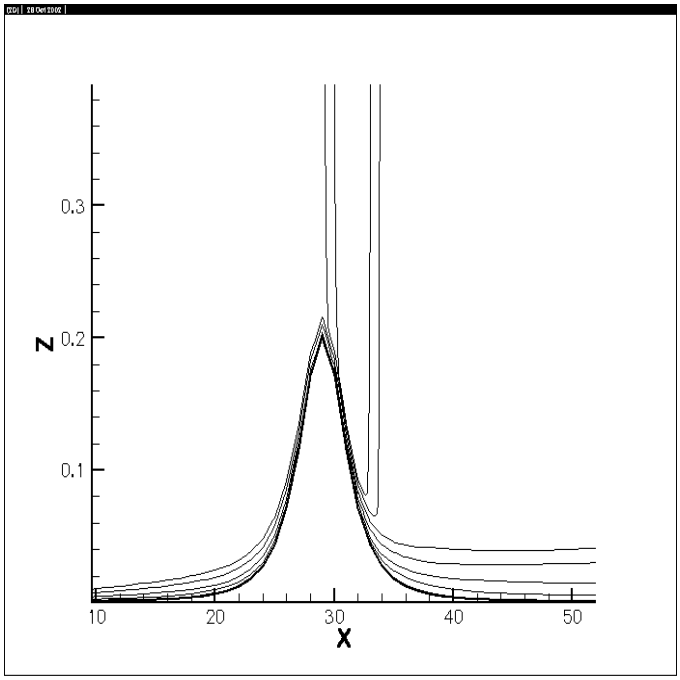

Figure 7.12: U velocity contour for $Re = 1 \times 10^8$ and $N = 0.0175$, Stable Atmosphere

7.6.3 Unstable atmosphere

Contrary to the stable atmosphere, unstable atmosphere has positive density gradient, so above definition of N is no longer valid. Moreover the buoyant force no longer acts as a restoring force to give us the harmonic motion. The density statification gives only the bouyancy force which acts upwards only. For this case let's define the Brunt-Vaisala frequency (N) as a measure of the density gradient in the form $N^2 = \frac{g}{\rho_0}\frac{\partial \rho}{\partial z}$. For unstable flow both the turbulent shear and buoyancy leads to production as shown in Figure 7.18,7.19,7.20.

Hence lee vortices can be observed downstream of the mountain if the production is sufficient enough. For $N = 0.0525$ concentration of the TKE is observed in lee of the mountain but negative velocity is not obtained, Figure 7.21,7.22. Further increasing the stratification the lee vortex is seen at the bottom of the mountain, Figure 7.23,7.24. No upstream blocking can be observed in this case as buoyancy gives positive momentum to overcome the potential of the mountain.

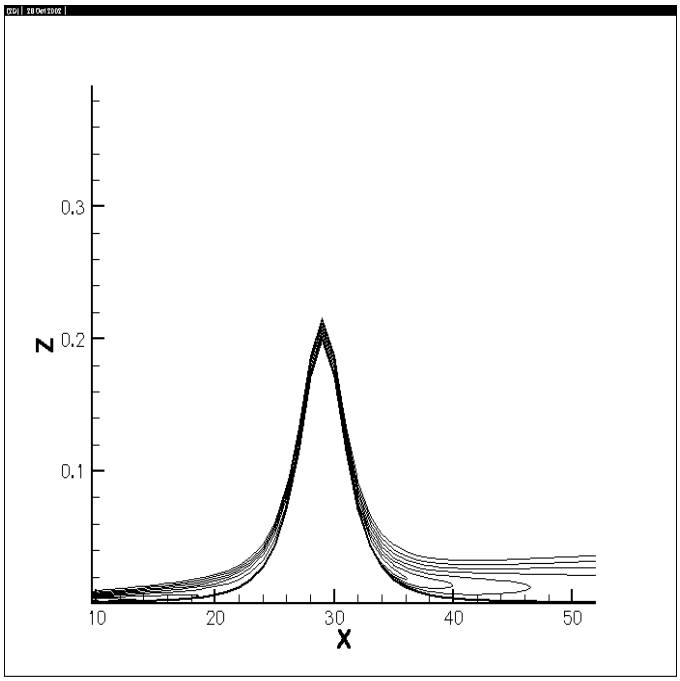

Figure 7.13: TKE contour for $Re = 1 \times 10^8$ and $N = 0.0175$, Stable Atmosphere

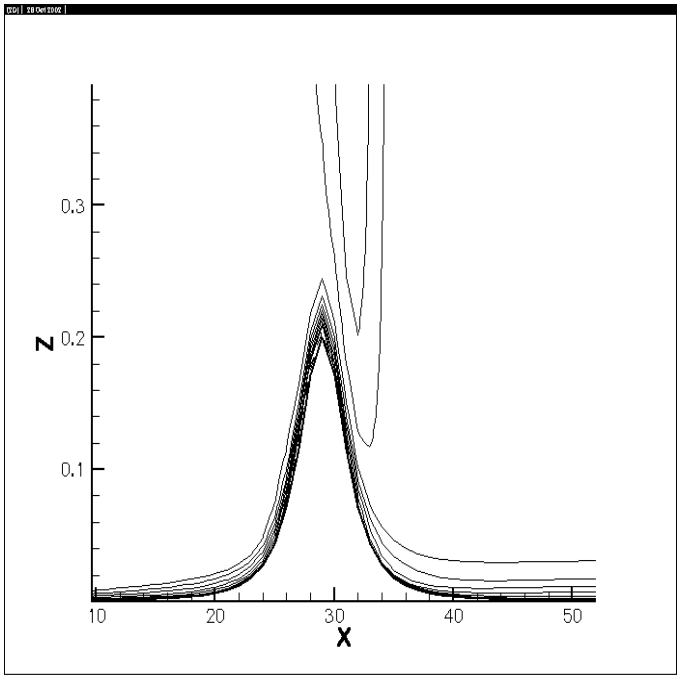

Figure 7.14: U velocity contour for $Re = 1 \times 10^8$ and $N = 0.0575$, Stable Atmosphere

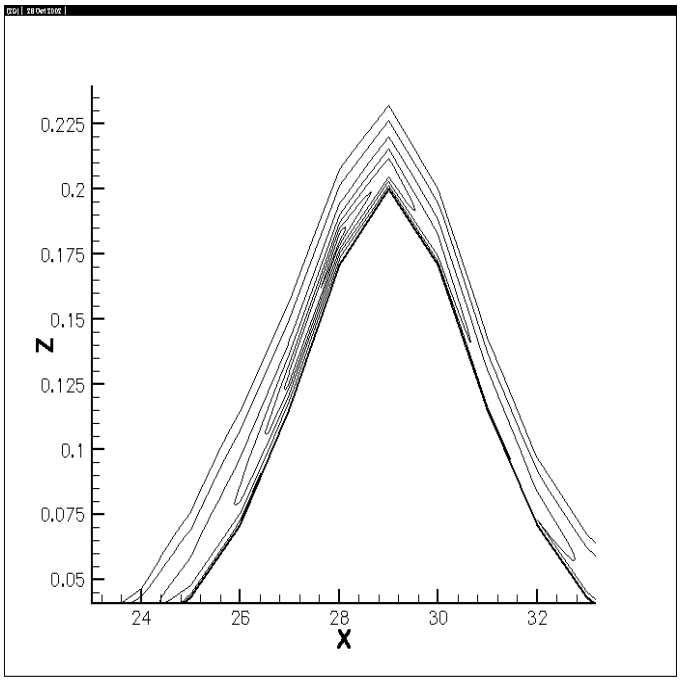

Figure 7.15: TKE contour for $Re = 1 \times 10^8$ and $N = 0.0575$, Stable Atmosphere, magnified

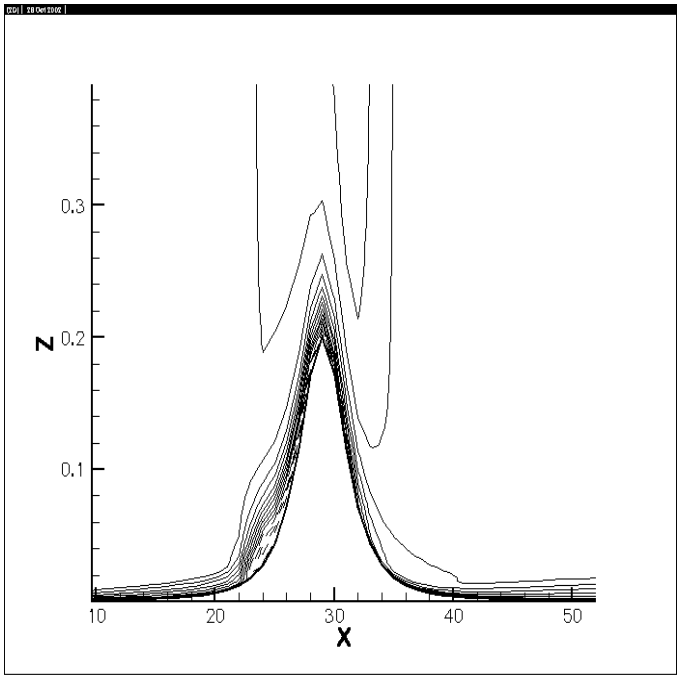

Figure 7.16: U velocity contour for $Re = 1 \times 10^8$ and $N = 0.0675$, Stable Atmosphere

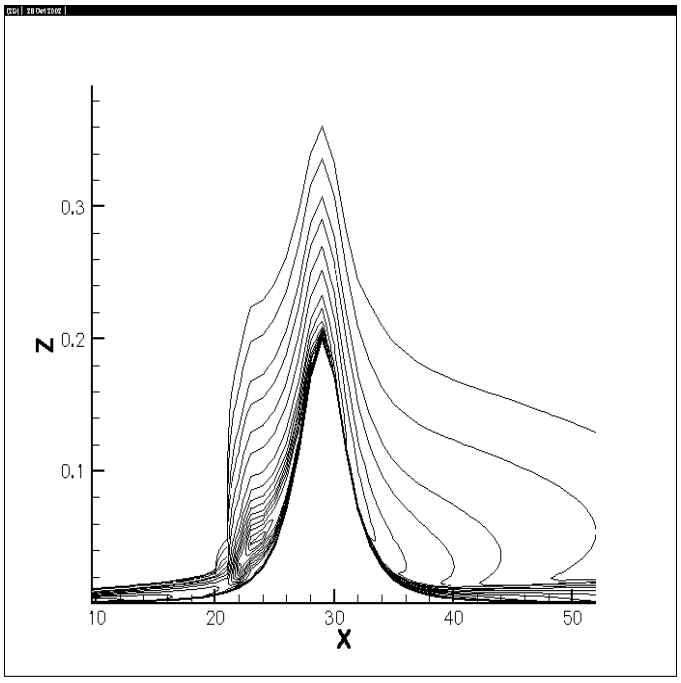

Figure 7.17: TKE contour for $Re = 1 \times 10^8$ and $N = 0.0675$, Stable Atmosphere

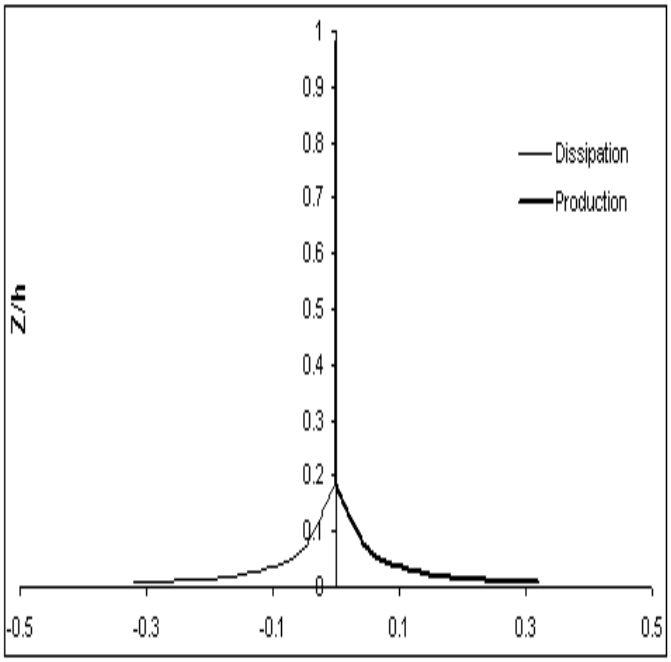

Figure 7.18: Production and Dissipation balance for unstable atmosphere, $10^4 m^2/s^3$

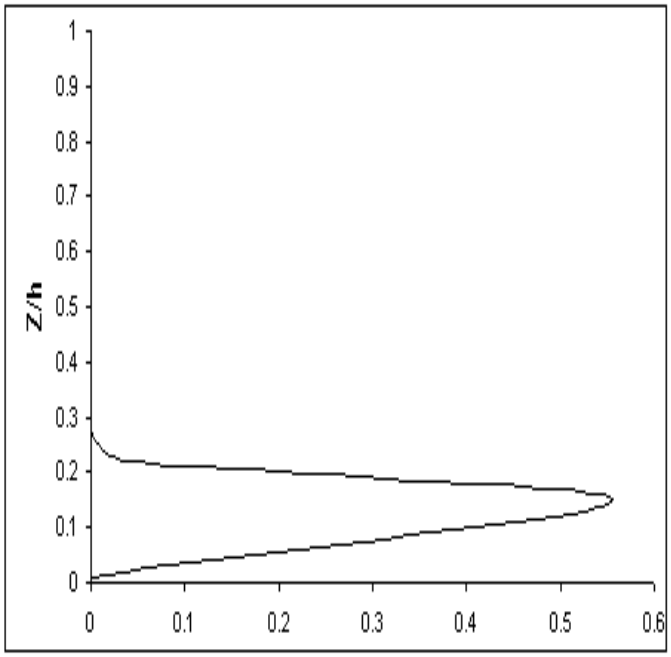

Figure 7.19: Production from subgrid stresses in unstable atmosphere, $10^3 m^2/s^3$

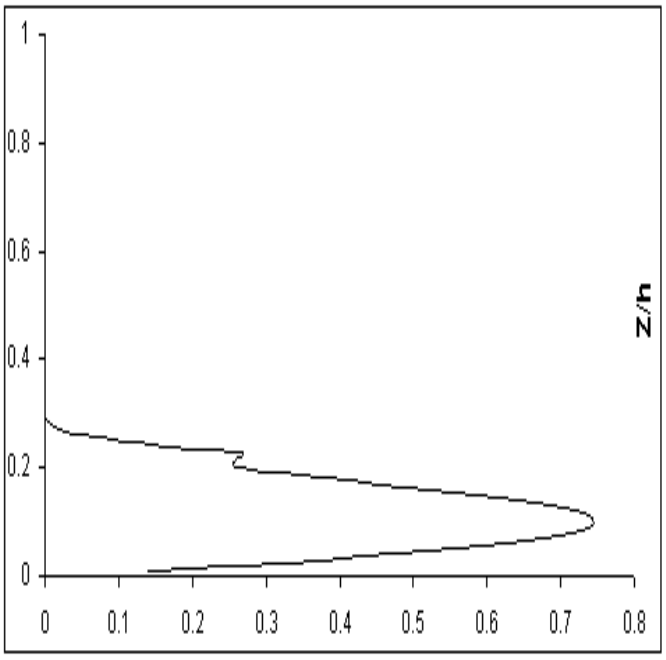

Figure 7.20: Production by buoyancy term in unstable atmosphere, $10^3 m^2/s^3$

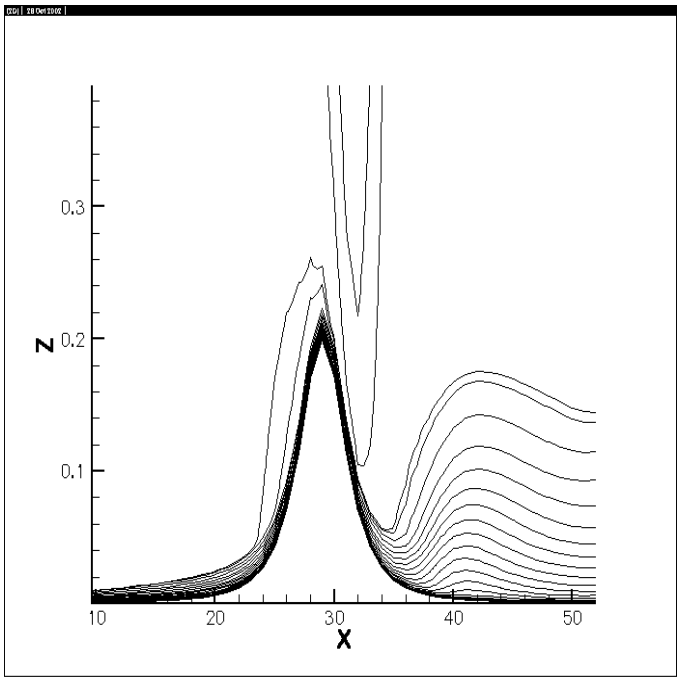

Figure 7.21: U velocity contour for $Re = 1 \times 10^8$ and $N = 0.0525$, Unstable Atmosphere

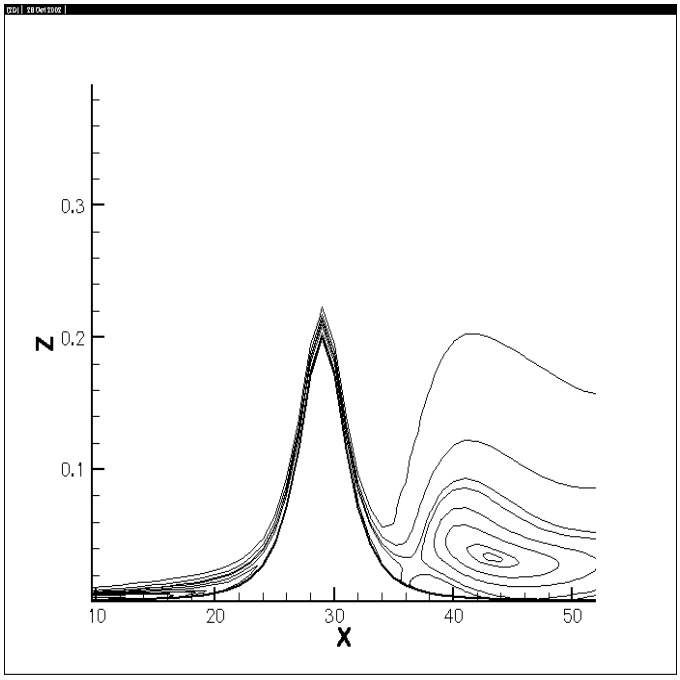

Figure 7.22: TKE contour for $Re = 1 \times 10^8$ and $N = 0.0525$, Unstable Atmosphere

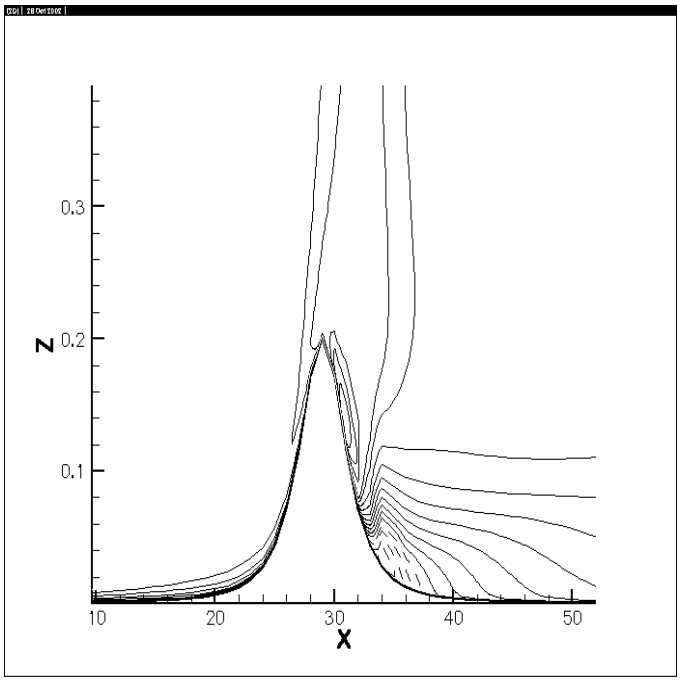

Figure 7.23: U velocity contour for $Re = 1 \times 10^8$ and $N = 0.0675$, Unstable Atmosphere

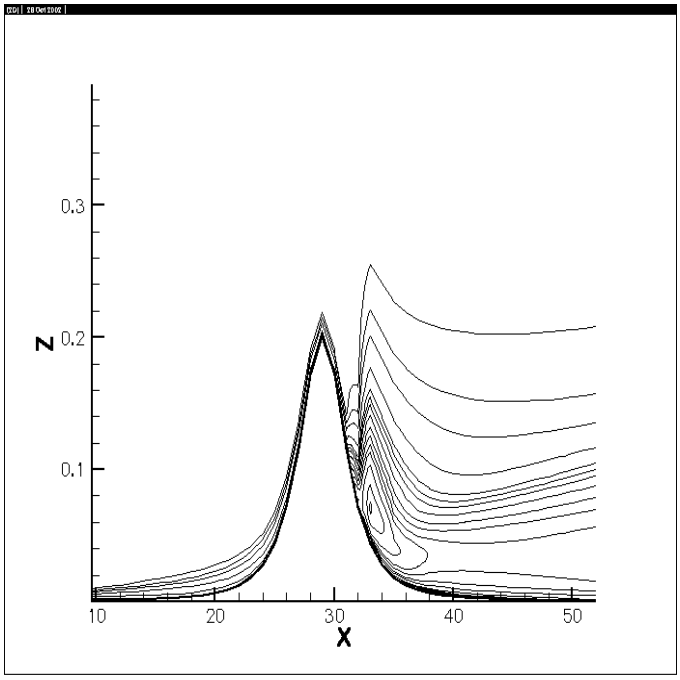

Figure 7.24: TKE contour for $Re = 1 \times 10^8$ and $N = 0.0675$, Unstable Atmosphere

CHAPTER VIII

DISCUSSION AND CONCLUSIONS

8.1 Discussion of Results

In this study we have used the " *Three-Dimensional Environmental Fluid Dynamics Code*" written by John M. Hamrick. The theoretical and computational aspects of the code has been discussed in a special report, [27]. The code solves the turbulent averaged, vertically hydrostatic equations with Boussinesq's assumption on sigma grid. The transport equation of scalar quantities such as salinity, temperature, dye, etc. are also solved, which finds its use in *mesoscale* atmospheric and oceanographic flows. The code is also capable of solving stratified flow. The numerical simulation is carried out by splitting the equation in external and internal mode equations and modeling them independently, which helps to obtain the solution for larger time step. Since the *shallow convection equations* are solved which require vertical scales to be much smaller than the horizontal length scales, the implicit filtering can be applied, to obtain the turbulent averaged equation, such that it is ensemble averaged in vertical direction and Gaussian filtered in horizontal direction. This helps us to model the vertical diffusion as Reynolds stress and horizontal diffusion as subgrid stresses [73] [70]. The vertical diffusion coefficient for the transport equations are obtained from the second moment closure scheme of Mellor and Yamada [26], [74]. The horizontal diffusion terms are obtained from the subgrid scale model as proposed by Smagorinsky [9]. The code is modified by introducing the new nonlinear model for the subgrid stresses and scalar fluxes with buoyancy effect.

Here we have proposed a new nonlinear model for the subgrid stresses, which has been obtained by extending the nonlinear constitutive equation for Reynolds stresses proposed by Warsi [23]. The turbulent eddy viscosity type term has been modeled using the subgrid scale kinetic energy and subgrid length scale rather than by rate of strain term as used by Smagorinsky [9]. An effort has been made to identify the terms of the model with the Leonard's, cross and

Reynolds stress terms. The model coefficients are obtained as universal constants by satisfying the dissipation criteria. Estimation of the dissipation is obtained from the isotropic turbulence thereby in the inertial subrange. The backscatter of the energy has also been considered which is estimated using the EDQNM theory. The model coefficients thus obtained are thus tested for the *plane homogeneous shear flow* and *plane strain flow* and good approximation was obtained. The model was further extended to include the buoyancy effect and for scalar fluxes. The model proposed here still lacks the proper modeling of the cross term. Thus far the physics contained in the cross term is the least understood and hence it's modeling is not discussed separately. When the new model is implemented in the code the solution obtained is not deterministic. This is because of the backscatter, which causes the solution to be stochastic in nature. The solution was rendered deterministic by clipping the dissipation term as suggested by Zang *et al.* [30]. This aspect has been studied by various authors [20], [25] and thus Lagrangian dynamic model was developed.

The code was run to generate velocity data for the backward facing step problem, where the inflow velocity profile was computed from the turbulent velocity profile for the flat plate [23]. The velocity data thus obtained is used to estimate the subgrid stresses using the *Smagorinsky*, *mixed nonlinear* and *new nonlinear* models and both are compared. We call this test an *a priori study*, although this is not exactly the *a priori study* as coined by Piomelli [89] which requires DNS data. From this comparison we study the physics contained in various models. We observe that there is considerable correlation of the *new nonlinear* model with the *Smagorinsky model*, whereas its behavior is same as that of the *mixed nonlinear model*. The normal stresses obtained from the new nonlinear model has a magnitude intermediate of the *Smagorinsky* and *mixed nonlinear model*. We can see the negative normal stresses which are a consequence of the backscatter term. For the mixed nonlinear model the backscatter term keeps on increasing as we move away from the wall, which is a consequence of the smaller coefficient of the eddy viscosity type term. For the new nonlinear model the backscatter decreases as we move away from the wall which seems reasonable. This is due to the fact that the backscatter of energy is modeled independent of the forward scatter [21]. The new nonlinear model gives more shear stress than the Smagorinsky model whereas the mixed nonlinear model gives less, but the peak of the shear stress by new nonlinear and Smagorinsky model lies approximately at the same position.

The flow over backward facing step forms a benchmark problem because of its fixed separation point and reattachment lengths. This problem has been studied extensively both experimentally and numerically for various parameters. Here the turbulent flow over a backward facing step is solved for the low Froude number, such that free surface elevation is small. We consider few of the parameters such as the expansion ratio, top boundary condition, effect of skin friction which helps us to apprehend the results obtained from the numerical simulation. Various authors have observed different recirculation zones in the different flow regimes and for different top boundary conditions. Based on the literature available we have tabulated the various recirculation zones that can be observed for the particular flow regime and top boundary condition. For our flow case we should have observed two recirculation zones one near the corner of the step called the secondary recirculation zone and the primary recirculation zones. However we observe only one recirculation zone, i.e the primary zone. It may be because of the sigma grid that has been used, which does not resolve the corner of the step. The reattachment length that has been obtained from the numerical simulation is 5.2 h, where h is the step height. The results from the literature available has been tabulated for the turbulent flow for the various upper boundary. The reattachment length varies from 5-8 h. However the result obtained here seems to be an underestimate, this may be because of the free surface condition which tends to decrease the reattachment length for turbulent flow, the near wall treatment as the equations are not solved right up to the surface. Moreover the nature of the equation which has been solved. The *a posteriori* test was performed on the results obtained. The velocity profile was compared with the experimental results [6]. The velocity profiles were compared in the corresponding recirculation, reattaching, attached and at far boundary. Good match with the experimental result was obtained both for the velocity profile and the turbulent kinetic energy. The production dissipation balance has been plotted at different sections, the subgrid scale production is small with respect to vertical shear production. The normal stresses decrease as we move away from the wall, whereas the shear stresses changes sign as we move across the reattachment zone has been shown.

The second problem that has been considered is the geophysical application of the model developed. Here we have considered constantly stratified flow over a two dimensional elliptic mountain ridge. This type of problem has been considered by many authors [104] [103] [105] [96] [95] but they have considered the transport of the potential temperature along with the

equations of motion. Hence the lee vortices formation is primarily due to the baroclinic effect. There has been little effort to study solely the effect of turbulence in such geophysical flows. Here we assume the stratification of the density is constant over the layer in time (which changes in time but due to barotropic effect). Hence the baroclinic instability cannot develop in between the density stratification layer, thereby the baroclinically produced vorticity is absent. The vorticity production is due to the turbulent shear and buoyancy effect only. The stratification thus results only in the buoyancy effect and solution of temperature equation is not required. The rate equation of the MSVF is modeled so that more insight can be obtained on the vorticity production mechanism. The results are obtained for neutral, stable and unstable atmosphere.

For the neutral atmosphere the buoyancy term is zero hence the vorticity generation is due to turbulent shear alone. The generation of the turbulent field requires apart from production and dissipation mechanism a trigger mechanism. In the present situation the mountain ridge acts as the trigger mechanism and hence the flow is turbulent on the lee of the mountain, which is evident from the concentration of the turbulent kinetic energy on the lee of the mountain. As the Reynolds number is increased the vorticity production increases thus the vorticity appears in the lee of the mountain at $Re = 4 \times 10^8$. The lee vortex generation is detected by a negative velocity contour or the concentration of TKE. The concentration point of TKE is also the concentration of vorticity as evident from the vorticity equation, as they both follow the same transport mechanism.

The stable atmosphere has a negative density gradient, hence the buoyancy produces a dissipation or inhibits the production mechanism. Since it has been observed from the neutral atmosphere that the shear production is not sufficient enough to produce the lee vortex at this Reynolds number, hence lee vortex cannot be produced for the stable atmosphere. This fact is validated by the numerical result with decreasing density gradient (increasing Brunt-Vaisala frequency). However when the density gradient is steep enough, upstream blocking effect is observed. This phenomenon can be supported from the momentum equation as put forward by Sheppard [106], which states that the fluid momentum is not able to overcome the buoyancy potential which increases with the density gradient and the potential of the mountain and hence the flow reversal takes place. The flow reversal for the baroclinically produced vortices occurs due to the upward moving columnar modes. The upstream blocking occurs for the $Fr = 2$, which is close to the value obtained by other authors.

The unstable atmosphere is defined for the positive density gradient and hence both buoyancy and shear terms adds up to the vorticity production mechanism. As the density gradient is increased the vorticity production increases and hence the lee vortices are formed. The vortex formation is identified by the concentration of the TKE, which moves to the bottom of the mountain with increasing gradient. No upstream blocking is observed since the buoyancy term acts against the mountain potential and hence adds up to the fluid momentum.

8.2 Conclusions

The *new nonlinear model* proposed here is obtained from the rate equation of the subgrid stresses and hence captures the physics of the subgrid stresses better than other existing models. The model terms are identified with the stress components which help us to compute the model coefficients. The backscatter term has distinctly been modeled form the forward scatter. The model coefficients are expressed as universal constants for the Gaussian filter. The model coefficients are tested for plane shear and plane strain flow and give good approximation. The physics contained in the cross term, which is least understood both in physical and spectral space, has been modeled with the Reynolds' term. Better understanding and modeling of this term is still a challenge for subgrid stress modeling.

A priori tests show that the new model has considerable correlation with Smagorinsky model and has the nature of mixed model. The *a posteriori test* has been performed for backward facing step and good match with the experimental result is obtained.

The turbulent flow behavior was studied for stratified flow over a two dimensional elliptic mountain ridge. Lee vortices were observed for 'unstable atmosphere' and for high Reynolds number flows. Upstream blocking was observed for 'stable atmosphere'. These vortex formation has been explained from the vorticity generation mechanism equation.

REFERENCES

[1] J. K. Eaton and J. P. Johnston, "A review of research on subsonic turbulent flow reattachment," *AIAA*, vol. 19, pp. 1093–1100, 1981.

[2] S. Thangam and D. D. Knight, "Effect of step height on the seperated flow past a backward facing step," *Physics of Fluids A*, vol. 1(3), pp. 604–606, 1989.

[3] B. F. Armlay, "Experimental and theoretical investigation of backward-facing step," *Journal of fluid mechanics*, vol. 127, pp. 473–496, 1983.

[4] C.W.Li and T.S.Yu, "Numerical investigation of turbulent shallow recirculating flows by a quasi-three-dimensional $k - \epsilon$ model," *International Journal For Numerical Methods in Fluids*, vol. 23, pp. 485–501, 1996.

[5] S. Jovic and D. Driver, "Reynold's number effect on the skin friction in seperated flows behind a backward-facing step," pp. 464–467, 1994.

[6] J.Kim, S. Kline, and J. Johnston, "Investigation of a reattaching turbulent shear layer: Flow over a backward facing step," *Journal of Fluids Engineering*, vol. 102, pp. 302–308, 1980.

[7] C. G. Speziale, "Analytical methods for the development of reynolds-stress closures in turbulence," *Annual Review of Fluid Mechanics*, vol. 23, pp. 107–157, 1991.

[8] C. W. Hirt *Phys. Fluids, Suppl. II*, pp. 219–227, 1969.

[9] J. Smagorinsky, "General circulation experiments with the primitive equations. i. the basic experiment.," *Monthly Weather Review*, vol. 91, pp. 99–164, 1963.

[10] J. W. Deardorff, "A numerical study of three-dimensional turbulent channel flow at large reynolds numbers," *Journal of Fluid Mechanics*, vol. 41, pp. 453–480, 1970.

[11] D. K. Lilly, "The representation of small-scale turbulence in numerical simulation experiments," in *Proc. IBM Sci. Comput. Symp. Enviorn. Sci*, pp. 195–210, 1967.

[12] D. K. Lilly, "A proposed modification of the germano subgrid-scale closure method," *Physics of Fluids, A*, vol. 4(3), pp. 633–634, 1992.

[13] A.Leonard, "Energy cascade in large-eddy simulations of turbulent fluid flows," *Advanced Geophysics*, vol. 18, pp. 237–248, 1974.

[14] P. J. Mason and N. S. Callen, "On the magnitude of the subgrid-scale eddy coefficient in large-eddy simulations of turbulent channel flow," *Journal of Fluid Mechanics*, vol. 162, pp. 439–462, 1986.

[15] D. C. Leslie and G. L. Quarini, "The application of turbulence theory to the formulation of subgrid modelling procedures," *Journal of Fluid Mechanics*, vol. 91, pp. 65–91, 1979.

[16] B. Kosovic, "Subgrid scale modelling for the large-eddy simulation of high-reynolds-number boundary layer," *Journal of Fluid Mechanics*, vol. 336, pp. 151–182, 1997.

[17] C. G. Speziale, "Galiliean invariance of subgrid-scale stress models in the large-eddy simulation of turbulence," *Journal of Fluid Mechanics*, vol. 156, pp. 55–62, 1985.

[18] S. B. Pope, *Turbulent Flows*. Cambridge University Press, 2000.

[19] C. Meneveau and J. Katz, "Scale-invariance and turbulence models for large-eddy simulations," *Annual Review of Fluid Mechanics*, vol. 32, pp. 1–32, 2000.

[20] S. Ghosal, S.Lund, P. Moin, and K. Akselvoll, "A dynamic localization model for large-eddy simulation of turbulent flows," *Journal of Fluid Mechanics*, vol. 286, pp. 229–255, 1995.

[21] J. R.Chasnov, "Simulation of the kolmogorov inertial subrange using an improved subgrid model," *Physics of Fluids A*, vol. 3(1), pp. 188–200, 1991.

[22] B. Galperin and A. A. Orszag, *Large Eddy Simulation of Complex Engineering and Geophysical Flows*. Cambridge University Press, 1993.

[23] Z. U. A. Warsi, *Fluid Dynamics, Theoretical and computational approach*. CRC press, 1998.

[24] P.J.Mason and D. J. Thompson, "Stochastic backscatter in the large-eddy simulations of boundary layers," *Journal of Fluid Mechanics*, vol. 242, pp. 51–78, 1992.

[25] C. Meneveau, T. S. Lund, and W. H. Cabot, "Lagrangian dynamic subgrid-scale model of turbulence," *Journal of Fluid Mechanics*, vol. 319, pp. 353–385, 1996.

[26] G. L. Mellor and T. Yamada, "Development of a turbulence closure model for geophysical fluid problems," *Reviews of Geophysics and Space Physics*, vol. 20(4), pp. 851–875, 1982.

[27] J. M. Hamrick, "A three-dimensional enviornmental fluid dynamics code : Theoretical and computational aspects," Tech. Rep. Special Report No. 317, Varginia Institute of Marine Science, May 1992.

[28] M. Germano, "Turbulence: The filtering approach," *Journal of Fluid Mechanics*, vol. 238, pp. 325–336, 1992.

[29] M. Germano, "A proposal for a redefinition of the turbulent stresses in the filtered navier-stokes equation," *Brief communication, Physics of Fluids*, vol. 29, no. 7, pp. 2323–2324, 1986.

[30] Y. Zang, R. L. Street, and J. R.Koseff, "A dynamic mixed subgrid-scale model and its application to turbulent recirculating flows," *Physics of Fluids, A*, vol. 5(12), pp. 3186–3196, 1993.

[31] M. Germano, P. M. Ugo Piomelli, and W. H. Cabot, "A dynamic subgrid-scale eddy viscosity model," *Physics of Fluids*, vol. 3(7), pp. 1760–1765, 1991.

[32] J. Bardina, J. H. Ferziger, and W. C. Reynolds, "Improved sub-grid models for large eddy simulation.," *AIAA*, vol. Paper 80, p. 1357, 1980.

[33] A. Scotti and C. Meneveau, "Generalized smagorinsky model for anisotropic grids," *Physics of Fluids, A*, vol. 5(9), pp. 2306–2308, 1993.

[34] C. E. Leith, "Stochastic backscatter in a subgrid-scale model: plane shear mixing layer," *Physics of Fluids, A*, vol. 2, pp. 297–299, 1990.

[35] P.J.Mason, "Large-eddy simulation of the convective atmospheric boundary layer," *Journal of Atmospheric Sciences*, vol. 46(11), pp. 1492–1516, 1989.

[36] P. Moin and J. Kim, "Numerical investigation of turbulent channel flow.," *Journal of Fluid Mechanics*, vol. 118, p. 341, 1982.

[37] V.M.Canuto and Y.Cheng, "Determination of the smagorinsky-lilly constant c_s," *Physics of Fluids*, vol. 9(5), pp. 1368–1375, 1997.

[38] J.W.Deardorff, "Three-dimensional numerical study of the height and mean structure of a heated planetary boundary layer," *Boundary-layer Meteorology*, vol. 7, pp. 107–123, 1974.

[39] J.W.Deardorff, "Three-dimensional numerical study of turbulence in an entraining mixed layer," *Boundary-layer Meteorology*, vol. 7, pp. 226–, 1974.

[40] A.R.brown, S.H.Derbyshire, and P.J.Mason, "Large-eddy simulation of stable atmospheric boundary layers with a revised stochastic subgrid model," *Q. J. R. Meteorological Society*, vol. 120, pp. 1485–1512, 1994.

[41] P.J.Mason and A.R.Brown, "On subgrid models and filter operations in large eddy simulations," *Journal of Atmospheric Sciences*, vol. 56, pp. 2101–2114, 1999.

[42] R. A. Clark, J. H. Ferzier, and W. C. Reynolds, "Evaluation of subgrid-scale models using an accurately simulated turbulent flow," *Journal of Fluid Mechanics*, pp. 1–16, 1979.

[43] R. H. Karaichan, "Eddy viscosity in two and three dimensions.," *Journal of Atmospheric Sciences*, vol. 33, pp. 1521–1536, 1976.

[44] B.Aupoix, "Subgrid scale models for homogeneous anisotropic turbulence," *Proceedings of Euromech Colloquium, Direct and large eddy Simulation of Turbulence, Muenchen FRG*, vol. 199, pp. 37–66, 1985.

[45] J. Bardina, *Improved turbulence models based on large eddy simulationof homogeneous, incompressible turbulent flows.* Stanford University, 1983.

[46] S. Liu, C. Meneveau, and J. katz, "On the properties of similarity subgrid-scale models as deduced from measurments in turbulent jet.," *Journal of fluid mechanics*, vol. 275, pp. 83–119, 1994.

[47] C. Pruett, J. S.Sochacki, and N. A.Adams, "On taylor-series expansions of residual stress," *Physics of Fluids, A*, vol. 13(9), pp. 2578–2589, 2001.

[48] C. Brun and R. Friedrich, "Modeling the test sgs tensor t_{ij}:an issue in the dynamic approach," *Physics of Fluids, A*, vol. 13(8), pp. 2373–2385, 2001.

[49] C. Meneveau and T. S.Lund, "The dynamic smagorinsky model and scale-dependent coefficients in the viscous range of turbulence," *Physics of Fluids, A*, vol. 9(12), pp. 3932–3934, 1997.

[50] F.Sarghini, U.Piomelli, and E.Balaras, "Scale-similar models for large-eddy simulations," *Physics of Fluids, A*, vol. 11(6), pp. 1596–1607, 1999.

[51] V.C.Wong, "A proposed statistical-dynamic closure method for the linear or nonlinear subgrid scale stresses," *Physics of Fluids, A*, vol. 4(5), pp. 1080–1082, 1992.

[52] S.B.Pope, "A more general effective-viscosity hypothesis," *Journal of Fluid Mechanics*, vol. 72(2), pp. 331–340, 1975.

[53] T. B. Gatski and C. G. Speziale, "On explicit algebraic stress models for complex turbulent flows," *Journal of Fluid Mechanics*, vol. 254, pp. 59–78, 1993.

[54] F.H.Champagne, "The fine-scale structure of the turbulent velocity field," *Journal of Fluid Mechanics*, vol. 86, pp. 67–108, 1978.

[55] U. Schumann, "Stochastic backscatter of turbulence energy and scalar variance by random subgrid-scale fluxes," *Proceedings of Royal Society of London, A*, vol. 451, pp. 293–318, 1995.

[56] P. J. Mason, "Large eddy simulation of convective atmospheric boundary layer," *Journal of The Atmospheric Sciences*, vol. 46, pp. 1492–1516, 1988.

[57] M. Lesieur, *Turbulence in Fluids.* Martinus Nijhoff Publishers, 1987.

[58] G. D. Stefano and O. V.Vasilyev, "Sharp cutoff versus smooth filtering in large eddy simulation," *Physics of Fluids, A*, vol. 14(1), pp. 362–369, 2002.

[59] C. H. Moeng, "A large-eddy simulation model for the study of planetary boundary-layer turbulence," *Journal of Atmospheric Sciences*, vol. 41(13), pp. 2052–2062, 1984.

[60] A.A.Townsend, "The uniform distortion of homogeneous turbulence," *Quarterly Journal of Mechanics and Applied Mathematics*, vol. 7(1), pp. 105–127, 1954.

[61] H.J.tucker and A.J.Reynolds, "The distortion of turbulence by irrotational plane strain," *Journal of Fluid Mechanics*, vol. 32(4), pp. 657–673, 1968.

[62] J.N.Gence and J.Mathieu, "On teh aplication of successive plane strains to grid-generated turbulence," *Journal of Fluid Mechanics*, vol. 93(3), pp. 501–513, 1979.

[63] J. Mathieu and J. Scott, *An introduction to Turbulent Flow.* Cambridge University Press, 2000.

[64] H. Schlicting and K. Gersten, *Boundary Layer Theory.* Springer-Verlag, 2000.

[65] C.Pantano and S.Sarkar, "A subgrid model for nonlinear functions of a scalar," *Physics of Fluids*, vol. 13(12), pp. 3803–3819, 2001.

[66] J. O. Hinze, *Turbulence: An introduction to its Mechanism and Theory.* McGRAW-HILL, 1959.

[67] K.R.Sreenivasan and R.A.Antonia, "The phenomenon of small-scale turbulence," *Annual Review of Fluid Mechanics*, vol. 29, pp. 435–472, 1997.

[68] J. R. Herring, "A comparative assesment of spectral closures as applied to passive scalar diffusion," *Journal of fluid mechanics*, vol. 124, pp. 411–437, 1982.

[69] R. B. Stull, *An introduction to Boundary Layer Metereology.* Kluwer Academic Publishers, 1988.

[70] R. A. Pielke, *Mesoscale Metereological Modeling.* Academic press, 984.

[71] S. P. Arya, *Introduction to Micrometereology.* Academic Press, 1988.

[72] P.Thunis and R.Bornstein, "Hierachy of mesoscale flow assumptions and equations," *Journal of Atmospheric Sciences*, vol. 53(3), pp. 380–397, 1996.

[73] GeorgeL.Mellor and A. F. Blumberg, "Modeling vertical and horizontal diffusivities with the sigma coordinate systems," *Monthly Weather Review*, vol. 113, pp. 1379–1383, 1985.

[74] B.Galperin, L.Kantha, S.hassid, and A.Rosati, "A quasi-equilibrium turbulent energy model for geophysical flows," *Journal of Atmospheric Sciences*, vol. 45(1), pp. 55–62, 1988.

[75] M. Vinokur, "Conservation equations of gasdynamics in curvilinear coordinate systems," *Journal of Computational Physics*, vol. 14, pp. 105–125, 1974.

[76] J. M. Hamrick, "Long-term dispersion in unsteady skewed free surface flow," *Estuarine, Coastal and Shelf Science*, vol. 23, pp. 807–845, 1986.

[77] R. V. Madala and S. A. Piacsek, "A semi-implicit numerical model for baroclinic oceans," *Journal of Computational Physics*, vol. 23, pp. 167–178, 1977.

[78] J. C. Tannehill, D. A. Anderson, and R. Pletcher, *Computational Fluid Mechanics and Heat Transfer.* Taylor and Francis Publishers, 1997.

[79] I. E. Barton, "Comparision of simple- and piso- type algorithms for transient flows," *International Journal For Numerical Methods in Fluids*, vol. 26, pp. 459–483, 1998.

[80] L. P. Hackman, G. D. Raithby, and A. B. Strong, "Numerical predictions of flows over backward-facing steps.," *International journal for numerical methods in fluids*, vol. 4, pp. 711–724, 1984.

[81] M. Beddhu and Z. Warsi, "A fractional time-stepping method for solving the compressible navier-stokes equations," *MSSU-EIRS-ASE-94-2*, 1994.

[82] M. J. Rabbitt, "Some validation of standard, modified and non-linear $k - \epsilon$ turbulence models," *International Journal For Numerical Methods in Fluids*, vol. 24, pp. 965–968, 1997.

[83] R. Ramos, J. P. Guerrero, and R. Cotta, "Statified flow over a backward-facing step: hybrid solution by integral transform," *International Journal For Numerical Methods in Fluids*, vol. 35, pp. 173–197, 2001.

[84] R. R. Hwang and Y. F. Peng, "Computation of backward-facing step flows by a second-order reynolds stress closure model," *International Journal For Numerical Methods in Fluids*, vol. 21, pp. 223–235, 1995.

[85] J. Keskar and D. Lyn, "Computations of a laminar backward-facing step flow at $Re = 800$ with a spectral domain decomposition method," *International Journal For Numerical Methods in Fluids*, vol. 29, pp. 411–427, 1999.

[86] V. Bellucci and C. Bruno, "Incompressible flows with combustion simulated by a preconditioning method using multigrid acceeration and muscl reconstruction," *International Journal For Numerical Methods in Fluids*, vol. 36, pp. 619–637, 2001.

[87] A. Chwang, S. Van, and H. Kim, "Computaion of flow over backward facing step without and with free surface," *Hydrodynamics: theory and applications; proceedings of the Second International Conference on Hydrodynamics, Hong-Kong*, pp. 521–526, 1996.

[88] K. Akselvoll and P. Moin, "Application of the dynamic localization model to large eddy simulation of turbulent flow over a backward facing step," *Engineering applications of large eddy simulations*, vol. 162, pp. 1–6, 1993.

[89] U. Piomelli, P. Moin, and R. Adrian, "Model consistency in large eddy simulation of turbulent channel flows.," *Physics of Fluids, A*, vol. 31, pp. 1884–1891, 1988.

[90] F. Ilinca, D. Pelletier, and A. Garon, "An adaptive finite element method for a two-equation turbulence model in wall -bounded flows," *International Journal For Numerical Methods in Fluids*, vol. 26, pp. 887–905, 1998.

[91] R. B. Smith, "Linear theory of stratified hydrostatic flow past an isolated mountain," *Tellus*, vol. 32, pp. 348–364, 1980.

[92] G. D. Crapper, "A three dimensional solution for waves in the lee of mountains," *Journal of Fluid Mechanics*, vol. 6, pp. 51–76, 1959.

[93] P. Drazin, "On the steady flow of a fluid of variable density past an obstacle," *Tellus*, vol. 13, pp. 214–224, 1961.

[94] H. Olafsson and P. Bougeault, "Nonlinear flow past an elliptic mountain ridge," *Journal of Atmospheric Sciences*, vol. 53, No. 17, pp. 2465–2489, 1996.

[95] Y. D. Afanasyev and W. R. Peltier, "The three-dimensionalization of stratified flow over two-dimensional topography," *Journal of Atmospheric Sciences*, vol. 55, pp. 19–38, 1998.

[96] M. H. Bauer, G. J. Mayr, I. Vergeiner, and H. Peltier, "Strongly nonlinear flow over and around a three-dimensional mountain as a function of the horizontal aspect ratio," *Journal of Atmospheric Sciences*, vol. 57, pp. 3971–3991, 2000.

[97] S.B.Vosper, "Three-dimensional numerical simulations of strongly stratified flow past conical orography," *Journal of Atmospheric Sciences*, vol. 57, pp. 3716–3739, 2000.

[98] A.E.Macdonald, J.L.Lee, and Y.Xie, "The use of quasi-nonhydrostatic models for mesoscale weather prediction," *Journal of Atmospheric Sciences*, vol. 57, pp. 2493–2517, 2000.

[99] M. G. Wurtele and A. Datta, "The propagation of a gravity-inertia wave in a positively sheared flow," *Journal of Atmospheric Sciences*, vol. 57, pp. 3703–3715, 2000.

[100] J. J. O'Brien and H. E. Hurlburt, "A numerical model of coastal upwelling," *Journal of Physical Oceanography*, vol. 2, pp. 14–26, 1972.

[101] C.-S. Yih, *Statified Flows*. Academic Press, 1980.

[102] R. R. Long, "Some aspects of the stratified fluids iii. continous density gradients," *Tellus*, vol. 7, pp. 341–357, 1955.

[103] P. K. Smolarkiewicz and R. Rotunno, "Low froude number flow past three-dimensional obstacles. part i: Baroclinically generated lee vortices," *Journal of Atmospheric Sciences*, vol. 46, No. 8, pp. 1154–1164, 1989.

[104] R. B. Smith, "Hydrostatic airflow over mountains," *Advances in Geophysics, VOL. 31*, 1989.

[105] P. K. Smolarkiewicz and R. Rotunno, "Low froude number flow past three-dimensional obstacles. part ii: Upwind flow reversal zone," *Journal of Atmospheric Sciences*, vol. 47, No.12, pp. 1498–1511, 1990.

[106] P. A. Sheppard, "Airflow over mountains," *Q. J. R. Meteorological Society*, vol. 82, pp. 528–529, 1956.

[107] P. G. Baines, "Upstream blocking and airflow over mountains.," *Annual Review of Fluid Mechanics*, vol. 19, pp. 75–97, 1987.

[108] J. B. Klemp and D. Lilly, "Numerical simulation of hydrostatic mountain wave.," *Journal of Atmospheric Sciences*, vol. 35, pp. 78–107, 1978.

APPENDIX A

A.1 Galilean Invariance of Subgrid stresses

Navier-Stokes equation and its filtered form is Galilean invariant, which requires that the description of the turbulence be the same in all inertial frame. Consider a reference system moving with constant transitional velocity, **U**. The velocities with respect to the new reference frame is

$$u_i^* = u_i + U_i \quad , \quad \hat{u}_i^* = \hat{u}_i + U_i \quad \text{and} \quad u_i'^* = u_i'$$

The Leonard, cross and Reynolds stress term in the new reference frame is

$$\begin{aligned} L_{ij}^* &= L_{ij} - U_i\hat{u}_j' - U_j\hat{u}_i' \\ C_{ij}^* &= C_{ij} + U_i\hat{u}_j' + U_j\hat{u}_i' \\ R_{ij}^* &= R_{ij} \end{aligned} \tag{A.1}$$

which shows that R_{ij} is Galilean invariant but L_{ij} and C_{ij} are not. Where as $L_{ij} + C_{ij}$ has a Galilean invariant form. The mixed model proposed by Bardina *et al.* approximated the cross term as

$$C_{ij} = c_r\left(\hat{u}_i\hat{u}_j - \hat{\hat{u}}_i\hat{\hat{u}}_j\right)$$

In the new reference frame the cross term transforms as

$$C_{ij}^* - U_i\hat{u}_j' - U_j\hat{u}_i' = c_r\left(\hat{u}_i^*\hat{u}_j^* - \hat{\hat{u}}_i^*\hat{\hat{u}}_j^*\right) - c_r\left(U_i\hat{u}_j' + U_j\hat{u}_i'\right)$$

Hence the model is Galilean invariant if the coefficient c_r is chosen equal to one. Bardina *et al.* however arrived at $c_r = 1.1$, which is modified to 1. It has been shown by Piomelli *et al.* and Houriuti in a *a priori* test that the above model is good approximation for the cross term. It can be further established that Galilean invariant form of cross term with Bardina's approximation is zero. Germano [28] introduced a set of generalized central moment, which are Galilean invariant,

defined by

$$\begin{aligned} \tau(u_i, u_j) &= \widehat{u_i u_j} - \hat{u}_i \hat{u}_j \\ \tau(u_i, u_j, u_k) &= \widehat{u_i u_j u_k} - \hat{u}_i \tau(u_j, u_k) - \hat{u}_j \tau(u_k, u_i) - \hat{u}_k \tau(u_i, u_j) - \hat{u}_i \hat{u}_j \hat{u}_k \end{aligned} \tag{A.2}$$

similarly other moments can be defined. The above moments are equivalent to $\overline{u_i' u_j'}$ and $\overline{u_i' u_j' u_k'}$ defined by Monin and Yaglom for Reynolds averaged equation. Introducing the decomposition of the variable into resolved and subgrid scale components in the second order moment the subgrid stress can be decomposed into three components

$$\begin{aligned} \mathcal{L}_{ij} &= \tau(\hat{u}_i, \hat{u}_j) \\ \mathcal{C}_{ij} &= \tau\left(\hat{u}_i, u_j'\right) + \tau\left(u_i', \hat{u}_j\right) \\ \mathcal{R}_{ij} &= \tau\left(u_i', u_j'\right) \end{aligned} \tag{A.3}$$

Hence follows the new Galilean invariant form of the Leonard, cross and Reynolds stress. Similarly the scalar flux, $H_{j\theta} = \widehat{u_j \theta} - \hat{u}_j \hat{\theta}$, in Galilean invariant form as

$$\begin{aligned} \mathcal{L}_{i\theta} &= \tau\left(\hat{u}_i, \hat{\theta}\right) \\ \mathcal{C}_{i\theta} &= \tau\left(\hat{u}_i, \theta'\right) + \tau\left(u_i', \hat{\theta}\right) \\ \mathcal{R}_{i\theta} &= \tau\left(u_i', \theta'\right) \end{aligned} \tag{A.4}$$

The buoyancy production term can be expanded as:

$$\begin{aligned} \widehat{w\acute{T}} - \hat{w}\hat{\acute{T}} &= \widehat{\hat{w}\acute{T}} - \hat{\hat{w}}\hat{\acute{T}} + \widehat{\acute{w}\acute{T}} - \widehat{\acute{w}}\hat{\acute{T}} \\ &= \mathcal{C}_{i\theta} + \mathcal{R}_{i\theta} - \left(\widehat{\acute{w}\hat{T}_0} - \widehat{\acute{w}}\hat{\hat{T}}_0\right) \end{aligned} \tag{A.5}$$

As for the synoptic scale temperature, $\hat{\hat{T}}_0 = \hat{T}_0$, hence the subgrid flux term producing the buoyant production can be modeled as cross and Reynolds terms only.

A.2 Triadic Interaction

In order to analyze the stresses and it's decomposition we transfer the subgrid stress in the wave number space. The Fourier transform of the subgrid stress term $\boldsymbol{\tau} = \widehat{\mathbf{uu}} - \widehat{\mathbf{u}}\widehat{\mathbf{u}}$ as given in Pope [18], Stefano and Vasilyev [58] is:

$$\grave{\boldsymbol{\tau}}(\mathbf{k}) = \grave{G}(\mathbf{k})\left[\grave{\mathbf{u}}(\mathbf{k}') \star \grave{\mathbf{u}}(\mathbf{k}'')\right] - \left[\grave{G}(\mathbf{k}')\,\grave{\mathbf{u}}(\mathbf{k}')\right] \star \left[\grave{G}(\mathbf{k}'')\,\grave{\mathbf{u}}(\mathbf{k}'')\right] \tag{A.6}$$

where $(\star)$ means convolution of two terms such that

$$\grave{\mathbf{u}}(\mathbf{k}') \star \grave{\mathbf{u}}(\mathbf{k}'') = \int_{\mathbf{k}=\mathbf{k}'+\mathbf{k}''} \grave{\mathbf{u}}(\mathbf{k}')\,\grave{\mathbf{u}}(\mathbf{k}'')\,d\mathbf{k}'$$

and $(\grave{a})$ is the fourier component of the quantity. If we consider wavenumber $\mathbf{k}_{LES}$ such that

$$\mathbf{k} < \mathbf{k}_{LES} \;\Rightarrow\; \grave{\mathbf{u}} = \grave{\widehat{\mathbf{u}}} \;\text{ and }\; \mathbf{k} > \mathbf{k}_{LES} \;\Rightarrow\; \grave{\mathbf{u}} = \grave{\mathbf{u}}' \;\text{ as }\; \grave{G}\grave{\mathbf{a}} = \grave{\widehat{\mathbf{a}}}$$

considering all the triadic interactions and substituting the limits of wavenumber in the above equation and bringing the terms together we get

$$\grave{\boldsymbol{\tau}} = \left(\grave{\widehat{\mathbf{u}}}\grave{\widehat{\mathbf{u}}} - \grave{\widehat{\mathbf{u}}} \star \grave{\widehat{\mathbf{u}}}\right) + \left(\grave{\widehat{\mathbf{u}}}\grave{\mathbf{u}'} + \grave{\widehat{\mathbf{u}}}\grave{\mathbf{u}'} - \grave{\mathbf{u}'} \star \grave{\widehat{\mathbf{u}}} - \grave{\widehat{\mathbf{u}}} \star \grave{\mathbf{u}'}\right) + \left(\grave{\mathbf{u}'}\grave{\mathbf{u}'} - \grave{\mathbf{u}'} \star \grave{\mathbf{u}'}\right) \tag{A.7}$$

On taking the Inverse fourier transformation we obtain the decomposition of stresses into Leonard's, cross and Reynolds' terms, following Leslie and Qurani [15]. Germano [29] obtained the above decomposition using the Galilean invariance form of the stress terms and Zang *et al.* [30] obtained it by decomposing the variables into resolved and subgrid components in the stress terms. Since the subgrid stresses cause the energy transfer berween resolved scale and subgrid scale motion, the physical behaviour of each term can be understood from the wavenumber interaction. The subgrid stress can be written as:

$$\grave{\boldsymbol{\tau}}(\mathbf{k}) = \int_{\mathbf{k}=\mathbf{k}'+\mathbf{k}''} \left[\grave{G}(\mathbf{k}) - \grave{G}(\mathbf{k}')\,\grave{G}(\mathbf{k}'')\right] \grave{\mathbf{u}}(\mathbf{k}')\,\grave{\mathbf{u}}(\mathbf{k}'')\,d\mathbf{k}' \tag{A.8}$$

The triad interaction associated with each component can be thus be obtained, from the information form Eq. A.6 and A.7. For the sharp filter we can befine the cut-off number $\mathbf{k}_c$ such

that all the wavenumber components larger than it are annhiliated, such that $\grave{G}(\mathbf{k} > \mathbf{k}_c) = 0$. Thus the Leonard's component is zero as expected [13], whereas cross and Reynolds' term represent the interactions of the type

$$\begin{aligned} \grave{\boldsymbol{\mathcal{C}}} \quad &\text{for} \quad \mathbf{k} < \mathbf{k}_{LES}, \;\; \mathbf{k}_{LES} < max(\mathbf{k}', \mathbf{k}'') < 2\mathbf{k}_{LES}, \;\; min(\mathbf{k}', \mathbf{k}'') < \mathbf{k}_{LES} \\ \grave{\boldsymbol{\mathcal{R}}} \quad &\text{for} \quad \mathbf{k} < \mathbf{k}_{LES}, \;\; \mathbf{k}' > \mathbf{k}_{LES}, \;\; \mathbf{k}'' > \mathbf{k}_{LES} \end{aligned} \tag{A.9}$$

The above interactions are exact only if we have a precise distinction between large scale and small scale. The smooth filters such as Gaussian filter or top-hat filter, does not give this precise distinctions hence more interactions occur. For smooth filter we define cut-off wavenumber $\mathbf{k}_{LES}$ such that $\grave{G}(\mathbf{k} > \mathbf{k}_{LES}) \neq 0$. Thus the Leonard's term involves the interaction of type

$$\grave{\boldsymbol{\mathcal{L}}} \quad \text{for} \;\; \mathbf{k}_{LES} < \mathbf{k} < 2\mathbf{k}_{LES}, \;\; \mathbf{k}' < \mathbf{k}_{LES}, \;\; \mathbf{k}'' < \mathbf{k}_{LES} \tag{A.10}$$

There are more interactions which appear which has not been discussed. From the triadic interactions, Eq. A.9, A.10, it must be observed that the Leonards term represent the energy transfer from the resolved scale motion to the subgrid scale motion, due to nonlinearity effect as described by Leonard [13], hence this term produces pure dissipation. The cross term stress satisfies the triangular property of $\mathbf{k}, \mathbf{k}', \mathbf{k}''$ for the wave numbers near the cut-off wave number and hence represent the near-local energy transfer. Whereas the Reynolds' term in the limit $\mathbf{k}' \gg \mathbf{k}_{LES}$ represent the non-local interaction. These interactions have been further explained using the triadic interaction sketches, Figure A.1.

A.3 Moment of Filter

The n^th moment of a filter function in one dimension is expressed as:

$$\int_{-\infty}^{\infty} x_i^n G(x_i)\, dx_i$$

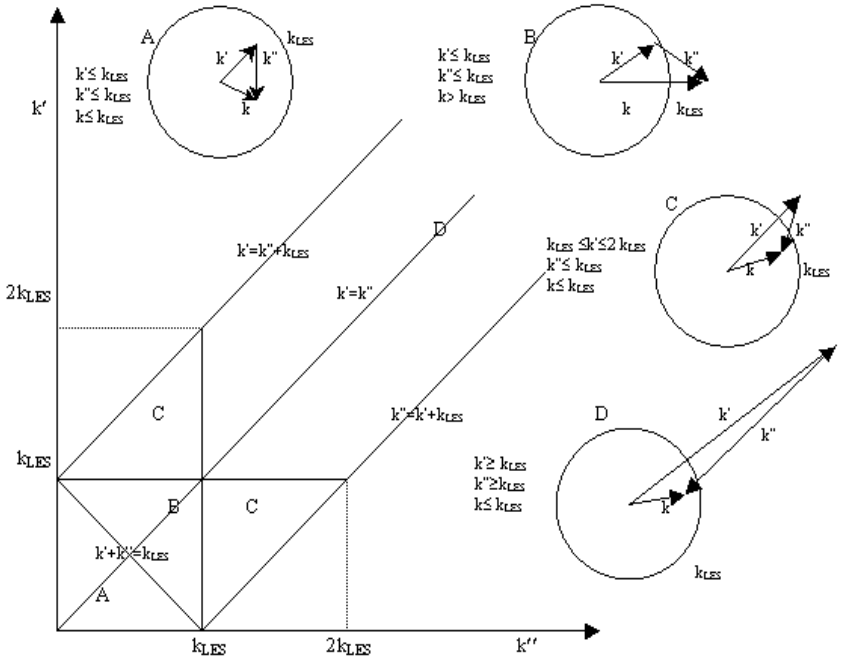

Figure A.1: The triadic interaction between $\mathbf{k}'$ and $\mathbf{k}''$ in one and two-dimensional space.

which can be expressed in terms of the transfer function of the filter as shown by Pruett and Sochacki [47].

$$\begin{aligned} \grave{G}(k) &= \int_{-\infty}^{\infty} e^{ikx_i} G(x_i)\, dx_i \\ \frac{\partial^n}{\partial k^n}\grave{G}(k) &= \int_{-\infty}^{\infty} (ix_i)^n e^{ikx_i} G(x_i)\, dx_i \\ \frac{\partial^n}{\partial k^n}\grave{G}(0) &= \int_{-\infty}^{\infty} (ix_i)^n e^{ikx_i} G(x_i)\, dx_i \end{aligned} \tag{A.11}$$

Thus the moment of the filter function in one-dimension can be obtained from the derivative of the transfer function. For the Gaussian, top-hat and sharp spectral filter the second filter moments are thus obtained as $\frac{\Delta^2}{12}$, $\frac{\Delta^2}{12}$, 0 respectively From the results obtained above the integral of the function, $\mathbf{r}^2 G(\mathbf{r})$, can be obtained as:

$$\int_{-\infty}^{\infty} \mathbf{r}^2 G(\mathbf{r})\, d\mathbf{r} = \sum_i \int_{-\infty}^{\infty} (x_i)^2 e^{ikx_i} G_i(x_i)\, dx_i = 3\frac{\Delta^2}{12} \tag{A.12}$$

which is applicable for symmetric filters only. However for anisotropic filter the choice of characteristic filter width as, $\Delta = (\Delta_1\Delta_2\Delta_3)^{1/3}$, is supported many authors [18] for obtaining the filter moment.

A.4 Leonard's Stress Expansion

Applying Taylor's series expansion of the filtered velocity following Brun and Friedrich [48] for symmetric filter (Gaussian) such that odd moments of the filter are zero we can get:

$$\begin{aligned}
\hat{\hat{u}}_m &= \hat{u}_m + b\frac{\partial^2 \hat{u}_m}{\partial {x_l}^2} + o(\Delta^4) \\
\widehat{\hat{u}_i\hat{u}_j} &= \hat{u}_i\hat{u}_j + b\frac{\partial^2 \hat{u}_i\hat{u}_j}{\partial {x_l}^2} + o(\Delta^4) \\
\hat{\hat{u}}_i\hat{\hat{u}}_j &= \hat{u}_i\hat{u}_j + b\left[\hat{u}_j\frac{\partial^2 \hat{u}_i}{\partial {x_l}^2} + \hat{u}_i\frac{\partial^2 \hat{u}_j}{\partial {x_l}^2} + o(\Delta^4)\right]
\end{aligned} \tag{A.13}$$

Where,

$$b = \frac{1}{2}\int_{-\infty}^{\infty} x_n^2 G(\mathbf{x}) dx_n$$

is half the second moment of the filter. The Leonard's stress

$$L_{ij} = \widehat{\hat{u}_i\hat{u}_j} - \hat{u}_i\hat{u}_j = b\frac{\partial^2 \hat{u}_i\hat{u}_j}{\partial {x_l}^2}$$

is up to fourth order accurate and give exact dissipation as the Leonard's stress as shown by Leonard [13]. The Galilean invariant decomposition of Leonard stresses as proposed by Germano is obtained as:

$$\mathcal{L}_{ij} = \widehat{\hat{u}_i\hat{u}_j} - \hat{\hat{u}}_i\hat{\hat{u}}_j = 2b\frac{\partial \hat{u}_i}{\partial x_l}\frac{\partial \hat{u}_j}{\partial x_l} + o(\Delta^4) \tag{A.14}$$

The dissipation due to the term $\hat{u}_i\hat{u}_j$ is zero for any filter, but the term $\hat{\hat{u}}_i\hat{\hat{u}}_j$ produces non zero dissipation for any other filter except spectral cut off filter. So the dissipation produced by the improved Leonards stress term can be computed using the triple correlation term. The improved Leonard's stress and its expansion produces the same dissipation.

For the scalar flux the Taylor's expansion of the Leonard's term can be obtained similar to the subgrid stress term

$$\mathcal{L}_{i\theta} = \widehat{\hat{u}_i\hat{\theta}} - \hat{\hat{u}}_i\hat{\hat{\theta}} = 2b\frac{\partial\hat{u}_i}{\partial x_l}\frac{\partial\hat{\theta}}{\partial x_l} + o(\Delta^4) \tag{A.15}$$

The dissipation due to the Leonard's term and its Taylor's series expansion form are same as computed for the isotropic turbulence.

A.5 Total and Resolved scale energy

Using the convention used by Warsi [23]. For homogeneous isotropic turbulence the two point velocity correlation is related to the internal structure of the wave number space as :

$$R_{jl}(r) = \langle u_j(x)\, u_l(x+r)\rangle \quad \text{and} \quad \Phi_{jl}(x,k) = \frac{1}{(2\pi)^3}\int\int_{\infty}^{-\infty}\int R_{jl}(r)\, e^{-ik\cdot r}dr$$

$$E_{jl}(x,k) = \int\int_s \Phi_{jl}(x,k)\, ds(k) \quad \text{and} \quad E(x,k) = \frac{1}{2}E_{jj}(x,k)$$

From the above definition of the energy spectra from the velocity correlation we get :

$$E(x,k) = \langle\int_{-\infty}^{\infty} R_{ii}(r)\, e^{-ikr}dr\rangle \tag{A.16}$$

The energy spectrum in the inertial subrange is known, so we need to express the filtered energy or resolved scale energy in terms of the filter function and energy spectrum. Resolved scale energy is is obtained from the correlation R_{ii}^f such that :

$$R_{ii}^f(r) = \langle\hat{u}_i(x)\,\hat{u}_i(x+r)\rangle$$

So the energy spectrum for the correlation term is:

$$E_f(x,k) = \int_{-\infty}^{\infty}\left[\int_{-\infty}^{\infty} G(y)\, u_i(x-y)\, dy\right]\left[\int_{-\infty}^{\infty} G(z)\, u_i(x+r-z)\, dz\right]e^{-ikr}dr$$

The above expression is obtained by expressing the filtered velocity as convolution between the velocity component and filter. Changing the order of integration we obtain:

$$E_f(x,k) = \int_{-\infty}^{\infty}\int_{-\infty}^{\infty}\left[\int_{-\infty}^{\infty} u_i(x-y)\,u_i(x+r-z)\,e^{-ik(r+z-y)}dr\right]G(y)\,e^{-iky}dyG(z)\,e^{ikz}dz$$

Using the above definition of energy spectrum we get:

$$E_f(x,k) = |G(k)|^2 E(k) \tag{A.17}$$

Similarly the filtered energy spectrum is defined from the correlation function $\hat{R}_{ii}$ as:

$$\hat{R}_{ii}(r) = \langle u_i(x)\widehat{u_i(x}+r)\rangle$$

$$\hat{E}(x,k) = \int_{-\infty}^{\infty}\left[\int_{-\infty}^{\infty} G(y)\,u_i(x-y)\,u_i(x+r-y)\,dy\right]e^{-ikr}dr$$

Changing the order of integration:

$$\hat{E}(x,k) = \int_{-\infty}^{\infty}\left[\int_{-\infty}^{\infty} u_i(x-y)\,u_i(x+r-y)\,e^{-ikr}dr\right]G(y)\,dy$$

which shows that :

$$\hat{E}(x,k) = E(x,k) \tag{A.18}$$

As for the filter function $\int_{-\infty}^{\infty} G(y)\,dy = 1$ from definition. The energy contained in subgrid scale motion (K_{sgs}) is therefore,

$$K_{sgs} = \hat{E} - E_f \tag{A.19}$$

A.6 Relating Subgrid scale energy and dissipation

The coefficient relating the subgrid scale energy (K_{sgs}) and dissipation (ϵ)

$$\epsilon = C_\epsilon \frac{K_{sgs}^{3/2}}{\Delta}$$

can be evaluated for homogeneous isotropic turbulence for cut-off wave number in the inertial subrange. The energy spectrum in the inertial subrange from the Kolmogrov's hypothesis follows the -5/3 law and is given by:

$$\grave{E}(k) = C_k \epsilon^{2/3} k^{-5/3}$$

. For the homogeneous isotropic turbulence turbulence energy in physical space is related to the turbulence energy spectrum in wave number space [23] as:

$$E = \int_0^\infty \grave{E}(k)\, dk \tag{A.20}$$

The above relationship helps us to relate resolved scale energy E_f to the energy spectrum in the inertial subrange as: $\grave{E}_f(k) = \grave{E}(k) |\grave{G}(k)|^2$, where $|\grave{G}(k)|$ is the averaged filter transfer function. We can further define the filtered energy field $\hat{E} = \widehat{u_i u_i}$ which can be expressed in wave number space as: $\grave{\hat{E}}(k) = |\grave{G}(k)| \grave{E}(k)$. For the isotropic homogeneous turbulence we obtain $E = \hat{E}$ as proof is outlined above [18]. From the above definitions of resolved and filtered energy field we can find the subgrid scale energy field $K_{sgs} = \hat{E} - E_f$ such that:

$$K_{sgs} = \int_0^\infty \left(1 - |\grave{G}(k)|^2\right) \grave{E}(k)\, dk \tag{A.21}$$

For the spectral filter $|G(k)| = H(k - k_c)$, where $H(.)$ is the heaviside function and k_c is the cut-off wave number. So for the sharp-spectral filter the above equation yields the value of $C_\epsilon = 0.93$ for $k_c = \frac{\pi}{\Delta}$. Some of the authors Mason, Schmidt and Schumann [14] have used the above relation to model the Smagorinsky coefficient where the value of constant is taken to be 0.7. Wong [51] suggested its value ranging from 0.63 to 0.85. For our model we will be using

Gaussian filter for which $|G(k)| = e^{\frac{-\Delta^2 k^2}{24}}$. The subgrid scale energy is thus computed as :

$$K_{sgs} = \int_0^\infty C_k \epsilon^{2/3} \left[1 - e^{\frac{-\Delta^2 k^2}{24}}\right] k^{-5/3} dk \tag{A.22}$$

From the above integral we get $C_\epsilon = 0.65146$. We will be using the above computed value for calculating the coefficient of the nonlinear model. Similarly for the scalar quantity the energy spectrum in the inertial subrange is given as

$$\grave{E}_\theta(k) = \beta \epsilon_\theta \epsilon^{-1/3} k^{-5/3}$$

The relation between the scalar dissipation and the turbulent kinetic is expressed in the form

$$\epsilon_\theta = C_{\theta\epsilon} \frac{K_{sgs}^{1/2} K_\theta}{\Delta}$$

The coefficient $C_{\theta\epsilon}$ is related to C_ϵ from the above relations to obtain its value, which gives $C_{\theta\epsilon} = \frac{C_k}{\beta} C_\epsilon = 1.575$, as compared to 2.02 for sharp spectral filter [55].

A.7 Estimating the Production/Dissipation

The production of energy due to different terms in the subgrid stresses can be estimated for the isotropic turbulence. We use the triple correlation relationship for two points as given in Hinze [66], Warsi [23] to estimate the term. Assuming that the velocity fluctuations are homogeneous and isotropic we should have the local equalbirium condition $P = \epsilon$ (Production= Dissipation). The subgrid stresses are the source of the dissipation (which occurs as Production in the equation of subgrid kinetic energy) of the Kinetic energy of resolved motion. The diffusion due to the subgrid scale terms are zero so we must have $\langle \hat{u}_i \frac{\partial \tau_{ij}}{\partial x_j} \rangle = -\langle \tau_{ij} \frac{\partial u_i}{\partial x_j} \rangle$. Where the stress term consists of all the three terms namely, Leonard, cross and Reynolds. The cross term and Reynolds term will be modeled together, so must account for the residual dissipation (total dissipation minus dissipation due to Leonard stress) and total backscatter. So we must estimate the dissipation due to the Leonards term.

$$\epsilon_L = \langle \hat{u}_i \frac{\partial \widehat{\hat{u}_i \hat{u}_j}}{\partial x_j} \rangle - \langle \hat{u}_i \frac{\partial \hat{\hat{u}}_i \hat{\hat{u}}_j}{\partial x_j} \rangle \tag{A.23}$$

The first term on the right can be estimated as shown in Leonard [13]. Where as the second term was not exactly the same as per the definition of Leonard. The Improved definition of the Leonard stress causes a significant change in the estimate of the dissipation due to this term. The dissipation due to the second term can be estimated from the Taylor's series expansion of the term such that:

$$\langle \hat{u}_i \frac{\partial \hat{\hat{u}}_i \hat{\hat{u}}_j}{\partial x_j} \rangle = \langle \hat{u}_i \frac{\partial \hat{u}_i \hat{u}_j}{\partial x_j} \rangle + b \left[\langle \hat{u}_i \frac{\partial}{\partial x_j} \left(\hat{u}_j \frac{\partial^2 \hat{u}_i}{\partial {x_l}^2} \right) \rangle + \langle \hat{u}_i \frac{\partial}{\partial x_j} \left(\hat{u}_i \frac{\partial^2 \hat{u}_j}{\partial {x_l}^2} \right) \rangle \right] \tag{A.24}$$

The first term on the left right is zero because of the continuity condition for incompressible flow. We need to express the second and third term in terms of the triple correlation function, $\hat{T}_{ij,k} = \langle (\hat{u}_i)_A (\hat{u}_j)_A (\hat{u}_k)_B \rangle$, so that they can be approximated for isotropic turbulence. The outline of the calculations are presented here for the Gaussian filter. The Triple correlation function is expressed as a function of single variable k, discussed in details Hinze [66] (Eqn 3-28), Warsi [23]. The derivatives can be expressed in terms of the distance between the points A and B by $\boldsymbol{\xi}$, where, $\xi_k = x_k|_B - x_k|_A$,such that $\frac{\partial}{\partial x_k}|_A = -\frac{\partial}{\partial \xi_k}$; $\frac{\partial}{\partial x_k}|_B = \frac{\partial}{\partial \xi_k}$, moreover as $(u_i)_A$ is not affected by the differentiation at point B and vice versa hence we can rearrange terms of the form as :

$$u_i u_j \frac{\partial^3}{\partial x_j \partial x_l \partial x_l} u_k = \frac{\partial^3}{\partial \xi_j \partial \xi_l \partial \xi_l} T_{ij,k}$$

$$\frac{\partial u_i u_j}{\partial x_k} \frac{\partial^2}{\partial x_l \partial x_l} u_m = -\frac{\partial^3}{\partial \xi_k \partial \xi_l \partial \xi_l} T_{ij,m}$$

Along with the invariance condition $T_{ij,k} = -T_{k,ij}$; Continuity equation $\frac{\partial \hat{u}_j}{\partial x_j} = 0$ and letting the two points A and B converge to a single point we get the desired result as:

$$\epsilon_L = -\frac{35}{24} K_{sgs}^{3/2} K_0''' (0) \Delta^2 \tag{A.25}$$

Where $\hat{q}^3 K_0''' = \langle (\frac{\partial \hat{u}_1}{\partial x_1})^3 \rangle$. The same result is obtained if the dissipation is computed from the Taylor's series expansion of the Improve Leonard term. It must be noted here that Leonard's definition of stress can be exactly modeled by second derivative, but improve definition requires only first derivative. Again, disspation due to $\mathcal{L}_{ij} \frac{\partial \hat{u}_i}{\partial x_j}$ also give the same result as obtained

above when computed using the sixth-order isotropic tensor form presented by Tenneskes and Lumley , Champagne and Robertson [54] given below. Which is a consequence of the isotropy consideration for which the diffusion is zero.

$$\langle \frac{\partial u_i}{\partial x_j}\frac{\partial u_k}{\partial x_l}\frac{\partial u_m}{\partial x_n}\rangle = \Big[\delta_{ij}\delta_{kl}\delta_{mn} - \frac{4}{3}\left(\delta_{ij}\delta_{km}\delta_{ln} + \delta_{ik}\delta_{lj}\delta_{mn} + \delta_{im}\delta_{jn}\delta_{kl}\right)$$
$$-\frac{1}{6}\left(\delta_{ij}\delta_{kn}\delta_{lm} + \delta_{il}\delta_{kj}\delta_{mn} + \delta_{in}\delta_{kl}\delta_{jm}\right) - \frac{3}{4}\left(\delta_{il}\delta_{kn}\delta_{jm} + \delta_{in}\delta_{kj}\delta_{lm}\right)$$
$$+\delta_{il}\delta_{km}\delta_{jn} + \delta_{in}\delta_{km}\delta_{lj} + \delta_{ik}\delta_{lm}\delta_{jn} + \delta_{ik}\delta_{ln}\delta_{jm} + \delta_{im}\delta_{jl}\delta_{kn} + \delta_{im}\delta_{jk}\delta_{ln}\Big]\langle\left(\frac{\partial u_1}{\partial x_1}\right)^3\rangle \quad \text{(A.26)}$$

Similar to the above approximation the scalar dissipation terms can be approximated. The Leonard's dissipation for the scalar quantity is approximated using the scalar correlation function, $T_{\theta,j\theta}$ such that

$$\hat{T}_{\theta,j\theta} = \langle \hat{\theta}_A \left(\hat{u}_j\hat{\theta}\right)_B\rangle$$

and has the properties

$$\hat{T}_{\theta,j\theta} = -\hat{T}_{j\theta,\theta} \;\;;\;\; \hat{T}_{j\theta,\theta} = \hat{T}_{\theta j,\theta} \;\;;\;\; \hat{T}_{\theta\theta,j} = 0$$

The expansion of the correlation term for isotropic turbulence has been discussed in details by Hinze [66]. The dissipation can thus be approximated using the above properties as:

$$\begin{aligned}\langle\theta\frac{\partial \mathcal{L}_{j\theta}}{\partial x_j}\rangle &= \int_{-\infty}^{\infty} G(\boldsymbol{\xi})\frac{\partial}{\partial \xi_j}T_{\theta,j\theta}d\boldsymbol{\xi} \\ &= -\frac{5}{12}K^{\theta}_{sgs}K^{1/2}_{sgs}K'''_{\theta}(0)\,\Delta^2 \end{aligned} \quad \text{(A.27)}$$

The coefficient K'''_{θ} can be obtained from the relation

$$\langle\frac{\partial^3 T_{\theta,1\theta i}}{\partial\xi_1\partial\xi_k\partial\xi_k}\rangle = 5K^{\theta}_{sgs}K^{1/2}_{sgs}K'''_{\theta}(0) = \langle\frac{\partial\theta}{\partial\xi_k}\frac{\partial\theta}{\partial\xi_k}\frac{\partial u_1}{\partial\xi_1}\rangle$$

The dissipation by the Taylor's expansion of Leonard's term is also approximated and gives the same value. The dissipation due to other terms can be obtained from the correlation function similarly.